Zeitschrift: IABSE reports = Rapports AIPC = IVBH Berichte
Band: 73/1/73/2 (1995)

Rubrik: Poster Session 1: Materials

Poster Session 1

Materials
Matériaux
Baustoffe

Leere Seite
Blank page
Page vide

Time-Dependent Load Changes in Integral Bridges

Variation des charges dans le temps de ponts monolithiques

Zeitabhängige Lastveränderungen in monolithischen Brücken

George L. ENGLAND
Professor
Imperial College
London, UK

George England is Professor of Mechanics and Structures at Imperial College. He holds PhD and D.Sc(Eng) degrees for original research into the time- and temperature-dependent behaviour of concrete structures. He acts as a consultant on bridge performance.

Neil C.M. TSANG
Research Student
Imperial College
London, UK

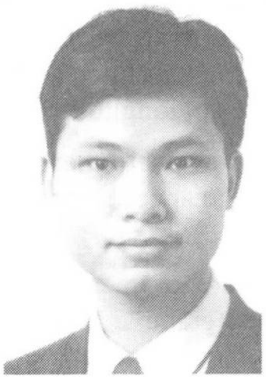

Neil Tsang is a Chartered Structural Engineer. He obtained his first degree in 1990 at the University of Sheffield, UK. Three years in a firm in England for designing concrete structures. Neil Tsang is currently conducting research study in the long term behaviour of prestressed concrete structures.

SUMMARY

The soil/structure interaction of bridge abutments is described in relation to experimentally observed behaviour of drained granular material subjected to cyclical strain loading. For integral bridges, repeated thermal displacements of the deck cause frictional flow in the granular material, and increases in the lateral soil stress behind the abutments. The composite behaviour is analysed in a novel manner, as an elastic-plastic shakedown problem. This approach allows the most influential parameters to be identified, and the limiting load cases for the structure to be defined.

RÉSUMÉ

L'interaction sol-structure des culées de pont est décrite en relation avec le comportement observé des matériaux granuleux subissant des allongements de manière cyclique. Dans les ponts monolithiques, la répétition des déplacements du tablier dûs aux variations de température provoquent des frottements dans le matériau granuleux et augmente les contraintes latérales du sol derrière les culées. Le comportement sol-structure est analysé pour la première fois en temps que problème élasto-plastique. Cette approche permet d'identifier les paramètres principaux du phénomène et de définir les cas de charges limites pour la structure.

ZUSAMMENFASSUNG

Es wird die Boden-Bauwerk-Wechselwirkung an Brückenwiderlagern angesprochen und zu experimentellen Beobachtungen in drainiertem körnigen Material unter zyklischer Dehnungsgeschichte in Beziehung gesetzt. In zusammenhängend gebauten Brücken bewirken die wiederholt auftretenden Temperaturdehnungen in der Fahrbahnplatte Reibungsdeformation im granularen Material und einen Anstieg des horizontalen Erddrucks hinter den Widerlagerwänden. Das Zusammenwirken wird erstmals als elastisches Shake-down-Problem analysiert. Bei dieser Vorgehensweise lassen sich Hauptparameter identifizieren und Grenzbeanspruchungsfälle des Bauwerks definieren.

1. INTRODUCTION

One major source of damage to highway bridges results from deicing salts leaking through deck joints onto sub-surface components. This process causes corrosion and immobilisation of movement joints and bearings, and represents a major element of conventional road bridge repair and maintenance costs. The Department of Transport in the UK has recently adopted the concept of continuous and integral (jointless) bridges as one of the options to avoid the corrosion problems. Integrating bridge deck to the abutment is also an option for retrofitting existing concrete bridges. In the UK, bridge abutments usually act simultaneously as soil retaining structures for the roadway embankment and are typically more than 6m in height. For medium span bridges of this type (length approx. 100m), environmental daily and seasonal temperature fluctuations of the bridge deck (up to 48°C) cause relative movements of the abutments. These in turn cause repeating displacements to be imposed on the granular backfill behind the abutments, where the nature of the soil/structure interaction is to create significant lateral stress escalation in the soil and atttendant increases in longitudinal force in the bridge deck.

Engineers require guidance to evaluate these thermally induced and cyclically-dependent lateral earth pressures acting over the rear face of the abutments and hence the axial force in the bridge deck for design purposes.

This paper describes the nature of the soil/structure interaction in relation to experimentally observed behaviour of drained granular material subjected to cyclical strain loading. An elastic-plastic shakedown model for the interaction between the bridge abutment and the granular backfill is presented. Finally, the most influential parameters are identified and the limiting load cases for the structure are defined.

2. INITIAL STRESS/STRAIN RESPONSE OF GRANULAR MATERIAL

The horizontal earth stress, σ_H, at a depth z is defined by γzK where γ is the unit weight of the granular material and K is the horizontal soil pressure coefficient (See Figure 1a.). During the initial heating (abutment moves towards the embankment) and then cooling (abutment moves away from the embankment), the horizontal soil stress path follows C-b-A in Figure 1b. In the case of cooling first *before* heating the path is C-a-B. The initial K value (point C) and profile of the initial responses curves (C-A or C-B) are dependent on density of the soil which is controlled by the degree of compaction. Point **a** and **b** are dependent on the temperature applied to the structure. During the second and subsequent thermal cycles, loading paths have origins which are no longer on the virgin loading curves, CB and CA.

3. SOIL/STRUCTURE INTERACTION

For a small number of cycles the volume of backfill which is strained plastically is difficult to identify. However, after many cycles, experimental observations of deformation patterns have revealed that β (see Figure 1) approaches unity. Initially, the deck is in compression due to the horizontal soil pressures at the abutments. Then for a temperature change ΔT (+ve for temperature rise), the *free thermal expansion* of the bridge deck is $L\alpha\Delta T$, where α and L are the coefficient of thermal expansion and length of the deck respectively. For a unit width of the abutment, this will cause a change in horizontal earth force, ΔF_2 (see Figure 1a.) and a complimentary equal change in the deck force, ΔP (+ve for compression). The corresponding deck displacement caused by the change of soil pressure, from the *free thermal length* $L(1+\alpha\Delta T)$ at one end of the deck, (symmetry assumed) is given by

$\delta_1 = \Delta P/k_b$ +ve for *contraction*, where,

$k_b = 2AE/L$ axial stiffness of the deck relative to P
$\Delta P = \Delta F_2$ thermally induced *increase* in axial compressive force

The corresponding displacement of the wall/soil interface is defined as, in Figure 1a, $\delta = (L\alpha\Delta T/2-\delta_1)$. This is absorbed within the soil wedge defined by β (=1).

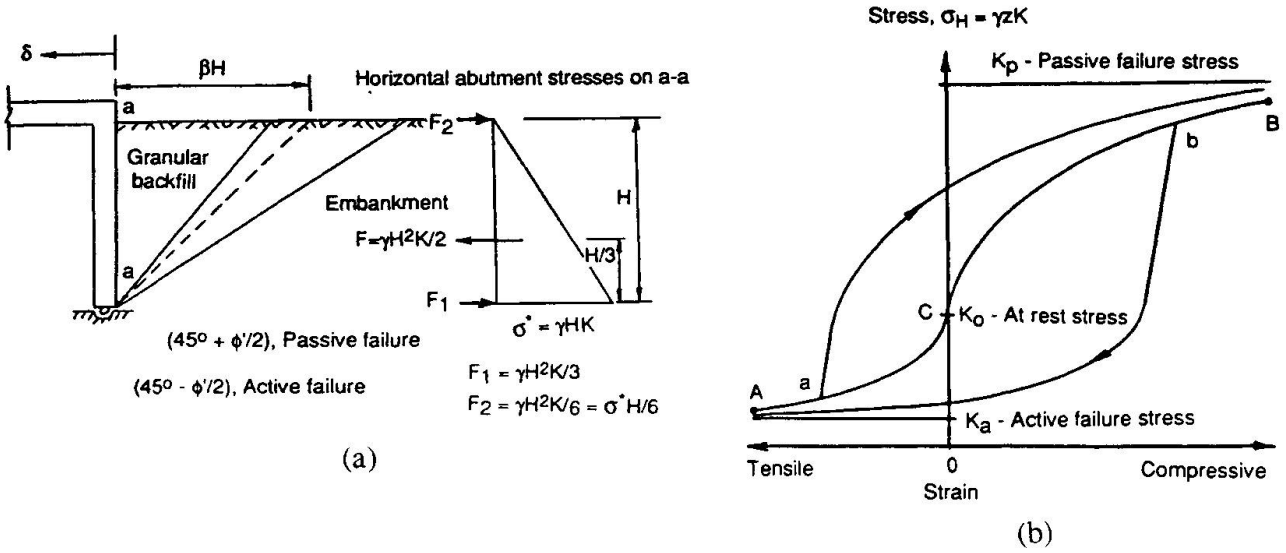

Figure 1. (a) Lateral soil pressure on a retaining wall type bridge abutment
(b) Initial Stress/Strain Response of Drained Granular Material
(i) unload **C-a** then reload **a-B** or (ii) load **C-b** then unload **b-A**

The analysis shown above represents an half-cycle temperature change. The daily and seasonal cyclic thermal movements of the bridge deck lead to a more complicated problem of continuous fluctuating strain changes in the granular backfill. A soil/structure interaction diagram is developed to enable a graphical presentation of the relationships between the stress paths of the soil, the stiffness of the bridge deck and the displacements of the deck/soil interface. Figure 2 represents a typical interaction diagram of this type for a "soft deck" structure, this will be further explained in next section.

Figure 2 has been derived from Figure 1(b) by suitable scaling of the axes; $\delta = \beta H\varepsilon_H$ and $F_2 = \sigma_H^* HK/6$. Lines **x-x** and **y-y** represent the bridge deck force/displacement responses at the two temperature limits. The effect of the cyclic temperature changes in the bridge deck creates an overall incrementally ratcheting inward displacement (towards the deck) of the wall/soil interface and an escalation of the horizontal force between the full-height retaining-wall abutment and the granular backfill embankment following the unclosed loops c-d-e-f-...of Figure 2.

4. SHAKE-DOWN STATE

During the cyclic straining process, the bulk volume of the soil particles may reduce and their packing arrangement changes. The horizontal earth pressure coefficient, **K**, will build up. Eventually the material tends either to (i) a *shakedown state*, or (ii) *failure* of the granular material (ie $K = K_p$ or K_a) or *failure* of the structure. The shakedown state is characterised by stresses which repeat on a cycle by cycle basis with no overall volume change and an upper stress ratio, K_u, which is always the reciprocal of the lower stress ratio, K_l, i.e. $K_u K_l = 1$. The existence of a shakedown state (see Figure 2) is dependent upon the magnitude of the imposed fluctuating soil strain ($\Delta\delta/\beta H$) from the bridge deck, the stiffness ($2AE/L$) of the deck and the horizontal residual

soil modulus ($\mathbf{E_g}$). It is defined by repeating elastic-plastic (friction) behaviour in the granular material and elastic behaviour in the structure. The existence of such a state has been verified experimentally [1] and values for the residual soil modulus for *sand* under cyclic strain loading have been observed to be proportional to the overburden pressure. $\mathbf{E_g}$ can be defined as $\mathbf{N\sigma_v}$ where σ_v is the vertical stress on the soil element considered and **N** is a constant coefficient. $\mathbf{E_g}$ is, therefore, dependent on the abutment wall height **H** and varies linearly with depth.

Because both the temperature change ΔT and abutment wall height **H** are governed practically by the environment and topographical conditions, the interaction diagrams, as shown in Figure 2 and 3, identify two types of integral bridge, depending upon deck stiffness :

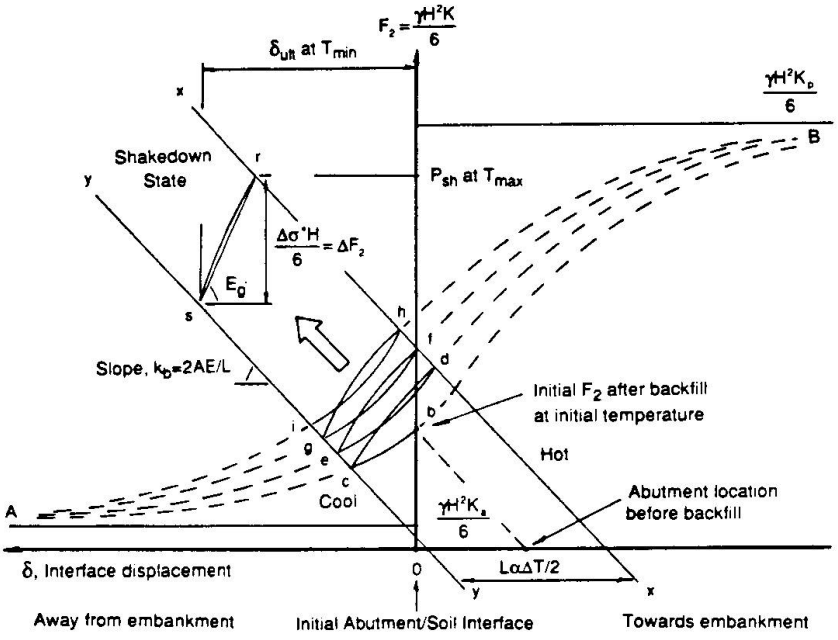

Figure 2. A Soil/Structure Interaction Diagram for "Soft Structure"

(i) **Soft deck**; small $\mathbf{k_b}$. Cyclically imposed displacements of the soft deck on the granular backfill lead to a *shakedown state* for any value of the residual soil modulus, $\mathbf{E_g}$. When this value is not known, a shakedown solution may still be obtained by using an upper bound value of $\mathbf{E_g} = \infty$. Then, the limiting upper bound value of the fluctuating stress, $\Delta\sigma_u^*$, at the toe of the abutment wall (see Figure 1) may be evaluated from Figure 2, as $\Delta\sigma_u^* = \mathbf{6AE\alpha\Delta T/H}$. The corresponding maximum fluctuating force in the deck is $\Delta\mathbf{P} = \mathbf{AE\alpha\Delta T}$. By applying one the shakedown requirements, $\mathbf{K_uK_l} = 1$, the maximum shakedown force in the deck, $\mathbf{P_{sh}}$, and maximum abutment displacement, δ_{ult}, can then be scaled from the interaction diagram of Figure 2.

(ii) **Stiff deck**; large $\mathbf{k_b}$. For a stiff bridge deck, the upper bound $\Delta\sigma_u^*$ evaluated by the formula in (i) above is larger than the maximum permissible stress defined by $(\mathbf{K_p} - \mathbf{K_a})$. This implies that the actual residual modulus, $\mathbf{E_g} \neq \infty$, of the granular backfill *at shakedown* should be determined and the corresponding fluctuating stress $\Delta\sigma^*$ (see Figure 3) should remain within the stress limits defined by $\mathbf{K_p}$ and $\mathbf{K_a}$ for a safe solution to exist. Otherwise, failure of the embankment will occur.

Figure 3 represents an interaction diagram for a *typical* highway bridge deck (stiff deck) and the granular backfill. The dimensions for the bridge are: length 100m, sectional area of the concrete deck per unit width $0.5m^2$ and abutment height 6m.

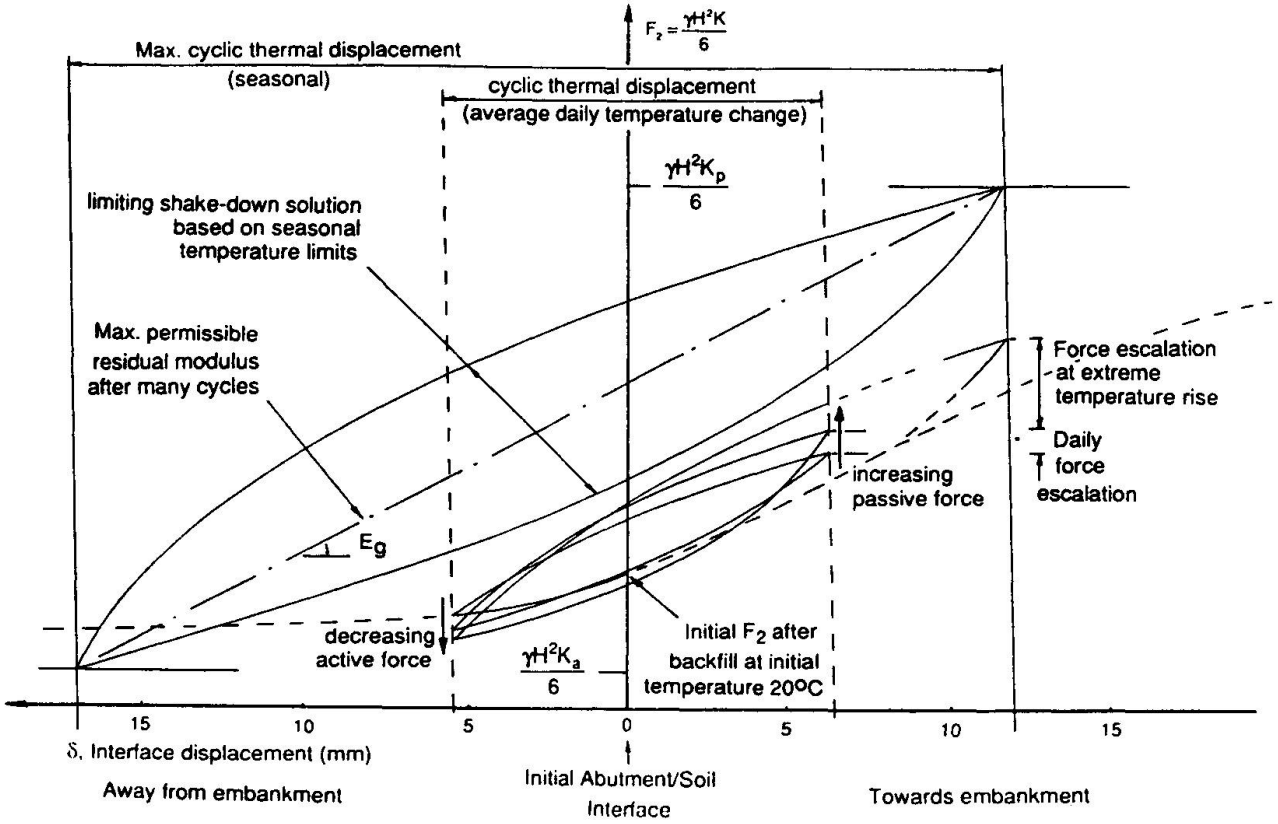

Figure 3. A Soil/Structure Interaction Diagram representing a typical highway concrete bridge (Stiff deck)

5. SHAKE-DOWN STATE FOR STIFF DECK

As shown in Figure 3, for a *typical* stiff bridge deck, the soil/structure interaction mechanism is strain-driven. Concerning the stability of the embankment, the shortening of the bridge deck due to the soil pressure is negligible. For a *Shake-down* solution to exist, the fluctuating horizontal soil stress at the toe of the wall, $\Delta\sigma_u^*$, should be less than the maximum permissible stress defined by $(K_p - K_a)$. It is then dependent on the residual soil modulus (variable with abutment height, **H**)and the fluatating soil/structure interface movement $\Delta\delta$ (variable with length of deck, **L**). Figure 4 represents the limiting relationship between the residual soil modulus coefficient **N** and the deck length **L**, with the wall height **H** for a temperature variation of 48°C. The residual modulus coefficient **N** increases with number of strain cycles. For sand, E_g has been found experimentally [1] in the range of 550 (15 cycles of 0.1% fluctuating strain) to 900 (100 cycles of 0.08% fluctuating strain). The actual movements that take place daily in most times of the year are always less than theoretically predicted. As shown in Figure 3, the number of cycles required to escalate the soil pressure by small daily movements is expected to be substantial. Althought the seasonal or extreme variations may give a more significant rise of soil pressure, the number of extreme cycles in the life time of the bridge will be limited.

6. CONCLUSION

6.1 A soil/structure interaction diagram relating the stiffness dimensions of an integral bridge to the soil preperties of embankment is presented. The composite behaviour is analysed as an elastic-plastic shakedown problem. Axial deck stiffness is the dominant feature in dividing the problem in two classes : *stiff* deck and *soft* deck.

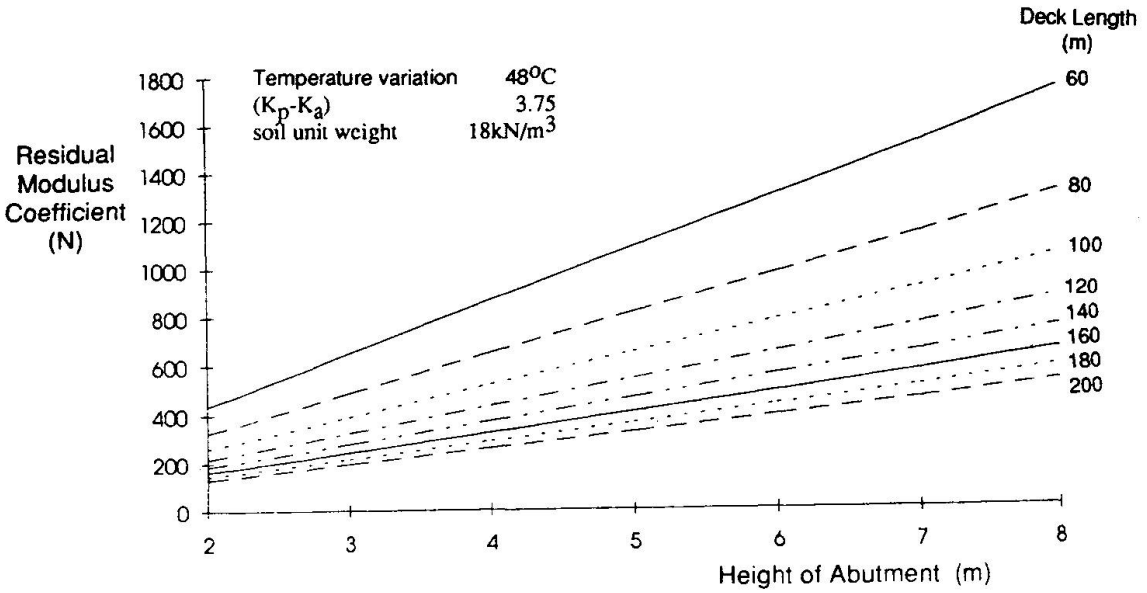

Figure 4. Maximum allowed residual soil modulus coefficient **N** for the deck length **L** and abutment height **H**.

6.2 Figure 2 shows that, an increase in deck length, **L**, increases the free thermal expansion $L\alpha\Delta T$ but reduces the axial stiffness, $k_b = 2AE/L$. Therefore, for the soft deck case, the maximum fluctuating stress in the granular backfill is independent of **L**, although the rate of approaching the shake-down state will be slower for larger **L**. However, due to the possible relatively higher interface displacement away from the soil, significant settlement in the region approaching the bridge deck may cause cracks at road surface.

6.3 Most bridge decks are classified as *stiff*. When the residual modulus of the granular material at shakedown predicts a failure, the bridge designer should consider either modifying the soil properties (E_g) by ground improvements or reducing the axial stiffness of the deck. Another alternative is to span the carriageway over the failure region by a run-on slab.

6.4 Further investigation is required to understand the combined effect of the number of strain cycles and their magnitudes to the ultimate residual soil modulus coefficient **N** and the rate of approaching this value.

6.5 Although the initial temperature and soil pressure during the completion of the bridge will not affect the ultimate shake-down stress imposed on the bridge deck, the ultimate soil/structure interface displacement and the volumetic change of the granular backfill are dependent on them and may cause unacceptable settlement of the embankment. Excessive initial compaction on granular backfill will either reduce the number of strain cycles required to reach the shake-down state or cause dilating failure to the embankment.

6.6 Although the problem of expansion joints has transferred from the bridge to the approaches, it is considered both (a) cheaper to repair damage to the junction between run-on slab and the carriageway and (b) easier to restore highway construction at grade.

REFERENCE

1. ENGLAND G.L., The Performance and Behaviour of Biological Filter Walls as affected by Cyclical Temperature Changes. Serviceability of Earth Retaining Structures, ASCE Geotechnical Special Publication No. 42, 1994, pp57-76.

Concrete Specifications for the Øresund Link

Spécifications du béton pour la liaison d'Øresund

Beschreibung der Betonsorten für die Øresund-Verbindung

Carsten HENRIKSEN
Engineer
RH&H Consult A/S
Copenhagen, Denmark

Laust LADEFOGED
Civil Engineer
A/S Øresundsforbindelsen
Copenhagen, Denmark

Niels THAULOW
Engineer
G.M. Idorn Consult A/S
Copenhagen, Denmark

SUMMARY

The construction of the Øresund Link between Denmark and Sweden involves, in addition to the sea crossing, several land-based concrete structures (bridges, tunnels etc.). These structures involve costs of approx. 800 million USD. A service life 100 years has been specified for these structures. To avoid that the individual consulting engineers spend unnecessary time and money in order to develop improved concrete specifications, the Owner has produced a guideline for the selection of concrete. The technical background of the specifications is described.

RÉSUMÉ

Outre la traversée proprement dite, la liaison d'Øresund entre le Danemark et la Suède comprend plusieurs constructions en béton tels que ponts, tunnels, etc. Ces constructions coûteront environ 800 million USD. La durée de vie de ces constructions a été spécifiée à 100 ans. Afin d'éviter que les ingénieurs conseils ne perdent du temps et de l'argent à développer des spécifications améliorées pour le béton, le maître de l'ouvrage a élaboré une directive pour la sélection du béton. Une description de la base technique des spécifications est donnée.

ZUSAMMENFASSUNG

Der Bau der Øresund-Verbindung zwischen Dänemark und Schweden umfasst neben der Verbindung von Küste zu Küste auch mehrere Festland-Betonkonstruktionen, wie z.B. Brücken, Tunnels, usw. Diese Konstruktionen sind mit Baukosten in Höhe von USD 800 Mio. verbunden und sind für eine Nutzungsdauer von 100 Jahren ausgelegt. Damit die beratenden Ingenieure keine unnötige Zeit für die Entwicklung von verbesserten Beton-sorten verbringen, hat der Bauherr, eine Anweisung zur Wahl der Betonsorte erarbeitet. Es wird der technische Hintergrund der Betonbeschreibung erläutert.

1. BACKGROUND FOR THE SELECTION OF THE CONCRETE TYPE/MIX DESIGN

The Øresund on-shore works on the Danish side comprise primarily of traditional bridge structures. There is extensive experience with design and execution of such bridge structures in Denmark, in accordance with the Danish Road Directorate's General Specification (AAB). Experience gained over a period of 50 years has shown that design and execution in accordance with these specifications generally results in sound and durable bridge structures. However, for certain severely exposed structural elements, experience shows considerably reduced durability when compared with the rest of the structure. The reason for reduced durability is usually design and/or execution errors which lead to unforeseen rapid development of damage by corrosion, frost and/or alkali silica reactions.

Based on this the concrete was to be selected according to the following overall requirements:

1) The choice of the concrete must be made in consideration of minimizing the risk of execution problems when placing the concrete.
2) The choice of the concrete mix-design, especially the water-cement ratio and the inclusion of additives, should secure a concrete with optimum workability and hence a satisfactory quality of the works.

Consequently, the specifications must reflect a number of individual considerations by the individual consulting engineer in order to achieve the optimum design and to ensure that the requirements can be handled later by both the contractor and the supervision.

2. SERVICE LIFE CALCULATIONS

2.1 Technical background

As stated in section 1 experience has shown that earlier standard specifications have to be tightened.

In order not to specify unrealistic demands or demands based on only assumptions it was decided to perform service life calculations.

The background for the service life calculations was an investigation made by the Danish Road Directorate in 1990 [2] to evaluate the cause and extent of the found damage to concrete bridges of the Danish highway network.

2.2 Specification of service life

The service life of a structure may be defined as one of four different time periods illustrated at figure 1.

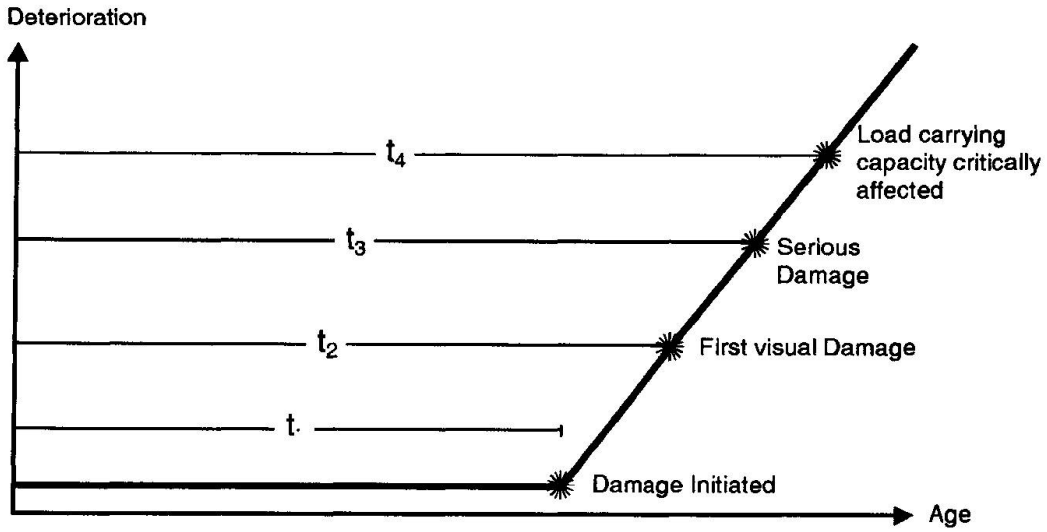

Figure 1: The figure illustrates the deterioration of concrete as a function of time.

Time periods t_2 and t_3 apply to this project and are defined in the following.

The requirement for the operation period for the structures, t_3, is a minimum of 100 years.

The requirement for the period t_2 is a minimum of 50 years. In this period the concrete must remain without damage and must be maintenance free except for maintenance of measures to extend the service life, e.g. a membrane on a bridge deck. Minor concrete repairs will be accepted after 50 years.

2.3 Calculation of service life, choise of environmental class

Corrosion caused by chloride ingress is considered to be the prime deterioration mechanism. Alkali silica reactions and freeze/thaw damage are other deterioration mechanisms. However there is extensive experience how to prevent them. So they are not considered to be problematic.

The service life of a concrete structure placed in chloride-contaminated environment can be calculated using Fick's 2nd law, as shown in figure 2. The values of surface chloride concentration C_s (0,1% and 0,2% mass of dry concrete) are based on the experience described in section 2.1 and [2]. The used values of the diffusion coefficient D are calculated from the formula: $D = (w/c)^5 \cdot 5000$. The calculation of D from this formula is in accordance with experimentally found values of D [2] for w/c ratios 0,45. The critical chloride content C_{cr} is estimated to 0,05% mass of dry concrete [2].

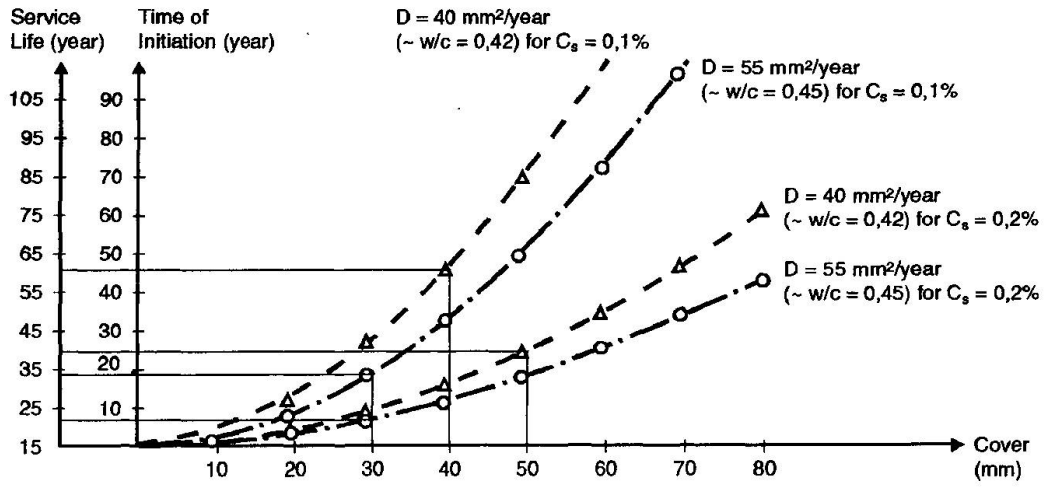

Figure 2 Theoretical time of initiation (t_1) and service life (t_2) as a function of D (diffusion coefficient) and cover for C_S = 0,2% and C_{cr} = 0,05%.

As a result of the calculations it was decided to use a w/c ratio of 0,42 (exist. requirements: 0,45) and a cover of 50 mm (exist. requirements: 30 mm) for structures in highly aggressive environment (C_s = 0,2%). A cover of 70 mm was specified for columns in sea-water, where C_s is estimated to 0,5%. For structures in a less aggressive environment (0,1%) a w/c ratio of 0,45 and a cover of 40 mm was required.

The decided parameters of 0,42 w/c ratio and 50 mm cover are seen to be theoretical insufficient to meet the requirement of 50 years of service life, before the first repairs can be accepted. However, a w/c ratio of 0,42 is within the limits of the concrete requirements that positively will meet the demand for a workable concrete to be cast without problems with a cover of 50 mm. Furthermore the requirement for sufficient drainage of traffic lanes will tend to place the structure in a less aggressive environment than the highly aggressive environment foreseen.

So the sound engineering judgement takes priority over the theoretical calculations based on which only even more tightened requirements should have been chosen with the consequence of increasing the risk of execution errors.

2.4 Accuracy

The evaluation of service life discussed above is, to a large extent, based on diffusion models from the laboratory and on parameter values which in practice are uncertain. Concerning the diffusion model used, experience has shown that values measured in practice are close to the theoretically calculated curve. However, the data is limited since it is based either on laboratory experiments or on data collected from existing structures of approximately same age (20-30 years). The general validity of the model for use in long term forecasts is there-

fore not demonstrated in practice. However, at the moment it is the only model which can be used in evaluation of service life.

Consequently, use of the model is acceptable provided due consideration is given to the uncertainties mentioned and that the model and the results are used only as a general guideline for the choice of concrete cover and w/c ratio respectively.

The calculated service life is considered to be on the safe side since the calculations do not take positive effects known from laboratory experiments into account.

3. MEASURES TO PROLONGE THE SERVICE LIFE

It is important to ensure that all elements of a completed structure achieve the same service life. It is therefore important to evaluate the future needs of repair and maintenance related to each structure. It may so be relevant to evaluate (technically and economically) the need for measures to prolonge the service life in order to avoid repeated repairs of the concrete as shown in the following example.

EXAMPLE:

In order to avoid repairs to columns in year 50 the recommendation could be the use of stirrups and main reinforcement of stainless steel. The extra cost of using stainless steel is per column about 1,000.- US $.

If only stainless steel stirrups are used the extra cost per column is about 110.- US $.

The cost of concrete repairs is 4,000.- US $ in 50 years and 8,000.- US $ in 75 years respectively.

The comparison between costs (in US $) is shown below:

Year	Mild steel	Stainless steel	Stainless stirrups
0		1,000	110
50	4,000		
75			8,000
Net present value*	600	1,000	550

* Discount rate 4%

From the example it is seen that an investment in stainless steel main reinforcement is not beneficial, but the use of stainless steel stirrups should be considered.

4. FINAL REMARKS

At the present time and with the present limited understanding of concrete technology the observed durability problems with some structures, dominate any discussion concerning concrete as a building material.

As a consequence, this might lead in the future to unrealistic requirements for concrete as the limited laboratory based experience, appears to call for tightening of the specifications. Especially even tighter requirements for the w/c ratio and the use of pozzolans to arrest chloride penetration has to be carefully considered. This is due to the fact that a reduction of the w/c ratio has resulted in an increased risk of execution problems which eliminates the theoretical benefits of a reduction in w/c ratio.

The evaluation of the choice of the concrete for the Øresund land-based structures has however, revealed that only minor changes to the existing requirements are needed to obtain remarkable benefits regarding prolongation of the expected service life without involving unacceptably high costs.

This is of course a prediction which can only be confirmed over time. The practical experience of 25 years of bridge maintenance in Denmark however supports the expectations.

With regards to the proposed concrete the experiences accumulated up till now on the Øresund Project with the use of the concrete show that it is workable and can be cast without problems and risk of honeycombs, cracks etc. The stress calculations which have been performed to avoid cracks due to temperature induced stresses and shrinkage can be problematic and have to be handle with care and a good understanding of the theoretical basis.

The results of the temperature/stress calculations have thus far proved to be realistic.

LIST OF REFERENCE:

[1] Guidelines for selection of concrete for Øresund On-shore works. A/S Øresundsforbindelsen 1992 and 1994.

[2] Chloride-induced Corrosion,
(The Danish Road Directorate, October 1991)

Filtration Stability of Cement Grouts for Injection of Concrete Structures

Stabilité au filtrage du mortier de ciment en vue de son injection dans les constructions en béton

Filtrierstabilität von Zementmörtel für die Injektion von Betonkonstruktionen

Per HANSSON
Senior Engineer
Vattenfall Utveckling AB
Älvkarleby, Sweden

SUMMARY

The most important property of a cement grout for injection, in terms of penetrability, is the filtration stability. A newly developed test method for measuring the filtration stability of cement grouts is presented. Results from the method, and related methods, are compared to different grouting situations simulated in the laboratory. The results show that it is possible to predict the penetrability of a grout by using this test method.

RÉSUMÉ

La propriété la plus importante d'un mortier de ciment pour injection, en termes de pénétrabilité, est la stabilité au filtrage. Une méthode d'essai développée récemment pour mesurer la stabilité au filtrage est présentée. Les résultats de cette méthode et de méthodes similaires sont comparés à différentes conditions d'injection simulées en laboratoire. Les résultats démontrent qu'il est possible de prévoir la faculté de pénétration d'un mortier pour injection à partir de cette méthode.

ZUSAMMENFASSUNG

Die wichtigste Eigenschaft eines Einpressmörtels ist, hinsichtlich der Erzielung einer guten Eindringfähigkeit, die Filtrierstabilität. Ein neuentwickeltes Prüfverfahren für das Messen der Filtrierstabilität von Zementmörtel wird präsentiert. Die Resultate dieses und ähnlicher Verfahren werden mit verschiedenen im Labor simulierten einpressähnlichen Situationen verglichen. Die Ergebnisse zeigen, dass die Eindringfähigkeit eines Einpress-mörtels mit Hilfe des präsentierten Prüfverfahrens vorausgesagt werden kann.

1. INTRODUCTION

To obtain a durable and high strength grouting of concrete subjected to cracking and leaching, it is necessary for the grout to be stable in terms of bleeding and sedimentation. Furthermore the w/c-ratio should be kept as low as possible to avoid a porous cement paste. Extensive laboratory tests on stable, low w/c-ratio, injection grouts shows that the most significant limitation to their penetrability is the tendency of cement grains to agglomerate into an impermeable filter cake. Grout refusal can also occur due to inappropriate rheology of the grout. Restrictions in penetrability due to the latter can in most cases be eliminated using superplasticizer. The ability of a grout to pass constrictions of the flow path without clogging can be designated filtration stability.

Development of a filter cake can occur at a ratio of channel width to maximum particle diameter (D_c/d_p) of as much as ten. If the grout is insufficiently dispersed, agglomerates or flocs of cement grains can certainly clog the channel due to excessive diameter of the agglomerate. However, even if the cement grains initially are dispersed, they can agglomerate if the grout is exposed to filtration situations such as entrances to cracks, fine cracks or porous material.

The filtration stability of a grout is generally improved by the following actions: increasing w/c-ratio, adding superplasticizer (SP), ensuring adequate dispersion and using a finer ground cement. Corresponding impairment is caused e.g. by: adding accelerating agent or by adding stabilizing agent. Exceptions to these rules of thumb occur.

The models available for assessing the risk of filtration are the D_{15}/d_{85} - ratio for soil injection and the groutability ratio (D_c/d_p) for crack injection. These models may be valid using thin grouts without additives but when dealing with stable grouts with additives they have proven to be inadequate. There is some relation between maximum grain size and penetrability but the exceptions are too common to rely on maximum particle size as a classification parameter for injection grouts. Since it is uncertain how much parameters such as chemistry and particle size distribution influence the filtration stability, it is convenient to determine it by measuring on the ready mixed grout.

2. MEASURING FILTRATION STABILITY

A new test method for evaluation of filtration stability has been developed with the aim that it would be suited both for laboratory work and site measurements. An outline of the equipment is shown in fig. 1. The grout is drawn into the device after which it is pressed out into a measuring vessel. The amount that has passed the filter is measured and registered as a qualitative measure of filtration stability. The filter consists of a woven metal wire cloth with a mesh width of 32, 45, 75, 100 or 125 µm depending on the expected performance of the grout to be tested.

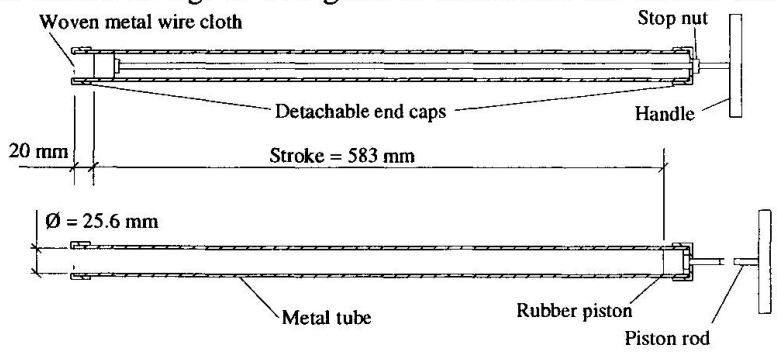

Fig. 1 Filtration device.

The filtration device works according to the cake filtration principle that is the filtration mechanism in effect e.g. at entrances to cracks. Other filtration mechanisms such as deep bed filtration and

physiochemical surface attraction applies to some of the laboratory situations presented in this paper.

Since cake filtration is the most basic principle it would be convenient if it was possible to correlate the different filtration mechanisms. Consequently it would be possible to reliably predict the penetrability of a grout by means of the simple filtration device test. The filtration device is considerably easier to handle and keep clean than for instance a sand column equipment.

3. LABORATORY TESTS

The scope of the laboratory tests presented in this paper is to find out whether the penetrability of a grout can be predicted with the filtration device. The tests are preliminary in the manner that the test methods may be improved during the continuance of the project.

All the filtration tests are carried out as single tests. On basis of repeated tests on different grouts, the repeatability of the filtration device test is estimated to be better than ± 10 % by a satisfactory margin.

Since the results from a filtration test is a qualitative measure for filtration stability, the two terms are used interchangeably.

3.1. Concrete crack grouting.

In order to evaluate the influence of filtration stability on the result of grouting crack in concrete studies a number of pilot tests have been carried out. A concrete crack was prepared by splitting a concrete specimen of the size 70 × 70 × 50 cm and drilling a centric grout hole. An outline of the specimen is shown in fig. 2. Before grouting the two halves was wetted and placed in a frame and forced together with a force three times the lifting force induced by the grouting pressure of 50 kPa. Immediately before grouting, the hydraulic crack width was assessed by water loss measurement and calculation assuming laminar flow.

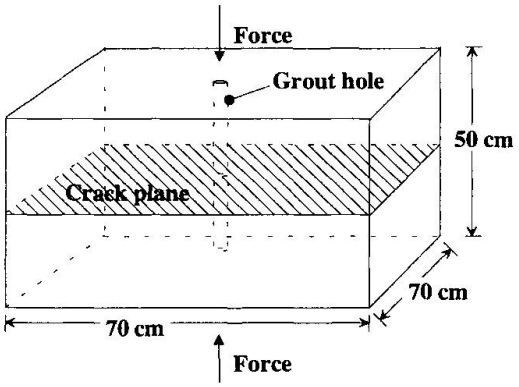

Fig.2 Concrete crack grouting specimen.

All the grouts were based on ultrafine Portland cement with d_{95} = 16 µm. The specific area of this cement determined by the BET-method is 1450 m²/kg. The SP was of an ordinary melamine type. All the grout mixes were designed to have as close to Newtonian rheological properties as possible in order to study the filtration effect separately.

Filtration device measurements (V_f) were compared to the time elapsed between start of grouting and grout refusal (grouting time, t_g) normalized to the hydraulic crack width (d_h). The normalization is made to compensate for the random variation in crack width that occurred due to the test equipment. The exponent on d_h is obtained by best fit calculations maximizing the correlation coefficient (r). Furthermore, V_f was compared to results from a modified filtration device with a sharp crack entrance as filtration site instead of a wire mesh. The amount of grout that passed the sharp entrance is denoted V_e. The test results are shown in table 1. The relation between filtration stability and normalized grouting time is shown in fig. 3.

ID no	1	2	3	4	5
w/c-ratio	0.6	0.7	0.8	0.9	1
SP [%C]	4	4	4	4	4
t_g [s]	990	990	1500	2220	6000
d_h [mm]	0.32	0.25	0.28	0.29	0.35
V_f [ml]	2	50	95	150	170
$t_g / d_h^{3.65} \times 10^{-5}$	0.64	1.57	1.57	2.05	2.78
V_e [ml]	17.3	25.3	29.9	35.0	78.0

Table 1 Results from concrete crack grouting.

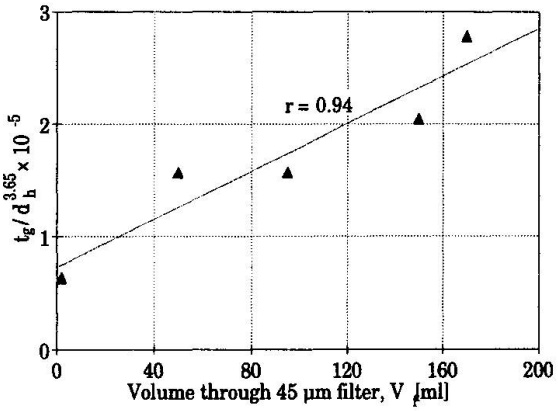

Fig. 3 Normalized grouting time vs. filtration stability.

Bearing in mind that the analysis is based on few tests, a clear tendency of correlation between filtration device measurements and grout take can be seen. It also seems likely that the crack width affects the result more than to the power of one since the best fit calculation resulted in an exponent of 3.65.

Fig. 4 shows the two different filtration devices compared to each other. The relationship in fig. 4 should be linear and some uncertainties in determining the V_e value of test no 5 brings that a linear relationship is possible. The filtration stability measured with the filtration device has proven to be strongly dependant on the w/c-ratio, fig. 5 shows this relationship.

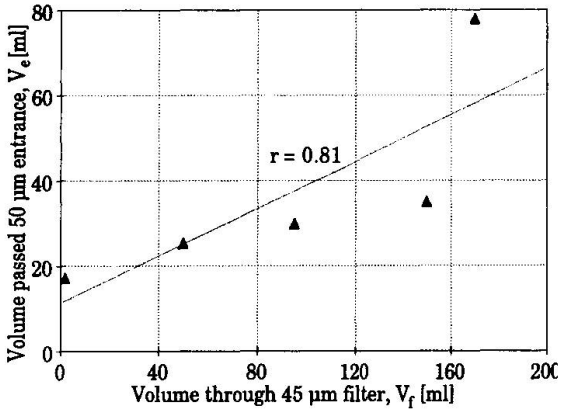

Fig. 4 Comparison between filtration devices.

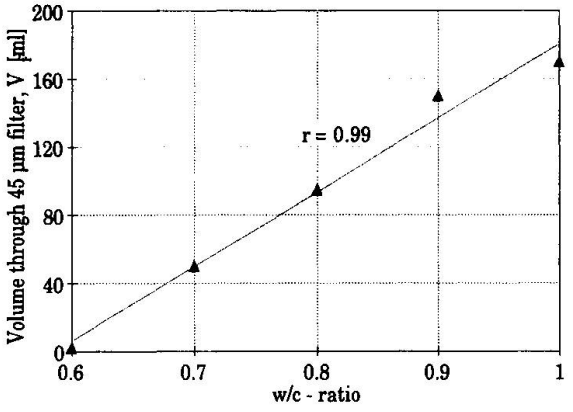

Fig. 5 Relationship between V_e and w/c-ratio

3.2. Sand column test

During the prequalification for a large tunnel project all the grout mixes were tested in laboratory [1]. Fig 6 shows the relationship between filtration stability and penetration of a sand column. The filtration stability is measured by a filtration device with a wire mesh sieve with a diameter of 90 mm and a sieve width of 125 µm. The filter is fed by a pressure tank with an air pressure of 50 kPa. The sand column test was carried out according to a pending CEN standard. The sand had an even particle size distribution between 0.63 and 1.25 mm. The feed pressure was 75 kPa.

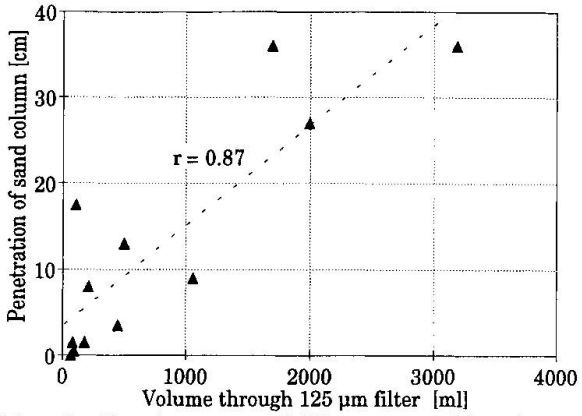

Fig. 6 Sand penetrability vs. filtration stability

Considering that the tests were made on grouts based on nine different types of cement, different additives and dosages and with different rheological properties, there is a tolerable correlation. Accordingly there is a tendency that sand injection results can be predicted by a filtration test.

3.3. Grouting of a smooth crack

An artificial smooth crack was made out of a ground steel plate with a glass plate tightly fastened on top. A constant aperture of 0.2 mm was accomplished by shims between the plates. The width of the channel was 50 mm and the length 1 m. The entrance to the aperture was rounded at a radius of 10 mm. The filtration device was the same as in previous section with the exception of the sieve that was a Fujiplate sintered filter with a sieve width of 150 µm. Both equipments were fed by a pressure tank with an air pressure of 50 kPa. The grouts were based on a Portland cement with d_{95} = 40 µm and a Blaine value of 600 m²/kg. The compositions of the grouts and the test results are shown in table 2 where volume through crack and volume through filter are designated V_{ac} and V_{f150} respectively.

w/c-ratio	SP [%C]	V_{f150} [ml]	V_{ac} [ml]
0.5	5	690	350
0.6	3	640	0
0.6	5	1180	650
0.7	1	430	1
0.7	3	570	120
0.7	5	1950	1400

Table 2 Test matrix and results from grouting of smooth crack.

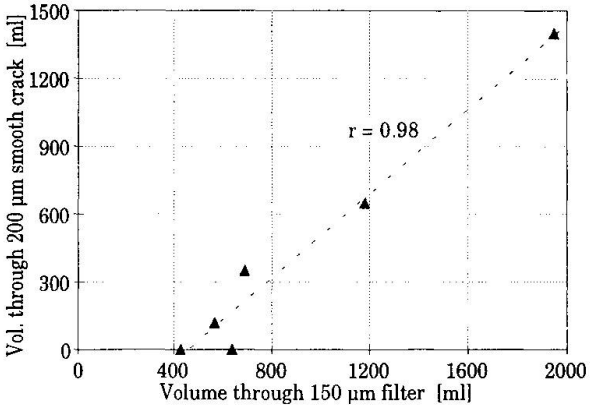

Fig. 7 Volume passed smooth crack vs. filtration stability

All the grout mixes were designed to have nearly Newtonian rheological properties. Fig 7 shows a comparison between volume of grout that passed the entire artificial crack and volume of grout through the filter.

3.4. Example of use - Dispersion time optimum

In order to establish an optimal dispersion effort using an Ultra-Turrax T25 dispersion tool, a series of laboratory tests was carried out. During the tests the dispersion time was varied in 15 seconds increments except an extreme value and the reference tests with superplasticizer (SP). The test sequence is described in [2].

The relation between dispersion time and amount passed the sieve of a 45 μm filtration device, that is a qualitative measure of filtration stability, is shown in fig. 8.

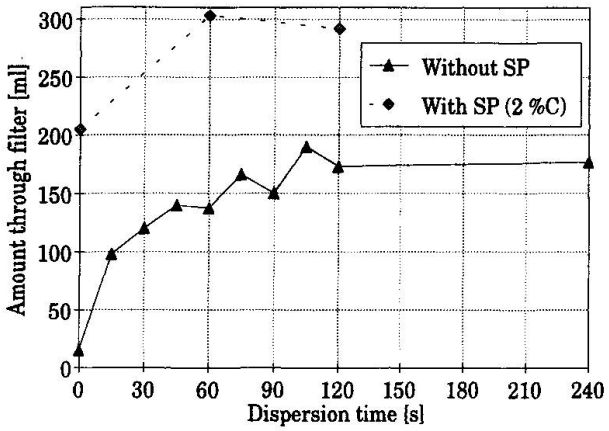

Fig. 8 Dispersion time versus filtration stability.

The effect of dispersion is clearly seen in fig. 8, as is the effect of the SP. However, the filtration stability does not increase much further after 90 s of dispersion why there is little reason to extend the dispersion time beyond that point.

This particular test is carried out in a small scale. However, the test procedure can very well be applied on production scale mixers.

4. CONCLUSIONS

The test results show that a relation between filtration test results and penetrability of cement grouts exists provided that the rheological properties of the grout is closely Newtonian. This regardless of the filtration mechanism that applies to the specific grouting situation. Furthermore there is a strong relationship between w/c-ratio and filtration stability.

Filtration tests can be used to evaluate the effectiveness of mixing as well as for assessing the performance of grout designs.

ACKNOWLEDGEMENTS

The research project dealt with in this paper is financed by ELFORSK AB - Swedish Electrical Utilities R & D Company. I also wish to thank Per-Erik Thorsell who carried out the main part of the laboratory tests.

REFERENCES

1. Hansson P. Injektering i Hallandsåsen - Utvalda tester. Proceedings. Bergsprängningskommitténs diskussionsmöte - 94. Stockholm 1994. (in Swedish).
2. Hansson P. Provningsmetoder för cementbaserade injekteringsmedel och deras användning. Proceedings. Vann og frostsikring av trafiktunneller. Trondheim 1995. (in Swedish).

Polymer-Modified Portland Cement Concrete at Temperatures up to 150°C

Béton modifié par polymères à des températures jusqu'à 150°C

Polymermodifizierter portlandzementgebundener Beton bei Temperaturen bis 150°C

Violeta BOKAN BOSILJKOV
Assistant
University of Ljubljana
Ljubljana, Slovenia

Violeta Bokan Bosiljkov, born in 1964, received her civil engineering degree in 1988, finished her M.Sc. thesis in 1991 at the University of Ljubljana. For six years she has been involved in research of ordinary and modified concrete.

Franc SAJE
Assistant Professor
University of Ljubljana
Ljubljana, Slovenia

Franc Saje, born in 1941, received his civil engineering degree in 1965, finished his Ph.D. thesis in 1990 at the University of Ljubljana.

Vlatko BOSILJKOV
Research Assistant
University of Ljubljana
Ljubljana, Slovenia

Vlatko Bosiljkov, born in 1964, received his civil engineering degree in 1991 at the University of Belgrade, Faculty of Civil Engineering.

SUMMARY

The flexural load-deflection curves of a styrene-acrylic copolymer modified concrete types, obtained three-point bending test carried out at temperatures between 20 and 150°C, are presented in the paper. The compressive stress-strain relationships for these modified concrete types are also given, but only at 20°C.

RÉSUMÉ

Le rapport examine la corrélation entre la charge et les déformations par flexion du béton modifié par le copolymère styrène-acrylique, dans un essai de flexion effectué à des températures entre 20°C et 150°C. Il est aussi possible de constater une relation entre l'effort de compression et les déformations du même béton, observé à 20°C.

ZUSAMMENFASSUNG

Die Biegelast-Biegungs-Linien für styrol-acrylatmodifizierte Betone, die an Balken mit einer Einzellast in der Mitte bestimmt wurden, sind bei Prüftemperaturen zwischen 20 und 150°C gegeben. Ebenso sind für dieselben Betone die Druckspannungsdehnungs-Linien dargestellt, in diesem Fall aber nur bei 20°C.

1. INTRODUCTION

New demands to improve the mechanical properties and durability of concrete in the case of chemical and/or physical influences are more and more frequent. One way to comply with these demands is represented by modifying structural concrete by the help of artificial materials. It is assumed that thermoplastic polymers used for modifications of portland cement concrete form a spatial network within inorganic binder [Konietzko A., 1988]. The polymer network plays an important role when loads are transmitted in the concrete in a complex manner. The thermal conditions, which prevail, affect significantly the loadbearing behavior of polymer-modified concrete types. At temperatures below the polymeric glass transition region, the addition of polymer results in a noticeable increase in tensile strength and strain capacity of concrete. On the other hand, at temperatures above the polymeric glass transition region the softened plastic leads to a considerable increase in ductility, and at the same time causes a reduction in strength.

The glass transition temperature (Tg) of styrene-acrylate copolymer which was used for modification equals about 19°C. The aim of our investigations was to establish a relationship between strength and deformation characteristics of modified concrete at temperatures above the polymeric Tg.

2. EXPERIMENTAL PROGRAMME

2.1 Details of mixes

Details of mixes made for the experimental study are given in Table 1. The constant quantity of portland cement in the amount of 400 kg per unit volume of concrete mix was used. For polymer-cement ratio (weight of polymer solids with respect to weight of cement, denotation P/C) ranging between 0.0 and 0.2, the water-cement ratio between 0.55 and 0.32 was adjusted in order to attain a fairly constant workability throughout. At polymer-cement ratio 0.1, 0.15 and 0.2 also the antifoaming agent in the amount of 0.5, 0.5 and 1.0 wt%, respectively, was added in order to attain the same porosity of all concrete mixes.

Mix	W/C	P/C	Vebe time (sec)	Vol. of Air (%)
FG01	0.55	0.00	2.0	2.5
FG03	0.37	0.10	4.0	2.6
FG04	0.34	0.15	3.5	2.6
FG05	0.32	0.20	3.5	2.8

Table 1 Details of mixes

Time (days)	Flexural strength (MPa)	Compressive strength (MPa)
3	5.5	31.8
7	6.8	38.1
28	7.7	47.8

Table 2 Strengths of standard cement mortar

2.2 Materials

Used were portland cement type PC 45B corresponding to the former Yugoslav Codes (JUS), river sand, and 8 mm maximum size gravel coarse aggregate. Flexural and compressive strengths determined on 4x4x16 cm standard cement mortar prisms according to JUS B.C8.022 are given in Table 2. As a modifier the water anion copolymer dispersion from ester acrylic acid and styrol without added plasticizer was used. It has a mean particle size of about 0.1μm, pH value between 7.0 in 8.0 and minimum temperature of film formation at about 30°C. The polymeric film formed from dispersion has a glass transition temperature at about 19°C, tensile strength between 7 and 10 MPa and strain at tensile strength between 500 and 800%.

2.3 Casting, curing and testing

From each mix, 100x100x360 mm prisms and 80x80x360 mm prisms were cast in steel moulds. The specimens were demoulded after 24 hours and were for the first 7 days cured in water at 20°C. Forthcoming curing took place under controlled ambient conditions at a temperature of 20°C and a humidity of 50%. Flexurally tested specimens at elevated temperatures were put into furnace with constant temperature which was equal to the forthcoming testing temperature 24 hours prior to testing. All the tests were carried out with specimens of 28 days age. For the tests a servo-hydraulic testing machine Instron type 1345 was used. The compressive stress-strain relationship was obtained by testing the 100x100x360 mm specimens under axial compression at laboratory conditions (about 20°C). The specimens were loaded by conducting the crosshead displacement of the testing machine with a velocity of 0.36 mm per minute. The measurements of the longitudinal strains were carried out using strain gauges. For each mix of concrete between 7 and 9 samples were tested. The flexural load-deflection curves were obtained at three point bending tests on 80x80x360 mm prisms. Since the aim was to get also the descending part of the flexural load-deflection curve, the testing samples were loaded by conducting the deflection of the sample with a velocity of 0.1 mm per minute, by the help of the extensometer. The flexural tests at a temperature of 20°C were carried out on all mixes, whereas at elevated temperatures (50, 75, 100 and 150°C) they were performed only on polymer-modified concrete mixes. In addition to above mentioned testing machine also the temperature chamber with a self-adaptive temperature controller and high temperature (water-cooled) extensometer of the same manufacturer as of the testing machine were used for testing at elevated temperatures. For each mix and each temperature 6 samples were tested.

3. RESULTS AND DISCUSSION

For each of both kinds of tests, for each concrete mix and temperature, the resulting curve was defined from the experimentally obtained curves by the help of

the neural network-like system with the estimation of conditional average [Grabec I., 1990]. This should make possible to avoid any a-priori assumptions regarding the relationship between the empirical data, and to permit the formation of any possible nonlinear relationship that, in the statistical sense, is best adapted to the empirical data.

3.1 Compressive stress-strain relationship

Figure 1 presents the compressive stress-strain curves for concrete modified with varying amounts of polymer. Due to the plastification effect of the added polymer and the demands for the same workability the maximum compressive stress of the modified concrete at the polymer-cement ratio 0.1 is increased for about 8 MPa, i.e. 23%. With further increase of the polymer-cement ratio, the maximum compressive stress of the modified concrete decreases. At the polymer-cement ratio 0.15 it is not even 6% higher than at the nonmodified concrete. Despite the insignificant difference in maximum stresses, the strain at maximum stress is about 20% larger than at the control mix. At the polymer cement ratio 0.2 the maximum stress is even about 12% lower than at the nonmodified concrete, but the strain at maximum stress is more than 65% larger. As compared to the other three mixes the ability to absorb energy in plastic range is at the polymer-cement ratio 0.2 also significantly increased.

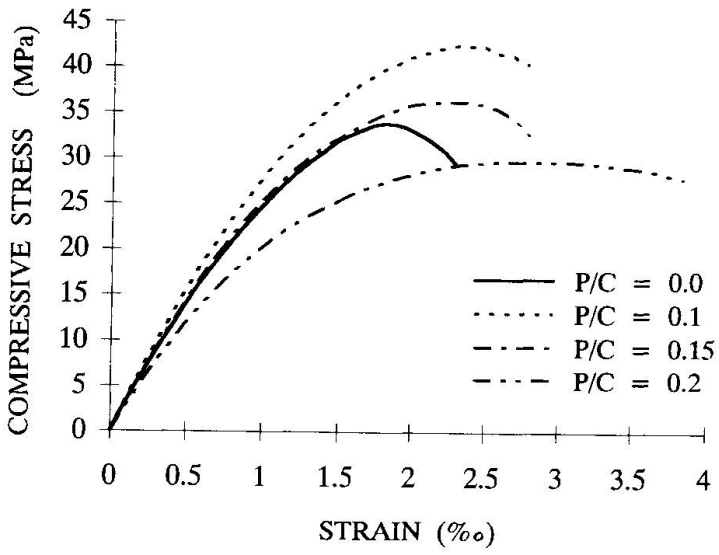

Fig. 1 Compressive stress-strains curves

3.2 Flexural load-deflection relationship at normal and elevated temperatures

For a particular polymer-cement ratio the flexural load-deflection curves, obtained at normal end elevated temperatures, are given in Figures 2 - 5. On each of those figures, comparison is given by the curve that show behavior of nonmodified concrete obtained at 20°C.

The maximum flexural load of modified concrete with the polymer-cement ratio 0.1 obtained at 20°C is about 120% higher than at control mix (Figure 2). The descending part of the flexural load-deflection curve was obtained only after instantaneous decrease of maximum load to 20% of its value. The maximum flexural

load at 50°C equals 7 kN, which is about 30% lower than at 20°C, but also about 50% higher than at control mix. At temperatures 75, 100 and 150°C, there is almost no difference in diagrams, which represents flexural load-deflection relationship, i.e., until maximum flexural load equals about 5.6 kN. The difference is in descending part of the diagrams, where toughness of concrete at 150°C is about 35 and 80% higher then at 75 and 100°C, respectively.

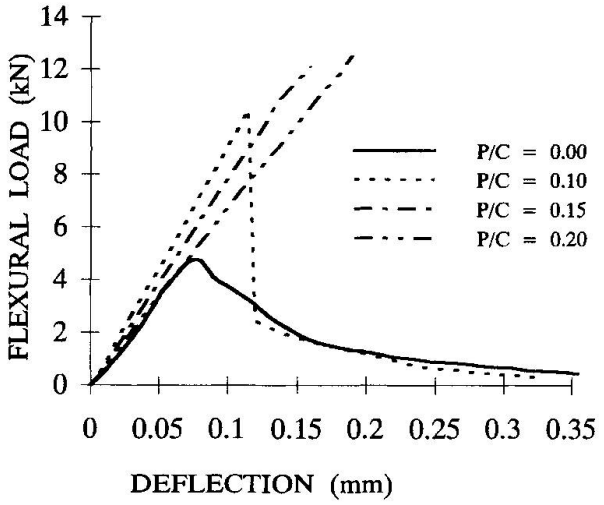

Fig. 2 Testing temperature 20°C

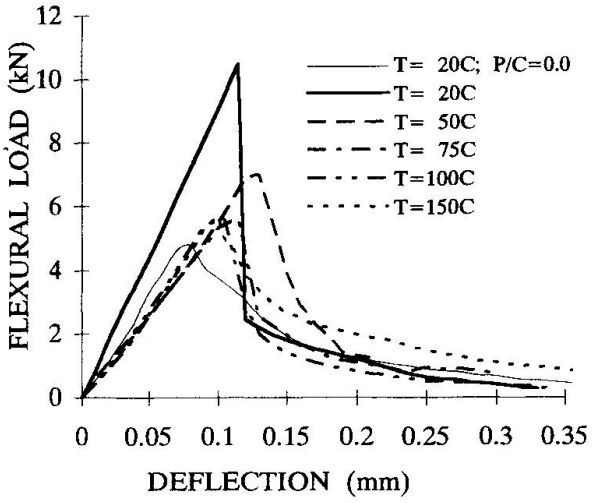

Fig. 3 Polymer-cement ratio 0.1

At the polymer-cement ratio 0.15 and normal temperature the maximum flexural load is 12 kN, which is about 150% higher than at control mix. Modulus of elasticity is lower than at the polymer-cement ratio 0.1, and the deflection at maximum load is thus increased. However, the maximum load is also the load of rupture. The reduction in strength at 50°C is about 60%

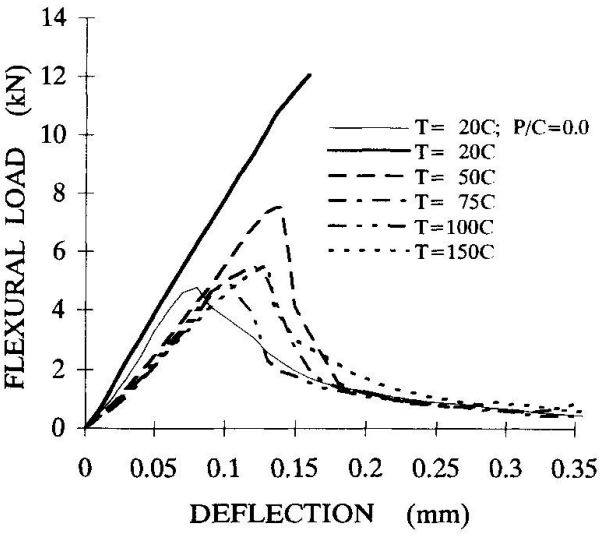

Fig. 4 Polymer-cement ratio 0.15

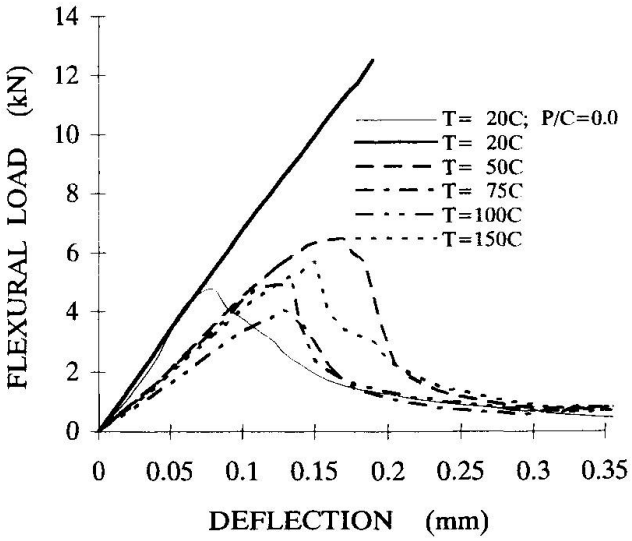

Fig. 5 Polymer-cement ratio 0.2

considering the strength at 20°C. Nevertheless, it is still about 60% higher than at nonmodified control mix. The ductility of modified concrete is also considerably increased. The maximum load of modified mix is at 75, 100 and 150°C almost the same or slightly higher than at control mix. The ability to absorb energy until the rupture is for the modified concrete at the above mentioned temperatures and for the nonmodified concrete highest at 150°C.

In the case of polymer-cement ratio 0.2 and a temperature of 20°C the maximum flexural load and its ability to absorb energy until the rupture are the highest of all. However, the rupture of material is brittle. At temperatures above the polymeric glass transition region the reduction in strength and at the same time the increase in ductility are enormous. The maximum flexural load at 50°C is only about 35% higher, at 75°C the same and at 100°C even about 20% smaller than at the control mix. At 150°C the maximum load is 20% and the ability to absorb energy about 30% higher than at the nonmodified concrete.

4. CONCLUSIONS

The results of tests carried out at temperatures above the polymeric glass transition region show considerable drop in flexural strengths of polymer modified concrete types, as compared to the strengths of modified concrete mixes at 20°C. On the other hand, adding between 10 and 20% of polymer by weight of cement, flexural strengths at 50°C are increased between 40 and 60%, as compared to the control mix which was tested only at 20°C. At the same time, the softened plastic leads to an important increase in concrete ductility. Maximal toughness pertains to the modified concrete with polymer-cement ratio 0.2 tested at 50°C. Only at 100°C and the polymer-cement ratio 0.2 the flexural strength is lower than at control mix, whereas at the polymer-cement ratio 0.15 and testing temperature 100°C is approximately equal to the flexural strength of control mix. Flexural strengths of other polymer-modified mixes tested at temperatures up to 150°C are up to 20% higher, and toughnesses pertaining to the above mentioned mixes are up to 30% higher, when compared to the control mix.

5. REFERENCES

1. GRABEC I., Modeling of natural phenomena by a self-organizing system. Proceedings of the ECPD NEUROCOMPUTING, Vol. 1, No. 1, 1990.
2. KONIETZKO A., Polymerspezifische Auswirkungen auf das Tragverhalten modifizierter zementgebundener Betone (PCC), Dissertation, 1988.

Methods of Treatment for Concrete Substrate Preparation

Méthodes de traitement du béton

Methoden der Betonuntergrundvorbehandlung

Volker KAUW
Civil Engineer
University of Technology
Aachen, Germany

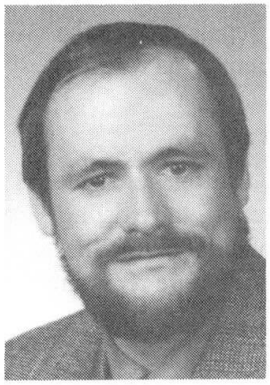

Volker Kauw, geboren 1962, studierte an der Rheinisch Westfälischen Technischen Hochschule Aachen Bauingenieurwesen. Wissenschaftlicher Angestellter am Institut für Baumaschinen und Baubetrieb der TH Aachen. Aufgabengebiet im Bereich Betoninstandsetzung.

Martin WERNER
Dr.-Ing.
Bausachverständiger
Aachen, Germany

Dr. Martin Werner, geboren 1958, studierte an der Rheinisch-Westfälischen Technischen Hochschule Aachen Bauingenieurwesen. 1991 Promotion über ein Verfahren für die Betoninstandsetzung. Freier Bausachverständiger.

SUMMARY

Different techniques can be used for concrete substrate preparation depending on the aim which has to be fulfilled. They can be subdivided into mechanical, thermal, and chemical techniques. All these different techniques have their special fields of application, advantages and disadvantages. They also differ in performance. The following article outlines the mechanisms of the main techniques for concrete substrate preparation as well as the advantages and disadvantages, the performance and costs of these techniques. These techniques are presented and the requirements for their application are given.

RÉSUMÉ

Il existe différentes techniques de traitement du béton. Le choix dépend des buts à atteindre. Il y a des procédés mécaniques, hydrodynamiques, thermiques et chimiques qui ont des domaines d'application particuliers et qui présentent des avantages et des désavantages. Leur efficacité est différente. L'article présente ces différentes techniques et leurs champs d'application.

ZUSAMMENFASSUNG

Es gibt eine Vielzahl unterschiedlicher Techniken zur Betonuntergrundvorbereitung. Die Auswahl richtet sich nach den zu erfüllenden Zielvorstellungen. Man unterscheidet mechanisch, hydrodynamisch, thermisch und chemisch arbeitende Verfahren. Alle diese Verfahren haben ihre speziellen Einsatzfelder sowie verfahrensspezifische Vor- und Nachteile. Sie unterscheiden sich auch in ihrer Leistungsfähigkeit. Der folgende Beitrag stellt die Wirkungsweise der gebräuchlichsten Techniken vor und geht auf deren Vor- und Nachteile sowie auf die Leistungsfähigkeiten ein. Einsatzfelder werden aufgezeigt.

1. INTRODUCTION

The preception of concrete as a building material has changed over the last decades, from concrete being viewed as a durable material requiring little maintenance, to the realisation that deterioration of concrete structures, such as concrete cancer, are serious problems requiring attention. The causes of concrete decay are manifold, ranging from errors in early design and detailing of the structure, to problems created during construction such as reinforcement being placed too close to the surface of the slab and finally environmental attack, such as chloride corrosion, which is a particulary significant problem in Germany. The imagery associated with concrete deterioration are now well known, rust appearing on the facade, cracking in the surface, shell shaped peeling and so on.

Repairing the deterioration of concrete buildings requires attention. Successful concrete repair needs to be carried out by experts from reliable companies experienced in the repair of concrete structures as repairing deterioration is usually more complex than constructing something new.

All methods of repair require the surface of the existing material to be prepared in order that the new material adheres successfully. Depending on the cause of the damage and the chosen method of repair, the existing surface will need to be treated by a combination of cleaning , roughening or removing material before the repair technique can be employed. The requirements to be fulfilled by the concrete surface before repairing measures can start are defined in [1] and [2].

2. CLEANING TECHNIQUES

Simply cleaning the existing surface may be sufficient if there is no structural damage to the existing concrete, for example, cleaning can be suitable preparation for the application of paint. Cleaning the surface does not remove any of the existing concrete from the structure, it only removes loose contamination such as layers of dirt, paint and coatings to an effective depth of 1 mm.

Conventional cleaning techniques include wire brushing by hand or machine, high pressure air blasting with oil-free air, water jetting, hot water jetting, steam jetting and treating the surface with chemical. High pressure water jetting is also effective in removing previous surface applications to concrete (Table 1).

3. METHODS FOR ROUGHENING

Techniques for roughening the surface of the concrete will also remove any loose or decayed concrete on the surface of the structure. The effective depth for roughening of the surface is approximately 3 mm, removing the cement skin. There are mechanical, hydrodynamical and thermal techniques available for treating the concrete surface.

One conventional mechanical technique is blasting the surface with solid agents. This can be done either dry or with the addition of a small amount of water against the dust. A vacuum system can also be adapted to remove the waste/blasting agent mixture from the process. The vacuum head is situated arround the blasting nozzle. A disadvatage of using an additional vacuum system is that the operator cannot observe the point where the blasting agent is hitting the concrete during the process and therefore the results are by the nature of the process approximate. The advantage of this method is that there is no dust appearing and disposal of the waste/blasting agent material is effective and the blasting agnet can be recycled and used again if desired. A better performance is achieved by using sand and water as the blasting agent. A problem can be the amount of

remains after blasting. The disposal of the water/abrasive mixture which also can be contaminated is always a problem.

The high-pressure water jet technique for roughening concrete is especially suitable for this purpose, using water pressures up to 250 MPa with a waterflow of up to 30 liter per minute. The waterjet is applied to the surface using a rotating nozzle. A high pressure water jet technique, combined with a vacuum system is in use and effective in removing waste material.

The flame treatment, used for removing dirt and surface applications is another popular technique. The maximum effective depth of this technique is 3 mm. Hand torches for vertical surface treatment and machine driven torches for horizontal surface treatment are in use. To use the technique a certain thickness of the concrete cover is needed to make sure that there will be no damage of the reinforcement. After using the flame technique, a mechanical treatment is required, such as wire brushing or blasting using steel balls as an abrasive (Table 1).

4. TECHNIQUES FOR CONCRETE REMOVAL

The field of concrete removal can be subdivided into planar removal and straight line removal or cutting. The removal depth can be varied depending on the requirement. Technuiques for concrete cutting include,
- chipping/caulking and sawing,
- high-pressure water jetting,
- high-pressure water jetting by use of additional abrasives.

Techniques for planar removal include,
- chipping/caulking, hammering, grinding and milling,
- high-pressure water jetting,
- high-pressure water jetting using additional abrasives.

Whilst flat peeling concrete it is essential to ensure that no additional damage is done to the surface and the structure other than what is desired. The stress of a jack hammer or miller on the surface may result in substructure cracking. Using any of these techniques requires a secondary treatment in order to adequately prepare the surface. This aftertreatment can be done by brushing machines, blasting with solid agents like sandblasting or water jetting. The risk of causing substructure damage is reduced considerably when hydrodemolition techniques are used for concrete removal. Hydrodemolition techniques treat the remaining material gentle. This principle was illustrated by SILFWERBRAND [3] when he compared different techniques for removing concrete.

Removing damaged concrete using the water jet technique has the advantage of only removing the concrete that has deteriorated, leaving the remaining material intact. Also the reinforcement remains intact. In addition, the surface of the structure after water jetting is ideal for the majority of repair techniques. Hydrodemolition techniques can be subdivided into two main machine types:
- systems working with a water pressure of 80 up to 120MPa using a waterflow of up to 300 litres per minute and
- systems working with a water pressure of up to 250MPa using a waterflow of max 30 litres per minute.

Advantages of the 80/120MPa systems are simplicity of construction, low maintenance and technical faults are not common. There are no special requirements concerning water quality and therefore filtered river water or recycled water from the water jetting process is acceptable. The disadvantage of this system is the high quantity of water required for the process and as a result, disposal of such a large quantity of water can be difficult considering that now water must be cleaned and recycled. A number of robotic water-jetting units, power guided systems are on the market which are able to remove 10 cm concrete surface in one go.

Regarding the problems with the wastewater, there are less problems by using the 250MPa systems. The maximum waterflow of these systems is 30 l/min. Therefore these systems are used for high rise structures where a huge amount of wastewater would be an additional problem. Any water running down the facade must be catched up and cleaned before it can be put into the sewage canal. It is also easy to handle a manual guided jet pistol on scaffolding. However, these machines are highly sophisticated and therefore require a lot more servicing than the 80/120MPa machines. The 250Mpa machines also require a high quality of the water. The water must be thoroughly clean without any impurities, in fact, cleaner than drinking water. Especially no suspended particles are allowed to be in the water. Typical uses for this system are cleaning and roughening of the surface using a rotating nozzle beam or removing concrete from reinforcing by using a hand manipulated jet pistol. This also removes the rust from the steel. This system can also be used to cut concrete. Table 1 is an overview of the different techniques available for concrete removal, roughening and cleaning.

REFERENCES

1. Richtlinie für Schutz und Instandsetzung von Betonbauteilen. Deutscher Ausschuß für Stahlbeton. Beuth Verlag GmbH, 1990.

2. ZTV-SIB 90 Zusätzliche Technische Vertragsbedingungen und Richtlinien für Schutz und Instandsettzung von Betonbauteilen. Bund/Länder-Fachausschuß Brücken- und Ingenieurbau. Verkehrsblatt-Verlag, 1990.

3. SILFWERBRAND J., Improving Concrete Bond in Repaired Bridge Decks. Concrete International. P. 61-66, Sept. 1990.

Method	Application	Requirements/Restrictions	Assessment
Chipping: Maually by hammer and chisel, jackhammer	(2), (3) Local for small areas	Danger of deeper damage caused by shocks and vibration. Danger of damaged reinforcement after chipping because of sharp tool. Special care with stressing tendons.	Low expenditure of machinery, can be used also for work in vertical and overhead position, low performance, dust, noisy.
Hammering: Needle gun	(1), (2), (4) Local for small areas		Low expenditure of machinery, can be used also for work in vertical and overhead position, low performance, dust, noisy.
Hammering: Mechanical hammer	(1), (2), (3) Depending on the size of the machine local or wide-area	Danger of deeper damage caused by shocks and vibration. Danger of damaged reinforcement after hammering because of sharp tool. Special care with stressing tendons. It is not possible to expose reinforcement.	Low expenditure of machinery, can be used for work in horizontal position only, dust, noisy.
Milling: Miller	(1), (2), (3) Wide-area removal from any even horizontal surface. Local removal from any even surface.	Concrete removal in each pass ≤ 5 mm, use of electronic levelling instruments nessecary for working on wide areas. It is not possible to expose reinforcement.	Often used technique for concrete removal from wide areas, noisy.

Table 1.1 Techniques for surface treatment (after [1] [2]).

Method	Application	Requirements/Restrictions	Assessment
Grinding: Grinder	(1), (2), (4) Local		Low expenditure of machinery, low performance, dust, noisy.
Brushing: Wire brushing with rotating brushes or brushing machines	(1), (2), (4) Local	After treatment for different techniques for surface preparation.	Low expenditure of machinery, low performance, dust, noisy.
Blasting with steel balls	(1), (2) Wide-area roughening of even horizontal or slightly sloping surface, local roughening of any even surface.	Can only be used on even surface.	Good for removing of coatings, possible aftertreatment after flame treatment.
Blasting with compressed air:			
Free blasting with solid agents (sandblasting)	(1), (2), (4) universal technique for local and wide-area use.	The removal depth is caused by the kind of abrasive, its size, its amount and the air pressure. Enormous appearance of dust, special regulations about dangerous goods need to be observed. The compressed air needs to be oil-free and water-free.	Universal, sufficient removal of rust from reinforcement, high performance, low costs, dust (housing necessary).
Dry blasting dustfree (suction apparatus)	(1), (2), (4) Local	The removal depth is caused by the kind of abrasive, its size, its amount and the air pressure. The compressed air needs to be oil-free and water-free	Sufficient removal of rust from reinforcement, low performance, recycling of abrasive possible.
Water-spray blasting dustfree	(1), (2), (4) Local and wide-area	The removal depth is caused by the kind of abrasive, its size, its amount and the air pressure. The compressed air needs to be oil-free. Cleaning of the surface after treatment necessary.	Suitable if requirements for low dust appearance are to be met, sufficient removal of rust from reinforcement but new rust appearing after treatment
Pressure (high-pressure) water blasting with water/abrasive mix	(1), (2), (3), (4) Local and wide-area	The removal depth is caused by the kind of abrasive and the water pressure. Cleaning of the surface after treatment necessary.	High performance, sufficient removal of rust from reinforcement but new rust appearing after treatment
Blasting with pressure water with or without suction of the blasting water and waste material	Local and wide-area	Appearance of huge amount of wastewater which needs to be disposed or recycled.	
< 20 MPa (40 MPa)	(1), (5) Surface cleaning	The cleaning result depends on the water pressure, water temperature, kind of nozzle and distance between surface and nozzle.	Disposal of wastewater necessary.

Table 1.2 Techniques for surface treatment (after [1] [2]).

Method	Application	Requirements/Restrictions	Assessment
40 - 120 MPa (high-pressure range)	(1), (2), (3), (4) Power guided device (robotic systems): wide-area, removal and roughening Manual guided tools: local	The removal depth depends on the water pressure, waterflow, duration and distance between nozzle and surface, uses an enormous amount of water up to 300 l/min.	Disposal of wastewater necessary, use of recycled water possible, above 100MPa, sufficient removal of rust from reinforcement but new rust will appear after treatment, noisy.
> 120 MPa (highest-pressure range) suction of water and waste material possible	(1), (2), (3), (4), (5) Power guided device: wide-area, removal, roughening and cleaning, Manual guided tools (jet pistols): local for concrete cutting	The removal depth depends on the water pressure, waterflow, duration and distance between nozzle and surface, waterflow up to 30 l/min.	Highly sophisticated technique, disposal of waste-water necessary, use of recycled water yet not possible, sufficient removal of rust from reinforcement but new rust will appear after treatment, noisy.
Flame treatment: Hand torch Machine driven torch	(1), (2) Wide-area roughening of even horizontal or slightly sloping surface, local roughening of any even surface.	Specially trained operators necessary. DVS guidelines 0302, min. speed and concrete cover. Removal up to 3 mm. It is not possible to expose reinforcement. After treatment with wire brushing or blasting with solid agent is nessecary.	Low expenditure of machinery, high performance.
Cleaning:			
Blowing	(5) Not horizontal areas	Compressed air oil-free.	Dust
Suction: Industrial vacuum cleaner	(5) Wide horizontal areas	Normal treatment before applying repair mortar or coating.	
Water jet Steam jet Hot water jet with or without chemical additives	(1), (5) Removal of dirt and loose contamination	Regulations for waste disposal need to be observed.	Disposal of wastewater necessary and possibly difficult.

Applications:

(1) = Removing of old coatings, after-treatment applications, surface contamination.
(2) = Removing of low-strength layers and cement skin.
(3) = Removing of damaged concrete and concrete repair material and exposing reinforcement.
(4) = Removing of rust from exposed reinforcement.
(5) = Cleaning off loose contamination, dust, loose material and water films.

Note:

"Compressed air oil-free" means, air with ≤ 0,01 ppm residual oil.

Table 1.3 Techniques for surface treatment (after [1] [2]).

Assessment of Water Blasted Concrete Structures

État de structures en béton, traités par jet d'eau

Beurteilung von wassergestrahlten Betonuntergründen

Martin HOFFMANN
Mineralogist
University of Technology
Aachen, Germany

Martin Hoffmann, born in 1962, studied mineralogy at Aachen Univ. of Technology. He is Scientific Assistant at the Institute of Construction Machinery and Management of the Aachen Univ. of Technology. His main field of research is repair work of natural stone facades.

Martin WERNER
Dr. Eng.
Aachen, Germany

Martin Werner, born in 1958, studied civil engineering at Aachen University of Technology. He completed his doctorate in 1991 about a special technique for concrete repair work.

SUMMARY

The use of a high pressure water jets is a normal procedure for preparing concrete substratae for repair. The concrete quality as well as the parameters for the high pressure water jet define the quality of the exposed concrete. This article presents the relationships between the parameters of the high pressure water jet and the concrete substratae, as well as an assessment of the treated concrete structure with regard to plainness, roughness and frequency of cracks.

RÉSUMÉ

La technique du jet d'eau à haute pression est un procédé habituel pour la préparation de structures en béton avant des travaux de remise en état. La qualité du béton de même que les paramètres concernent le jet d'eau ainsi que les conditions de chantier influencent la qualité de la réparation. L'article présente les relations entre les paramètres du jet d'eau et la structure traitée ainsi qu'une appréciation de la surface traitée ou de la fréquence des fissures.

ZUSAMMENFASSUNG

Die Hochdruckwasserstrahltechnik ist ein gebräuchliches Verfahren zur Vorbereitung von Betonuntergründen vor Instandsetzungsmassnahmen. Die Betonqualität sowie die betrieblichen und strahlseitigen Einflussgrössen bestimmen dabei die Beschaffenheit des Untergrundes. Im vorliegenden Beitrag werden Abhängigkeiten des hydrodynamischen Abtrages diskutiert, sowie eine Beurteilung des Traggrundes hinsichtlich Ebenheit, Rauheit und Risshäufigkeit vorgenommen.

1. INTRODUCTION

Since the beginning of the 1980´s the use of the high pressure water jet technique in the building industry has increased significantly. This is due to the ongoing need for repair work on existing buildings coupled with advances in the standard of the technique itself. The high pressure water jet technique is now used in all cases where this method provides particular advantages, ranging from cleaning, roughening and removing to drilling and cutting. In carrying out concrete repair work for the preliminary treatment of concrete substrates, the water jet technique can be applied to remove concrete skin and weak concrete layers as well as solid concrete of any thickness to any range from small to large quantities. Precondition for optimal economic implementation of the high pressure water jet is a thorough knowledge about the removal mechanisms. The behaviour of the mechanisms is determined by specific working and tool parameters as well as the material mechanics of the substrate. In addition to the structure of the removed concrete the structure of the blasted concrete substrate is particulary interesting. So, it is inevitable to prepare an even, adhesive subsurface to enable a firm and durable bond between concrete substrate and the protective - or concrete substitution system which is placed on the top. The concrete substrate should not contain any cracks or delaminated concrete parallel to the surface and should possess sufficient roughness, strength and water content.

The following article outlines the range of scientific research that has been undertaken on the concrete behaviour when the high pressure water jet is used for repair work. Furthermore, results will be presented concerning the fulfillment of set requirements in the structure of the concrete substrate after treatment.

2. AIM OF RESEARCH

The investigation of operational and tool parameters is designed to procure the capacities for concrete treatment of the high pressure water jet in dependancy on the adjustable parameters. Operational parameters are i.e. jet distance and working speed, whereas the most important tool parameters are water flow and jet pressure which determine the jet speed. Different constellations of the mentioned parameters should optimize the technique in accordance to the individual requirements of each possible application situation.

The concrete substrate after treatment will be evaluated with regard to outer appearance, roughness and plainness of the substrate. Particular attention will be paid to the eventual initiation of cracks by the high pressure water jet.

3. OPERATIONAL AND TOOL PARAMETERS

3.1 Water flow and jet pressure

In Figure 1 the volume of removed concrete is shown in dependency on jet pressure and nozzle diameter. The volume of removed concrete in relation to time is of particular interest because this relation describes the capacity for removal in the field of concrete repair measures. A strong progressive dependency of the time related volume of removal on the nozzle diameter and jet pressure can be observed. The amount of removed concrete disproportionally increases at a pressure of 100 MPa in dependency on the nozzle diameter. This can be explained by an increase of the water flow caused by larger nozzle diameter in combination with high jet pressure. Furthermore, an investigation of the width of the notch, caused by water jet, shows that higher pressure and especially larger nozzle diameters lead to an enlargement of the notches. Now,

on the one hand, this might be due to the fact that the water and removed concrete particles must leave the produced notch with clearly reduced speed. On the other hand, the deeper the notch the more material has to be removed while the slit width stays the same size. Both factors lead to a disproportionate widening of the notch and to a progressive concrete removal. As has been expected, an increase of the jet pressure from 100 MPa to 200 MPa by small nozzle diameters does not effect a significant rise in the volume of removed concrete because the water flow of the high pressure water jet increases at a considerably lower rate. Accordingly, the effectiveness of the water flow for concrete removal is more characterised by the nozzle diameter than by jet pressure.

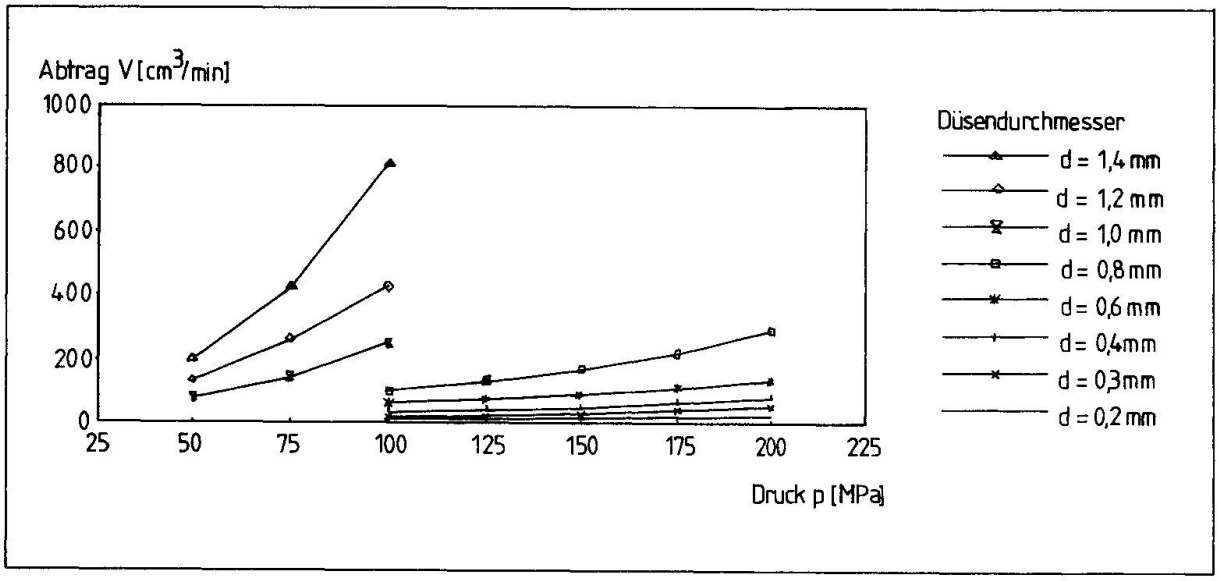

Fig.1 Volume of removed concrete (Abtrag) in dependency on jet pressure (Druck) and nozzle diameter (Düsendurchmesser).

Under economical considerations neither the jet pressure nor the nozzle diameter alone can account for a characterisation of the removal process. Here, it is necessary to additionally investigate the power expenditure. The power expenditure is the energy which is necessary to remove one measure of concrete. The specific removal energy, as the power expenditure is called in Figure 2, results from the ratio of jet capacity and the volume of removed concrete in time. The jet capacity is defined as the product of jet pressure and water flow. Figure 2 shows that a jet pressure of 100 MPa is the lowest power ependiture needed for the here considered concrete, independent of the nozzle diameter. Below and above this value the removal capacity is smaller. If a maximisation of the amount of removed concrete is another central issue, the largest nozzle possible should be used. The use of two or more small nozzles with the same power expenditure used for one large nozzle results in a smaller amount of removed concrete. But, the latter is advisable in those cases where no deep removal is desired, where the aim is a roughening of the subsurface [1].

3.2 Operational Parameters

In addition to the tool parameters, operational parameters as operational speed, distance and angle of jet can be changed. The most influental operational parameters for the removal capacity are jet distance and operational speed. With decreasing distance the removal capacity increases disproportionally. Especially when using small nozzles already minimal distance changes have a significent influence. Additional tests with varying

distances and different nozzle diameters showed that for every nozzle diameter within an economically sensible pressure range the smallest distance was at the same time the most favourable and efficient one in energetic terms. The choice of high operational speed leads to a significant increase of the removed amount of concrete and, as expected, to a decrease of the depth of the removed lift. Furthermore, it can be observed that repeated passing over the same spot with a consistent stress duration and distance achieves a higher capacity for removal than a single pass with low operation speed. The jet angle, a further influental parameter, has almost no influence on the removal capacity when small nozzles are used, but with larger diameter a jet in advance has proved favourable.

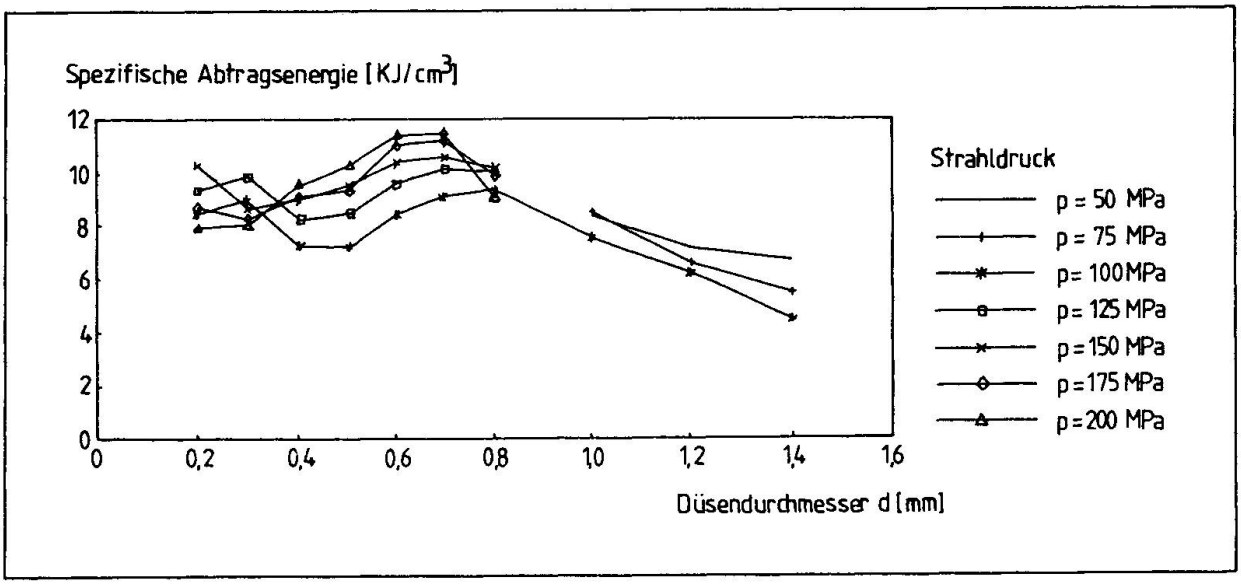

Fig.2 Specific removal energie (sp. Abtragsernergie) in dependency on jet pressure (Strahldruck) und nozzle diameter (Düsendurchmesser)

4.0 THE CONCRETE SUBSTRATE AFTER TREATMENT

4.1 The structure of the substrate

The preparation of the substrate prior to the placement of repair concrete and mortar or the protective system has to improve the strength, secure the compatibility and improve the bonding behaviour of the concrete substrate and the protective layer. Therefore, the remaining concrete substrate should not contain any cracks or delaminated concrete running parallel to the surface, or shell shaped in the surface ambient. It should, furthermore, be of sufficient roughness and strength [2]. If removal work on decayed concrete is carried out, it has to be regarded that not too much material will be removed by the implemented technique and the remaining concrete will not be damaged. When using the high pressure water jet technique the profile of the remaining concrete is determined by a complex set of interrelated parameters. A geometrically exact removal is impossible with this technique. This can be put down to the high pressure water jet´s working mechanisms. So, the resulting surface after removal is mostly determined by the strength of the concrete substrate. In consequence, after a treatment by high pressure water jet the substrate is uneven but usually very strong. Depending on the individual concrete´s structure one has to reckon with crates as deep as or even many times deeper than the nominal depth of the layer to be removed [3]. With increasing strength of the concrete, shell like delaminations appear more often, whereas the depth of removal decreases. As the cementing material poses

small resistance to the water jet, the breaking off of large parts occurs very seldom. Rather, only the grains are washed clear, which in turn leads to a smaller time-related removal amount. If the cement stone is of a relatively high strength and if furthermore a strong compound between cement stone and concrete aggrergate exists, one can expect a more grain-breaking removal. With less concrete strength the preferred technique is to remove the cement stone because of the different strength values of cement stone and concrete aggregate. This results in a more grain surrounding removal.

4.2 Plainness and Roughness

Until now, there have existed no standardized criteria for the evaluation of roughness or evenness of concrete substrates after treatment. An examination of evenness follows, therefore, the DIN 18202 [4]. Concrete substrates treated with high pressure water jet serve as testing samples. The removed concrete has to be of a nominal depth of 20 mm. For the evaluation of the relief a length of 100 cm is taken as a basis. As a comparative basis, in accordance with the DIN 18202, a line above the remaining peaks is chosen which is gained by laying a screed onto the treated substrate.

Meß-punkt cm	1 mm	2 mm	3 mm	4 mm	5 mm	6 mm	7 mm	8 mm
0	7	51	5	18	53	5	23	35
10	0	21	15	12	46	8	31	47
20	29	15	33	25	48	23	30	31
30	25	26	29	30	22	28	23	23
40	27	7	21	18	33	24	20	45
50	29	14	48	8	24	0	12	14
60	38	35	17	33	12	14	18	18
70	7	17	26	33	14	30	2	20
80	27	22	18	22	17	17	7	18
90	19	20	17	13	18	14	11	14
100	41	7	13	4	7	12	7	10
Mittel -wert	24	19	19	19	22	27	15	22

Table 1 Profiles for examination the evenness

Starting from this basis in intervalls of 10 cm the distances between screed and concrete substrate are measured. The results of 8 sections are shown in table 1. Distinctive features for the substrate-surface after treatment are created landscapes with extreme peaks and hollows. The extreme values vary between 0 and 53 mm. The mediate values of the analysed sections range from 15 to 27 mm and are situated close to the nominal depth of 20 mm. Such variations of the depth of the removed concrete are to be considered normal with the high pressure water jet technique. They can be put down to the selective way of removal of the water jet and finally to the inhomogeneities within the concrete strength.

The roughness of the substrate is evaluated visually. It is understood that roughness of the substrate is the profile of remaining concrete in the small range of a few millimeters. A surface as rough as possible is aimed at, to achieve a strong bond between substrate and concrete-substitution or protective system. To achieve a rough surface the grain breaking method of removal is the better method than the grain surrounding one, because the latter one procures smooth stonesurfaces. Via an estimation of the crushed grain portion of the concrete substrate an evaluation of roughness can be undertaken.

4.3 Crack Investigations

For microscopical investigations field and laboratory concrete cores were taken before and after concrete removal by a high pressure water jet. These sample cores were impregnated with fluorescent resin, so as to avoid any cracking due to the sample preparation. With each thin section one to two cracks due to the removal technique could be detected on a length of 50 mm. The cracks are between 0.5 mm and 2.5 mm deep, 2 to 10 mm long, and between 5 and 15 micrometers wide. Most of the cracks run parallel to the surface structure of the cement stone, are grain surrounding and branch off with increasing depths. The examination shows that there are only a few crack initiations caused by the water jet technique. But, it has to be mentioned that the investigations took into account only one class of concrete strength. During current research uncertainties and contradictions arose concerning the crack initiation, when dealing with concrete of higher strength. So, the macroscopical appearance of concrete substrates with high strength hints a significant development of cracks which could not be detected with concrete of a low strength. Bazong [5] also reports on the development of cracks due to the treatment with the high pressure water jet and the resulting decrease of the adhesion properties. A clarifying, more detailled microscopical investigation of concrete after treatment which takes varying degrees of strength and further features into account has still to be carried out. Therefore, enhancing investigations on the structure of the concrete substrate after treatment with high pressure water jet are in planning.

REFERENCES

1. WERNER M., Einflußparameter und Wirkmechanismen beim Abtrag von Mörtel und Beton mit dem Hochdruckwasserstrahl. Diss. Aachen, 1991

2. RICHTLINIE FÜR SCHUTZ- UND INSTANDSETZUNG VON BETONTEILEN; Deutscher Ausschuß für Stahlbeton, Beuth Verlag GmbH, Berlin, 1990

3. WERNER M., KAUW V., Gutachterliche Stellungsnahme zur Frage der Ebenheit im Zusammenhang mit dem Objekt "Tunnel am Lindener Berg", unveröffentlicht, 1993

4. DIN 18202 Ausgabe 05.86, Toleranzen im Hochbau, Bauwerke, Beuth Verlag GmbH, Berlin, 1986

5. BADZONG H.J., Anforderungen an den Betonabtrag mittels hydrodynamischer Verfahren, Bericht 90-1, Tiefbauamt Kanton Solothurn, Schweiz, 1990

Conservation of Buildings by Filling of the Pores with Paraffin

Conservation de bâtiments par remplissage des pores avec de la paraffine

Erhaltung von Gebäuden durch Porenfüllung mit Paraffin

Jürgen DREYER
Professor
Hochschule Wismar
Wismar, Germany

Jürgen Dreyer, geboren 1941, promovierte und habilitierte an der Hochschule für Architektur und Bauwesen in Weimar. Er arbeitete als Hochschullehrer in Dresden, Cottbus und Wismar auf dem Gebiet der Bauphysik. Sein spezielles Arbeitsgebiet ist die Untersuchung thermisch-hygrischer Prozesse in Bauwerken.

SUMMARY

The reason for the destruction of stones and elements of construction is the moisture, which penetrates in the pores and destabilizes, through several processes, the matrix of the construction material. Therefore it is very important to decrease the moisture content. An effective method is the filling of the pores with paraffin. If the building materials are warm enough, paraffin penetrates and fills the pores completely. Paraffin is an absolutely benign material. It can penetrate in the material over the surfaces through irrigation, flood-ing or plunging or through injection in holes. After the treatment, the water-absorbing ca-pacity, the moisture transfer and diffusion of the material is nearly null. The strength of damaged material increases.

RÉSUMÉ

L'humidité pénétrant dans les pores détruit l'équilibre d'un matériau de construction par des processus différents et entraîne la destruction des pierres et des éléments de construction. Pour cette raison, il est très important de réduire la teneur en humidité. Une méthode efficace est le remplissage des pores avec de la paraffine. Si le matériau de construction est assez chaud, la paraffine pourra pénétrer et remplir les pores complètement. La paraffine est une substance favorable à l'environnement. Elle peut pénétrer dans le matériau par irrigation, saturation et injection. Après traitement, des propriétés du matériau comme la capacité d'absorber de l'eau, le transport d'humidité et la diffusion sont infiniment petites. La résistance du matériau déjà endommagé peut être améliorée.

ZUSAMMENFASSUNG

Der Grund für die Zerstörung von Steinen und Bauteilen ist die Feuchtigkeit, die in die Poren eindringt und durch verschiedene Prozesse die Matrix eines Baumaterials destabilisiert. Deshalb ist es sehr wichtig, den Feuchtegehalt zu vermindern. Eine effektive Methode ist die Porenfüllung mit Paraffin. Ist das Baumaterial ausreichend erwärmt, kann das Paraffin penetrieren und die Poren vollständig füllen. Paraffin ist ein absolut umweltverträglicher Stoff. Es kann über die Oberfläche durch Berieseln, Tränken oder Injizieren eingebracht werden. Nach der Paraffin-Behandlung ist die Wasseraufnahme, der Feuchtetransport und die Diffusion verschwindend gering. Die Festigkeit von bereits geschädigtem Material wird erhöht.

1. INTRODUCTION

Moisture is the main reason for deterioration of stones, bricks, constructions and buildings. It penetrates into the pores and causes by several processes, such as frost-dew-alternation, chemical corrosion and material removal and transfer the deterioration of the material matrix, reduction of stability, changing of thermal and other qualities, development of heterogeneous structures among other consequences. That is why when attempting to preserve damaged and endangered buildings one tries to influence the moisture balance in a way that reduces the moisture contents in building materials. An effective method is the using of pore-sealing materials. These mediums have to fulfil the following requirements:

1. The pore must be sealed completely and with high reliability.
2. The spreading of the medium inside the building material must be determinable and controllable.
3. The medium should be compatible with the building material and should not cause any secondary effects.
4. The environmental compatibility should be very high.

Paraffin is a medium fulfilling these demands to a high degree. It is compatible with the building materials and the environment. Important for the effects of the stone-protecting and the stone-stabilising systems is the penetration of the medium (i.e. paraffin) deeply into the constructions so that the treatment takes not only place on the surface.

Treatments with paraffin and wax have been already used for centuries. But with the historical restrictions people had they could achieve a limited degree of protection.

The building material may be extensively filled with paraffin by warming it sufficiently and spraying, soaking or injecting with paraffin. Because there are no chemical or volatilisation processes while filling and locking the pores (only a sufficient temperature is required), you may practice the treatment as long as the process of sealing the pores is completely accomplished and deeply inside the building material.

2. THERMALLY STIMULATED INJECTION OF PARAFFIN TO BUILD UP SUBSEQUENT MOISTURE BARRIERS INSIDE THE WALL

Building up subsequent moisture barriers belongs to the most difficult tasks in the area of building reconstruction. The barrier has to be placed in base walls, which are decisive for the building's stability. Because this problem can't be solved with simple structural methods there exist several strategies with different modes of operation and results. Besides mechanical and electrophysical methods, above all injection methods are used. The damaging moisture transport in porous building materials takes place in the pores and capillaries where especially pores and capillaries with a radius of R=0.001mm are effective. That is the reason for injecting a pore-sealing or water repellent material. If the pores and capillaries are sealed or treated with a water repellent no moisture can be transported and the treated area operates as a moisture barrier. To realise these moisture barriers, the injection medium has to be brought into the walls in a way which assures that the whole wall cross-section is affected. This is done by boring holes with distances of 10 cm up to 12 cm into the wall. The depth of the bore holes should be compatible with the wall's strength. The injection medium is introduced into the

holes with or without pressure. With the pressure-less methods the capillary forces distribute the injection medium inside the building material. This process is accelerated with external pressure using pressure injection.

The injection methods mainly differ through the used injection medium. Silicates, water glass mixes, silicones, silanes and stearates serve as water repellent substances. By means of several methods, for example vaporisation of solvents, reaction with coal dioxide or moisture with low alkalinity, the silicon resin molecules form a chain and the water repelling silicon resin covers the pore walls. If the pores are filled with water or there is not enough moisture, if not enough solvent diffuses to the outside or not enough coal dioxide diffuses to the inside of the massive and wet wall, the water repellent effects of the mentioned methods will decrease or not appear.

As pore-sealing substances commonly cement suspensions, resins and paraffin are used. Cement suspensions and resins are generally introduced into the wall under pressure. This is necessary because after producing or mixing these substances the hardening process starts after a so called pot-time and the mediums have to first fill the pore space. Furthermore these materials can not be sufficiently transported through the capillaries because of their high viscosity. Therefore pressure is required.

Using paraffin as a pore-sealing substance, many of the above mentioned problems can be solved. Liquid paraffin is able to penetrate by means of capillary forces or pressure support. Therefore the treated wall has to be warmed up to a temperature above the melting-point of paraffin before, or while, the treatment takes place. Through this heating process the moisture vaporises and the moisture-damaged masonry becomes dry. Thus the pore space may be freed from moisture, filled and sealed with the heated paraffin. Paraffin injection is practised in the following way: heating sticks are introduced into the bore holes and after a sufficient drying and warming the paraffin is filled in. Simple technologies work with cans and storage

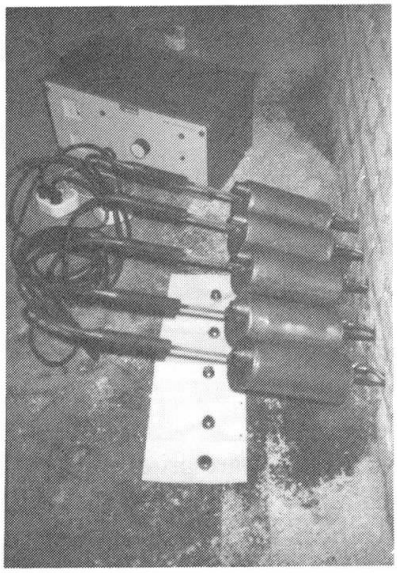

Fig. 1 Device of a paraffin infection

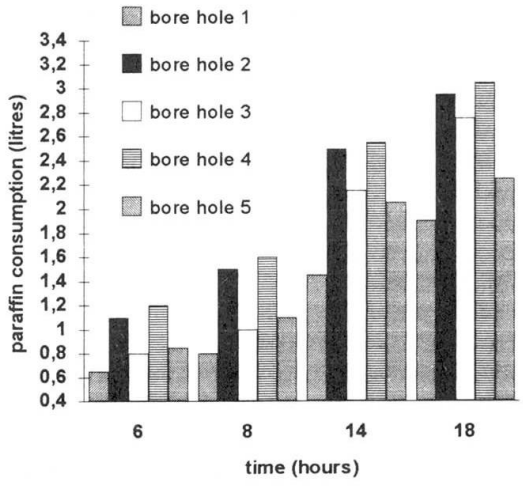

Fig. 2 Penetrating volume of paraffin during a paraffin injection

containers. The capillary forces then secure the distribution. It is also possible to accelerate the distribution of paraffin under pressure by using pressure aggregates. The sufficient warming of the masonry is important for these variants lest the paraffin stiffens during the penetration process.

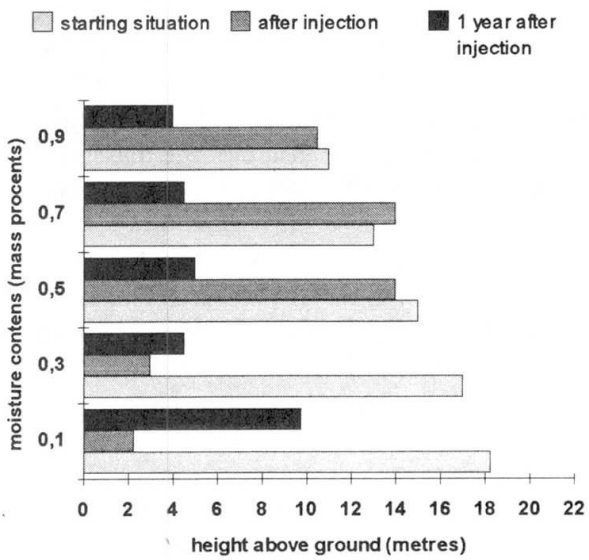

Fig. 3 Moisture distribution inside a wall before and after a paraffin injection

With another variant of paraffin penetration you heat inside the bore holes and simultaneous fill them with as much paraffin out of the storage containers as the bore hole admits. This method ensures that the maximum absorbable volume of paraffin is available. Fig. 1 formal represents the injection method. While using this device the heating stick inside the bore hole is continuously surrounded by liquid paraffin. The heat transmission is greatly enhanced through that compared with methods where the heating sticks warm the masonry before the paraffin injection starts. And it leads to an intensive warming, to an increase in efficiency and through this to performance decrease of the heating systems. The relatively big quantities which are able to penetrate by this method are comparable with the pore space to be sealed and indicate the high degree of pore filling. Fig. 2 shows the paraffin consumption by a bore hole injection with an injection into five bore holes. The paraffin injection method distinguishes itself with a certain operating mechanism because the solidifying process and the pore seal only depend on temperature and no other reaction conditions are required. Furthermore paraffin is absolutely compatible with the environment. Its use presents no negative hygienic or ecological consequences for the population and the environment.

Fig. 3 shows three moisture distributions measured before, immediately after and half a year after a paraffin treatment. Clearly recognisable is the direct drying effect through the heating and the certain barrier effect of the treated area.

3. INCREASING THE DURABILITY OF POROUS STONES BY PARAFFIN IMPREGNATION

A large number of damaging processes which affect stones and building materials are produced by water or steam entering the pore space and causing several damaging reactions. By preventing the moisture entry by a pore seal the moisture balance of the endangered building-construction improves. This leads to the slowing down or ending of the damaging processes. Present experiences with the paraffin treatment of porous stones prove that almost all pores can be sealed. Fig. 4 shows the water admission of impregnated stones before and after the paraffin treatment. The drastic water admission decrease clearly proves the pore-sealing effect of paraffin. This can be simply shown by the absorption quantities. The treatment with paraffin has to be done in a way through which the moisture is not locked in and treated areas can not

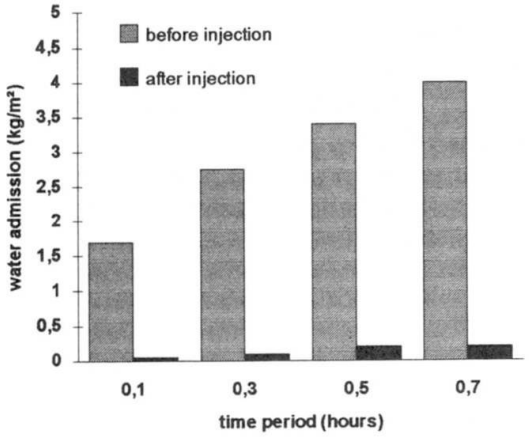

Fig. 4 Water admission of paraffin-treated and non-treated stones

be by-passed. To achieve this it is essential that sufficient depths are achieved and complete areas are treated. Impregnations with these effects can be easily done with paraffin. The prerequisite is warming up the areas to be treated to temperatures above the melting point of paraffin. As long as these temperatures exist the paraffin may spread by capillary forces and reach large areas. Whereby due to the laws of capillary material transport the process takes an extended period of time. The paraffin's ability to penetrate depends only on the temperature, therefore long treatment times are technically possible and in principle uncomplicated. Fig. 5 shows the entry of a paraffin front into sandstone. Filling the pores with paraffin does not only stop the processes of moisture exchange and moisture movement but also changes the mechanical properties of the treated building material. Fig. 6 demonstrates the increasing of pressure firmness of bricks by paraffin impregnation.

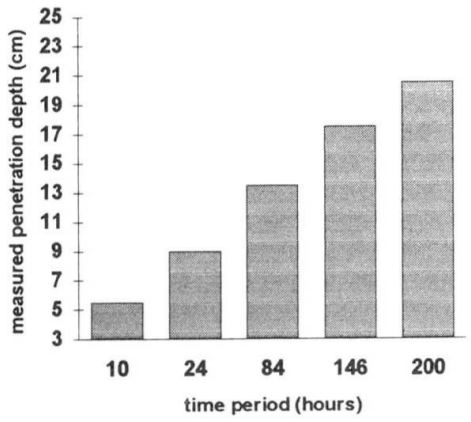

Fig. 5 Penetration depth of paraffin inside sandstone

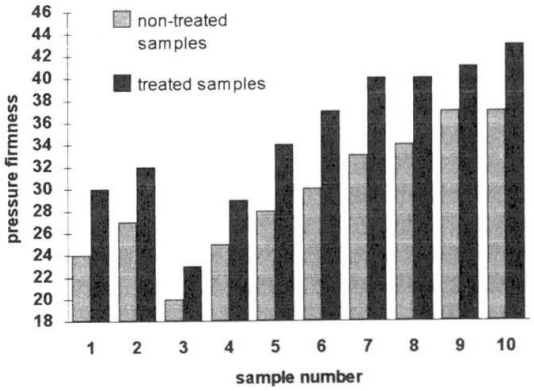

Fig. 6 Increase of pressure firmness

For these experiments old stones, which had already been damaged or weakened through frost-dew-alternation and salt crystallisation have been used. Several samples were obtained out of these stones to compare treated and non-treated stones. Increases of firmness of up to thirty percent, as shown in Fig. 6, could be achieved. Similar results were found by Franke [1] with comparable experiments.

4. SUMMARY

The treatment of stones to be protected with waxes and paraffins is an old method which can be used very effectively with today's technical possibilities. The penetrated areas are absolutely impermeable for water so that safe barrier layers can be built up. The paraffin spreading is tied to temperatures above 50°C. Through this it is possible to determine the spreading zones of paraffin penetration and adapt them to the requirements of moisture- and stone protection. Filling the pores with paraffin also changes the mechanical stone properties. Firmness increases could be proved with damaged stones and stones of limited firmness.

BIBLIOGRAPHY

1. FRANKE, L., BENTRUP, H.: Paraffininjektionsverfahren zur Trockenlegung von Mauerwerk - Beurteilung der Wirksamkeit, Bautenschutz+Bausanierung 16 (1993) p. 5-8

2. DREYER, J.: Thermisch stimulierte Injektion von feuchtegeschädigten Wänden mittels Paraffin, Bautenschutz+Bausanierung 6 (199) p. 22-28

External Reinforcement of Concrete Beams Using Fibre Reinforced Plastics

Renforcement de poutres en béton à l'aide de plaques composites

Aussenliegende Bewehrung von Betonbalken mittels faserverstärkten Kunststoffen

Hamid VARASTEHPOUR
Civil Engineer
University C. Bernard
Lyon, France

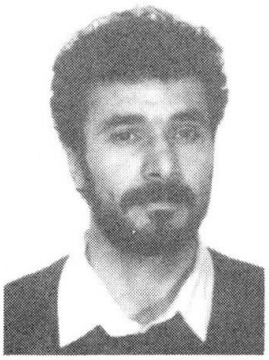

Born in 1959 in Iran, Hamid Varastehpour has engineering degrees from UTI, Iran, and INSA, France. He is presently a PhD student at the Univ. C. Bernard in Lyon. His research is in structural applications of fibre reinforced plastics.

Patrice HAMELIN
Professor
University C. Bernard
Lyon, France

Born in 1949, Patrice Hamelin has a science and engineering degree from INSA, Lyon, and a Ph.D. from UCBL France. He is Professor and Head of the Materials and Mechanical Engineering Laboratory at the Univ. C. Bernard Lyon.

SUMMARY

Strengthening of concrete structures in situ with externally bonded fibre-reinforced plastic (FRP) using epoxy resins appears to be a feasible way of increasing the capacity and stiffness of existing structures. A series of 32 small beams strengthened using FRP plates was tested to failure under four-point bending to measure load versus deflection and compare with predicated value in order to study the effectiveness of the different two-part epoxy and FRP types. An iterative analytical method capable of simulating material non-linearity and slip bonding based on the compatibility of deformations and equilibrium of forces was developed to predict the ultimate forces and deflections.

RÉSUMÉ

Renforcer des ouvrages en béton à l'aide de plaques composites (FRP) collées sur la face extérieure, peut augmenter leur capacité et leur rigidité. Une série de 32 poutrelles renforcées par FRP a été testée jusqu'à la rupture pour étudier l'efficacité des différentes colles et FRP. Un nouvel essai a été proposé pour déterminer les propriétés mécaniques de l'interface béton/colle/plaque et une méthode d'analyse itérative capable de simuler la non-linéarité des matériaux et le glissement des plaques a été développée pour prévoir le comportement des poutres renforcées et calculer les forces et les flèches ultimes.

ZUSAMMENFASSUNG

Für die nachträgliche Verstärkung bestehender Betontragwerke bieten sich faserverstärkte Kunststoffe mit Epoxidharzen an. Um die Wirksamkeit zweier unterschiedlicher Epoxid- und Faserkunststoffarten zu untersuchen, wurden 32 kleiner Versuchsbalken mit Klebebewehrung im 4-Punkt-Biegeversuch bis zum Bruch belastet, wobei das Last-Durchbiegeverhalten gemessen und mit vorausberechneten Werten verglichen wurde. Zur Bestimmung der Merkmale der Kontaktfläche (Beton/ Kleber/ Faserkunststoffplatte) wurden einzelne Klebestösse getestet. Mit einem iterativen Berech-nungsverfahren können die Werkstofflinearität und Verbundschlupf berücksichtigt und aus der Dehnungsverträglichkeit und dem Kraftgleichgewicht das Bruchverhalten bestimmt werden.

1. INTRODUCTION

Deterioration of older structures due to loss of material properties, inferior design, action of climate, or increases in traffic loads in the case of bridges, often requires the invention of new rehabilitation techniques. In recent years, with the development of strong structural adhesion, the use of steel plate, bonding on the tension face of beams is a relatively well known technique for strengthening. This technique is very successful by the simplicity and speed of application but it also has some disadvantages. The use of composite plate is an interesting alternative to avoid this inconvenience due to their high strength, high stiffness, resistance to corrosion and low weight. This paper briefly reports the results of tests carried out on different small beams strengthened by different FRP plates. The tests were divided into four series, in each series different adhesives were used to study the influence of a two-component epoxy on the ultimate capacity and the failure mode. To study the bond interface between plate/concrete and for the determination of an interface law (needed as input to the computational analysis), different single lap specimens on large scale were constructed and tested. An iterative analytical method capable of simulating the bond-slip and material non linearity based on the compatibility of deformations and equilibrium of forces was developed to predict load-deflection relationship, strength and failure mode.

2. EXPERIMENTAL PROGRAM AND TEST SPECIMENS

As shown in fig.1, each small beam had a cross-section of 70 mm x 70 mm and a total length of 280 mm. The experimental set-up consisted of a simple supported beam subjected to two concentrated loads, symmetrical about mid span.

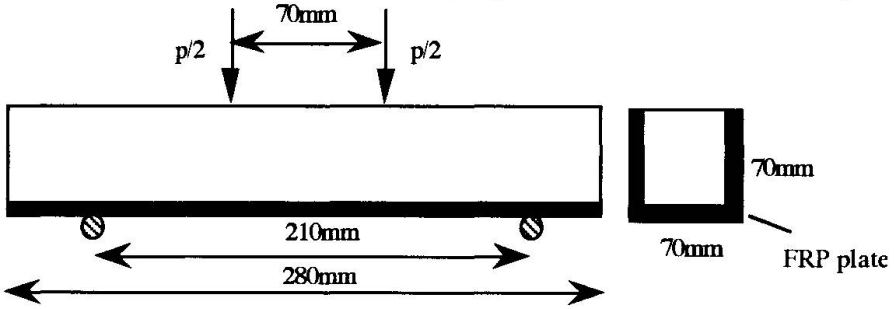

Fig.1. Beam test set-up

Similarly mixed concrete was used for all small beams The cement: sand: gravel proportions in the concrete mix were 1:2.2:3 by weight. The water/cement ratio was 0.52 and type I Portland cement (CPA55) was used. The maximum size of the aggregate was 12.5 mm. Twelve 160 mm x 320 mm concrete cylinders were cast and tested to determine the mechanical properties of the hardened concrete. The average compressive strength was 43.5 MPa and the flexural tensile strength was 6.35 MPa. The concrete had an average elastic modulus of 31 GPa for compression and 26 GPa for tension.

Plate	Code	Pattern	Weight (gr/m2)	Nominal thickness (mm)	Young's modulus (GPa)	Ultimate strength (MPa)
Glass1	1581	Satin	320	0.24	22	450
Glass2	1309	Satin	315	0.22	37.5	770
Carbon1	43377	Satin	285	0.33	57	560
Carbon2	46320	plaine weave	330	0.31	117	1350

Table 1 Physical and mechanical properties of plate

The fiber-composite material consisted of glass or carbon bonded together with an epoxy matrix. Four types of plates were utilized (70 mm x 280 mm). All the plates were subjected to longitudinal tensile tests (according to EN2561) to

determine elastic modulus and ultimate strength. The FRP exhibited a linear elastic behaviour up to failure. Summary of the plate properties used in the experimental study is given in table 1. Four adhesives, including epoxies and acrylics were selected for exploration in this study after consultation with a number of manufacturers about this particular application. A summary of the properties of the adhesives is given in table 2.

Properties		Sikadur (31)	Sikadur (910)	Ciba (XB-5323)	Hexcel (HP-330)
Modulus	Mpa	8500	600	6200	-
com.Strength	Mpa	70-80	80	75	-
Ten.Strength	Mpa	20-30	20	24	21
Density	g/cm3	1.5	1.1	1.6	1.36
Viscosity	cPs	Thixotrope	2800	9000	Thixotrope

Table 2 Properties of adhesives

2.1 Preparation of test specimens and fabrication

The FRP sheets were bonded to the tension face and the lateral faces of the specimen, 28 days after casting. Before applying the epoxy the concrete surface was roughened by sand blasting and was cleaned using an airjet, to insure a good bond between the epoxy glue and the concrete surface. The surfaces of the FRP plates were sanded to remove the shine and were cleaned with propanol.

Beam	Fiber type	Plate thickness (mm)	Adhesive	Beam	Fiber type	Plate thickness (mm)	Adhesive
B111	Glass 1	0.75	Sikadur31	B113	Glass 1	0.75	Hexcel
B211	Glass 2	0.5	"	B213	Glass 2	0.5	"
B311	Carbon 1	0.65	"	B313	Carbon 1	0.65	"
B411	Carbon 2	0.7	"	B413	Carbon 2	0.7	"
B121	Glass 1	1.8	"	B123	Glass 1	1.8	"
B221	Glass 2	2.5	"	B223	Glass 2	2.5	"
B321	Carbon 1	2	"	B323	Carbon 1	2	"
B421	Carbon 2	2.6	"	B423	Carbon 2	2.6	"
B112	Glass 1	0.75	Sikadur910	B114	Glass 1	0.75	Ciba
B212	Glass 2	0.5	"	B214	Glass 2	0.5	"
B312	Carbon 1	0.65	"	B314	Carbon 1	0.65	"
B412	Carbon 2	0.7	"	B414	Carbon 2	0.7	"
B122	Glass 1	1.8	"	B124	Glass 1	1.8	"
B222	Glass 2	2.5	"	B224	Glass 2	2.5	"
B322	Carbon 1	2	"	B324	Carbon 1	2	"
B422	Carbon 2	2.6	"	B424	Carbon 2	2.6	"

Table 3 Notation of the small beams

The epoxy was hand mixed and hand applied at an approximate thickness of 1.5 mm using a metal spatula (the adhesive was applied to both the FRP and the concrete surfaces). Bond thickness was not specifically controlled, but excess epoxy was squeezed out along the edges of the plate, assuring complete epoxy coverage. After the plate was positioned, it was held down with concrete weights during a curing period of minimum three days. The specimens were instrumented with electrical strain gauges and a LVDT, the strain gauges were positioned at the plate and on the compression zone of the concrete,a LVDT was placed in the neutral axis at mid span. The notation of the small beams are given in table 3.

3. EXPERIMENTAL PROGRAM FOR DETERMINATION OF INTERFACE MATERIAL LAW

This section describes the experimental set up of the proposed single lap specimen, used for the determination of the interface properties and the study of the interaction between the concrete/glue/plate interface. Fig. 2 shows the details of the specimen proposed, which essentially consists of two L-shaped concrete blocks which are bonded by a FRP plate 2 mm thick and 140 mm wide. The distance along the glued line was kept constant at 180 mm and glue thickness was maintained as 2 mm.

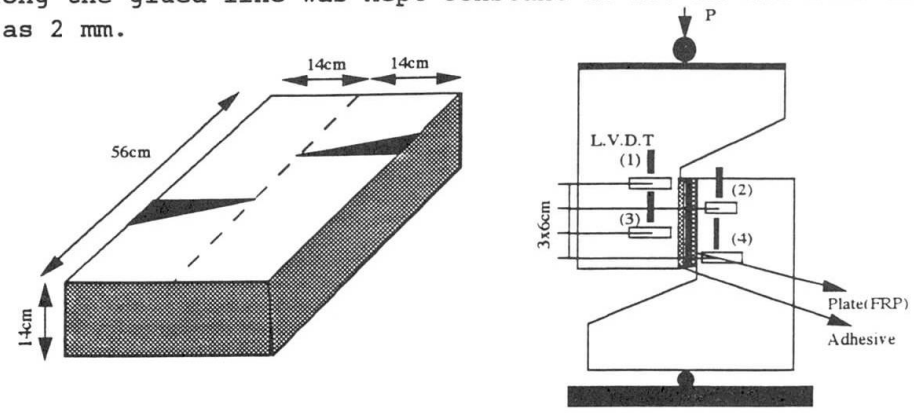

Fig. 2 Single lap specimen test details and experimental set-up

The whole assembly was subjected to a compression loading test. To determine the relative slip between the two blocks of concrete, the specimen was fitted with four LVDT's fixed at different points. The exact location of the LVDT's is shown in fig. 2. The loading was at a constant deformation rate with 0.2 mm per minute. Fig. 3 shows shear stress versus shear strain of the interface for the different interfaces types. shear stress versus the strain as determined from the LVDT reading divided by glue line thickness. The slopes of the plots indicate the shear modulus of the interface (Gint). The test results show a bi-linear behaviour between shear stress and bond slipping. The mechanical properties of the interface appears to be greatly dependent on the adhesive type. Table 4 lists the ultimate loads, shear strength and shear modulus (average result of different test), these results were used for construction of the interface model, needed as input to the computational analysis.

Adhesive	Ultimate load (KN)	Shear strength τmax(MPa)	Shear modulus Gint (MPa)
Sikadur910	77.5	4.6	50
Hexcel	141	8.5	160.5
Ciba	128	7.6	256
Sikadur31	146	8.8	240.5

Table 4 Result of shear test

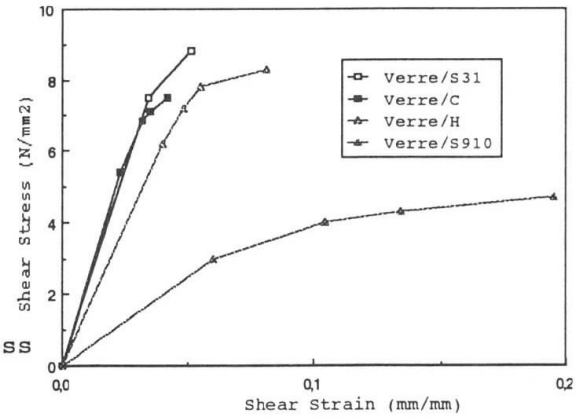

Fig. 3 Interface shear stress versus shear strain

4 THEORETICAL ANALYSIS

The method developed in this study to predict the strength and stiffness of RC beams strengthened by FRP plates is an iterative analysis technique, practicable by computer. Several assumptions commonly made in reinforced concrete theory are used, including a)plane sections remain plane, b)no slip occurs between any longitudinal reinforcement and concrete and c)stress-strain relationships of materials as determined by standard tests. This iterative analysis is capable of simulating material non-linearity including concrete cracking in tension and associated tension stiffening, plasticity of concrete in compression, plasticity

of reinforcing steel and non-linearity due to bond-slip between plate and concrete (Fig. 4). This model is able to predict the ultimate strength in bending, the load-deflection characteristics and failure mode due to tensile fracture of the FRP, crushing of concrete in compression or plate separation.

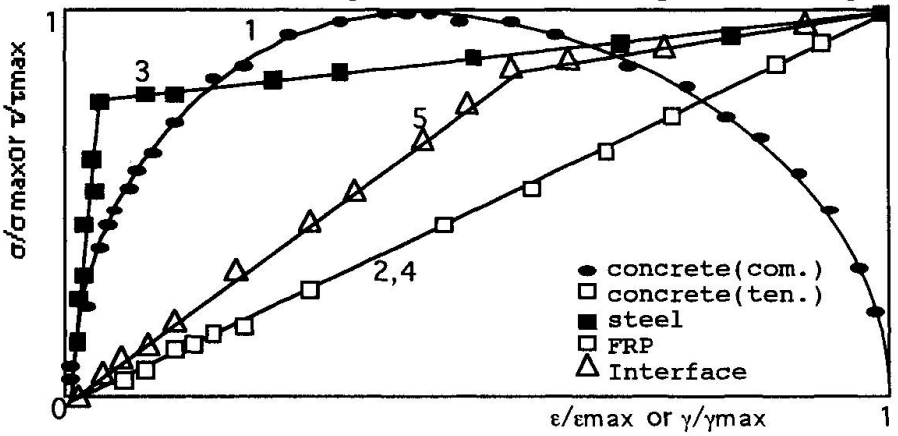

Fig. 4 Normalized stress-strain curved for idealized materials

4.1 Data required and calculating algorithm

At first, all dimensions of the beam (height, width, depth of steel, external plate dimensions) must be known. Also the span and the external load points are required to determine the load-deflection relationships. The entire stress-strain relationships of the steel, the FRP plate, the concrete (tensile, compression) and the interface material law must also be known with precision. First, a top fiber concrete strain and a neutral axis depth are assigned. The

Beam	Ultimate load(KN)			Failure mode	Beam	Ultimate load(KN)			Failure mode
	T*	T'**	E***			T	T'	E	
B111	47	46.6	41	FRP failure	B113	44	43.5	38	FRP failure
B211	50	49.5	45.5	"	B213	47	46.7	43.5	"
B311	67	66.3	65	"	B313	62	61	45	Plate separation
B411	92	89.1	63.4	plate separation	B413	85	83	44	"
B121	71	68.9	65	"	B123	65	63	62	"
B221	100	94.8	82	"	B223	92	88	63	"
B321	108	100.1	83.5	"	B323	99	90.8	64	"
B421	175	105	99	"	B423	162	92.8	63	"
B112	44	43.3	42	FRP failure	B114	47	46.7	45	FRP failure
B212	47	46.2	N.A	N.A	B214	50	49.6	41	"
B312	62	61	44	Interface	B314	67	66.4	62	Plate separation
B412	85	69	45	"	B414	92	89.3	55	"
B122	65	63.7	62	"	B124	71	70.1	72	"
B222	92	72	55	"	B224	100	93.5	75	"
B322	99	65.7	44	"	B324	108	96.5	68	"
B422	162	69.3	60	"	B424	175	98.2	84	"

* Theoretical ** Theoretical (With bond-slip effect) *** Experimantal

Table 5 Ultimate load and failure mode for each small beam

depth of the beam is divided into 200 slices, using the average strain for each slice, the compression and tensile stress can be found using the concrete stress-strain curve. Multiplying this by the area of the slice gives the compressive and tensile force. A similar method is used to determine the two tensile forces of the reinforcing steel and external plate. The tensile force of the external plate must be corrected due to the bond-slips in every iteration by determining the shear stress in the interface. The neutral axis is then adjusted until the sum of the compressive forces equals the sum of the tensile forces

(equilibrium). When this is achieved, the moment and the curvature are determined. This calculation continues until the maximum strength of the beam.

5. RESULTS OF EXPERIMENT AND DISCUSSION

Experimental results for all specimens are summarized in table 5. Also the theoretical results using the iterative analysis are mentioned (with and without interface effect). The ultimate load of the control specimen (unplated small beam) is 10.5 KN. Out of the 32 small beams tested, 8 failed by FRP rupture, 6 by interface failure and the others by debonding due to plate separation. The results show that the adhesive's effect is very important in the success of this technique. Fig. 5 shows load versus deflection for two series tests using different adhesives. Notice that the epoxy properties are very important to improve cracking behaviour and stiffness.

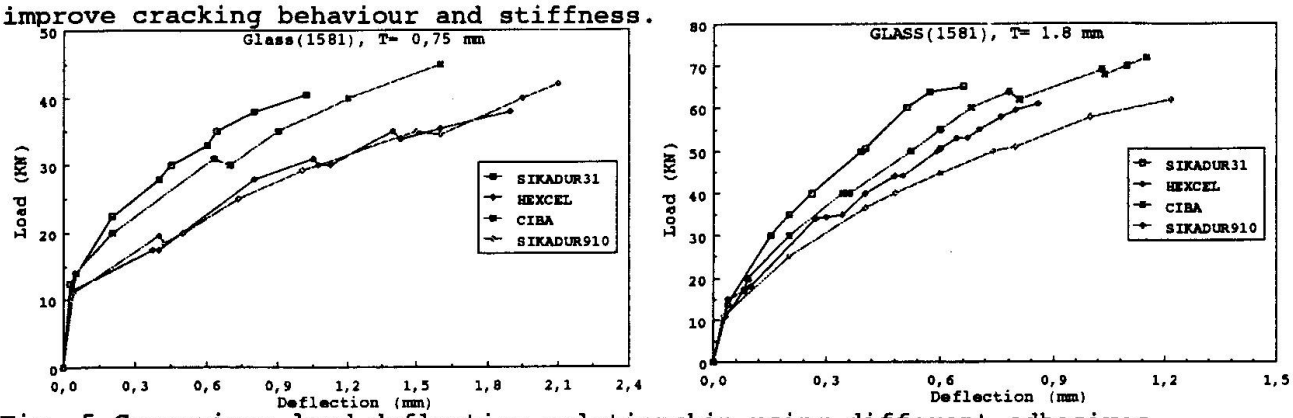

Fig. 5 Comparison load-deflection relationship using different adhesives

6 CONCLUSION

As result of the experimental and the theoretical studies, the following conclusions can be made:

1: The results of the test performed in this study indicate that significant increase in the flexural and shear strength can be achieved by bonding FRP plates to the tension face and the lateral faces of reinforced concrete beams.

2: The new single-lap test set-up introduced, proved to be a reliable specimen for measurement of the parameters necessary for the characterization of the concrete/glue/plate interface.

3: The selection of a suitable epoxy is very important in the success of this technique. The test results have shown that full FRP action can be achieved by using a rubber toughened epoxy.

4: The computer model in the form of a non-linear program developed in this study appears to be a good method for prediction of flexural strength, ultimate deflection and failure mode.

REFERENCES

1. DEBLOIS M., PICARD A., BEAULIEU D., Renforcement de poutres en Béton Armé à l'Aide de Matériaux Composites. Advanced composite Materials in Bridges and structures, 1st International Conference, Canada, 1992, P.265-275

2. HAMELIN P., Renforts d'ouvrages en Béton. Textiles à Usages Techniques, 3e Trimestre, N°13, 1994, P.36-38

3. MEIER U., KAISER H., Renforcement des structures par des stratifiés en Fibre de Carbone. Revue composite, N°2, Mars-Avril 1992, P. 42-48

4. SAADATMANESH H., EHSANI M.,RC Beam strengthened with GFRP Plates, I: Experimental Study. Journal of the structural Division, ASCE, V.117, N°11, 1991, P. 3417-3433

Extending the Life of Cables by the Use of Carbon Fibers

Prolongement de la durée de vie des câbles par l'utilisation de fibres de carbone

Verlängerung der Lebensdauer von Kabeln durch Anwendung von Kohlenstoffasern

Urs MEIER
Professor
EMPA
Dübendorf, Switzerland

Urs Meier, born in 1943, graduated in civil engineering from the ETH in Zürich. Since 1971 he has been involved in testing and research on advanced composites and he is now Director of the Swiss Federal Laboratory for Materials Testing and Research (EMPA). He is also Professor at the ETH Zürich.

SUMMARY

Since 1980 research and development has been carried on carbon fiber reinforced plastic (CFRP) cables for cable stayed and suspension bridges. The excellent properties of the parallel wire bundles include corrosion resistance, very high specific strength and equivalent modulus and outstanding fatigue behaviour. The key problem facing the application of CFRP cables, and thus their widespread use in the future, is how to anchor them. A new reliable anchoring scheme produced with gradient materials based upon ceramics and epoxy is described.

RÉSUMÉ

Depuis 1980, des recherches et développements sont réalisés pour des câbles en matière plastique renforcée de fibres de carbone (PRC) pour les ponts suspendus et les ponts à haubans. Ces câbles à faisceaux de fils parallèles présentent d'excellentes caractéristiques telles que résistance à la corrosion, résistance mécanique et module d'élasticité idéalisé et comportement à la fatigue remarquable. La difficulté de leur mise en oeuvre pratique réside dans l'ancrage des faisceaux de fils parallèles. Le présent rapport décrit une nouveau système d'ancrage fiable utilisant un matériau composite à gradient de concentration en céramique/résine époxyde.

ZUSAMMENFASSUNG

Seit 1980 werden Kabel aus kohlenstoffaserverstärkten Kunststoffen (CFK) für Hänge- und Schrägseilbrücken erforscht und entwickelt. Die ausgezeichneten Eigenschaften der Paralleldrahtbündel beinhalten Korrosionsbeständigkeit, sehr hohe Festigkeit, sehr hoher ideeller Modul und hervorragendes Ermüdungsverhalten. Die Schwierigkeit liegt bei der Verankerung der Paralleldrahtbündel. Im vorliegenden Bericht wird ein neuartiges, zuverlässiges auf einem Keramik/Epoxidharz-Gradientenwerkstoff basierendes Verankerungs-System dargestellt.

1. INTRODUCTION

During the past 20 years, the bridge engineering community has experienced more and more damage on stay and suspender cables [1]. Cables are suffering due to increased corrosion and fatigue loading. Most bridge engineers seem to agree that the corrosion and fatigue resistance of such cables has to be enhanced. Researchers proposed modern approaches using non-metallic that means non-corrosive materials [2-5]. The introduction of carbon fiber reinforced plastics (CFRP) instead of steel has been proposed since the early eighties [6]. From the lifetime point of view studies indicated superior results for carbon fiber composites compared to aramid or glass. It was found that the future potential of carbon fibers is highest [7].

The purpose of this work was to develop an anchorage system capable of successfully handling the huge potential of CFRP wires and to achieve the high reliability of parallel wire bundles made of such advanced composites.

2. CARBON FIBERS

The ideal construction materials are based on the elements found principally toward the middle of the Periodic Table. These elements, including carbon, form strong, stable bonds at the atomic level. Materials held together by such bonds are rigid, strong and resistant to many types of chemically aggressive environments up to relatively high temperatures. Furthermore their density is low and raw materials are available in almost unlimited quantities. Carbon fibers are made by carbonizing (charring) an organic polymer or pitch yarn with a fiber diameter normally in the 5-10-micrometer range. There are commercial carbon fibers available with elastic moduli ranging from 230 to 650 GPa and strengths from 3500 to 7000 MPa. The elongation at failure is varies between 0.6 and 2.4 %. The fiber mostly used within this study was the Torayca T 700S having a strength of 4900 MPa, an elastic modulus of 230 GPa and an elongation at failure of 2.1%. The density is 1.8 g/cm^3. The axial thermal expansion coefficient is approximately zero. In October 1994 these fibers were priced at 37 Swiss Francs (27 US $) per kg.

3. CARBON FIBER REINFORCED PLASTIC WIRES

An advanced composite material built up of parallel fibers and a matrix might seem unnecessarily complicated at first sight. Why not simply take a solid carbon wire for the parallel bundle of a cable? Carbon would be, as was pointed out above, a very rugged material having the outstanding properties shared by elements from the middle of the Periodic Table. Such materials have however seen little use as structural materials in the past due to their brittle behavior. A fine notch at the surface or a small flaw within the bulk can lead to a sudden, premature and catastrophic failure of a structural element made of such a material. Considerations of the chemical structure and statistics show that the strength of carbon can be greatly increased and made highly reliable in the form of fibers. Furthermore the crack in a composite wire does not propagate as suddenly as in a solid body. A flaw in a fiber does not inevitably lead to the failure of a structural element. When

a fiber is embedded in an polymer matrix, it can again take up full load a short distance away from a crack. For these reasons CFRP wires are very reliable.

CFRP wires are produced by pultrusion, a process for the continuous extrusion of reinforced plastic profiles. Rovings (strands of reinforcement) are drawn (pulled) through an impregnating tank with epoxy resin, the forming die, and finally a curing area (e.g. radio-frequency exposure). The fibers have a good parallel alignment and are continuous. The fiber volume content of the wires used in this study was in the range of 65 to 70%. The axial properties of a CFRP wire (modulus, strength) can simply be calculated with the rule of mixture. Measured properties are listed in Table 1. The wires used in this project have a diameters of 5 or 6 mm.

Tensile strength σ_u (longitudinal)	3300	MPa
Elastic modulus E (longitudinal)	165	GPa
Density	1.56	g/cm³
Fiber content	68	Vol-%
Thermal expansion (longitudinal)	0.2×10^{-6}	m/m/°C

Table 1 Properties of wires pultruded of T700S fibers

4. CFRP CABLES

The cables are built up as parallel wire bundles. The principal objectives are minimal strength loss of the wires in a bundle as compared to single wires. Since CFRP wires are corrosion resistant there is no corrosion inhibiting compound or grout required. However it is still necessary to protect the wires against wind erosion and ultraviolet radiation attack because the combination of these two attacks could degrade the wires. A poly-tetra-fluoroethylene sheath would be adequate for shielding.

When a load is applied to a cable with a horizontal as well as a vertical span, the elongation consists of the material deformation augmented by a geometric deformation due to the straightening out of the cable sag. The ratio of the applied stress to the observed "strain" (elongation/original distance between the end points) is called the relative equivalent modulus. The low mass density of CFRP cables gives them an advantage in comparison to steel cables with increasing horizontal cable span. Some data are given in Table 2.

Horizontal cable span [m]	Relative equivalent modulus [GPa]	
	Steel	CFRP
0	210	165
500	196	165
1000	163	163
1500	128	162
2000	98	159

Table 2: Relative equivalent modulus for 720 MPa

5. THE ANCHORAGE OF CFRP CABLES

The key problem facing the application of CFRP cables and thus the impediment to their widespread use in the future is how to anchor them. The outstanding mechanical properties of CFRP wires mentioned above are only valid in a longitudinal direction. The lateral properties including interlaminar shear are relatively poor. This makes it very difficult to anchor CFRP wire bundles and obtain the full static and fatigue strength.
The EMPA has been developing CFRP cables using a conical resin-cast termination similar. The evaluation of the casting material to fill the space between the metallic cone of the termination and the CFRP wires was the key to the problem. This casting material, also called load transfer media (LTM) has to satisfy multiple requirements:

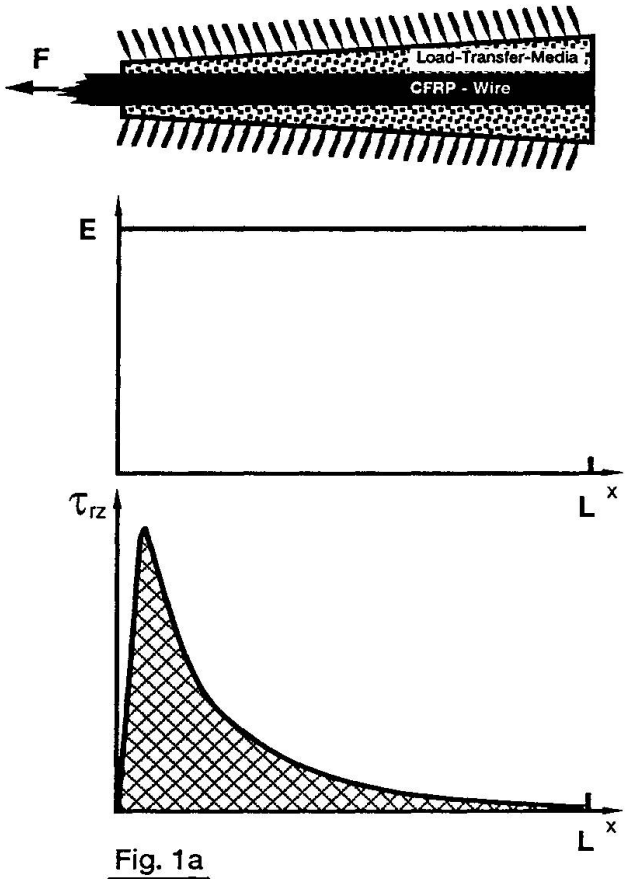

Fig. 1a

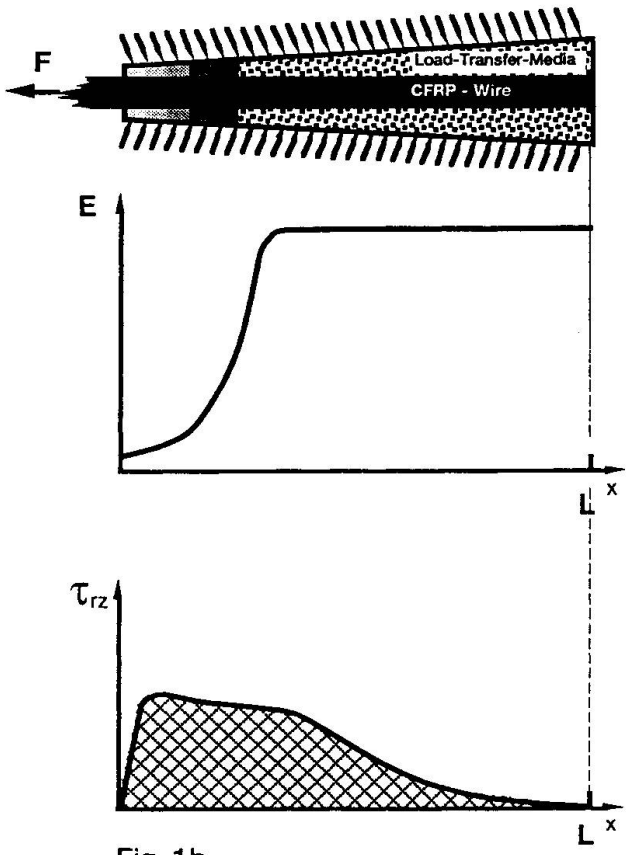

Fig. 1b

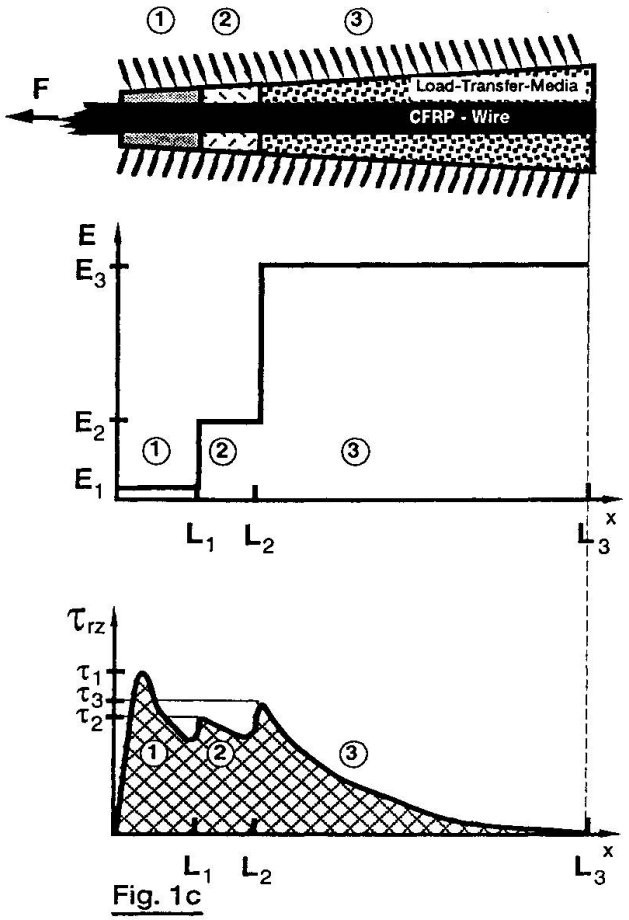

Fig. 1c

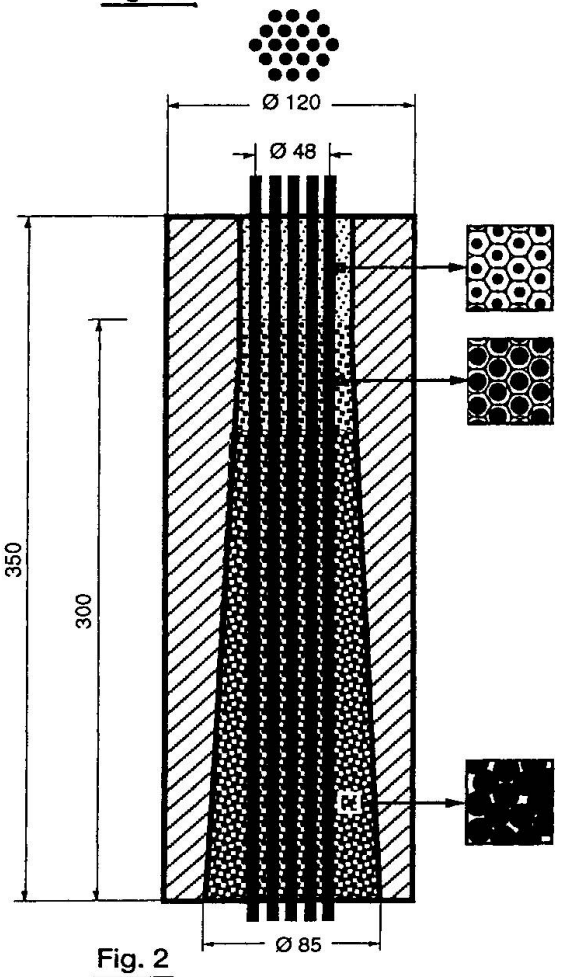

Fig. 2

- The load should be transferred without reduction of the high long time static and fatigue strength of the CFRP wires due to the connection.

- Galvanic corrosion between the CFRP wires and the metal cone of the termination must be avoided. It would harm the metal cone. Therefore the LTM must be an electrical insulator.

The conical shape inside the socket provides the necessary radial pressure to increase the interlaminar shear strength of the CFRP wires. The concept is demonstrated in the Figures 1a to 1c using for this example a one-wire-system. If the LTM over the whole length of the sockets is a highly filled epoxy resin there will be a high shear stress concentration at the beginning of the termination on the surface of the CFRP wire (Fig. 1a). This peak causes pullout or tensile failure far below the strength of the CFRP wire. We could avoid this shear peak by the use of unfilled resin. However this would cause creep and an early stress-rupture. The best design is shown in Fig. 1 b. The LTM is a gradient material. At the beginning of the termination the modulus of elasticity is low and continuously increases until reaching a maximum. This way a shear peak can be avoided. Experiments at EMPA have demonstrated that the 3-step-modulus LTM shown in Fig. 1c is the optimum design from the technical and economic point of view . The LTM is composed of aluminum oxide ceramic (Al_2O_3) granules with a typical diameter of 2 millimeters. All granules have the same size. To get a low modulus of the LTM the granules are coated with a thick layer of epoxy resin and cured before application. Hence shrinkage can be avoided later in the socket. To obtain a medium modulus the granules are coated with a thin layer. To reach a high modulus the granules are filled into the socket (Fig. 2) without any coating. With this method the modulus of the LTM can be designed tailor-made. The holes between the granules are filled by vacuum-assisted resin transfer molding with epoxy resin.

The termination of a 19-wire-bundle is shown in Fig. 2. Many such bundles were tested at EMPA in static and fatigue loading. The results prove that the anchorage system described is very reliable. The static load carrying capacity generally reaches 92% of the sum of the single wires. This result is very close to the theoretically determined capacity of 94% [8]. Fatigue tests performed on the above described 19-wire cables at EMPA showed the superior performance of CFRP under cyclic loads [7]. The anchorage system is patented (CH 01'270/94-3).

6. CONCLUSIONS

Suspenders in suspension bridges are regularly replaced throughout the world. Stay cables caused very high maintenance costs in the past 20 years. Many such cables are in need of replacement. There is no doubt that from the technical standpoint CFRP is today the best suited material for suspenders and stay cables. However since initial cost is the major and often the only parameter used by bridge owners in decision making it is very difficult for CFRP to compete against steel. Even if the carbon fiber price would decrease within the next five years to a level of 25 Swiss Francs (18 US $) per kg (1 kg CFRP is 5.2 times lighter than steel) it will be very difficult for CFRP cables to compete unless the entire life is considered in the costs. A few clients for bridge cables such as the Department of Transport increasingly require more and more life cycle costing to be

carried out. This takes into account the predicted inspection and maintenance costs over the lifetime of the bridge, usually taken as 100 years. Costs are evaluated by calculating the net present value of the expenditure stream using a cash discount rate of typically 6 %. CFRP cables benefit considerably compared with steel in such comparisons.

The most important factor to remember is not the cost per kg of materials, but rather the cost effectiveness of the finished product, installed, considering the life expectancy and the costs of the alternatives. This has worked to the advantage of the CFRP sheet bonding technique for rehabilitation of structures [9] and there is a high probability that this will also be the case for CFRP cables in future.

REFERENCES

[1] WATSON St. C., STAFFORD D., Cables in trouble, Engineered Design and Construction, ASCE, Civil Engineering, April 1988, Vol. 58, No. 4.

[2] RIZKALLA S. H. and ERKI M.-A., Joints, Connections and Anchorages, Advanced Composite Materials with Application to Bridges, Edited by: Mufti A. A., Erki M.-A. and Jaeger L. G., State-of-the-Art Report, Canadian Society for Civil Engineering, May 1991, pages 238-245.

[3] ERKI, M.-A. et. all, Creep Relaxation Characteristics of a Prestressed Kevlar Cable / FRP Tube Structural System, Advanced Composite Materials in Bridges and Structures, Editors: Neale K. W. and Labossière P., The Canadian Society for Civil Engineering, 1992, pages 445-454.

[4] KIM P. and MEIER U., CFRP Cables for Large Structures, Advanced Composite Materials in Civil Engineering Structures Proceedings MT Div/ASCE Las Vegas, 1991, pages 233-244.

[5] YEUNG Y. C. T. and PARKER B. E:, Composite Tension Members for Structural Applications, Composite Structures, Edited by I. H. Marshall, Elsevier Applied Science, London, 1987, pages 309-320.

[6] MEIER U., MÜLLER R. und PUCK A., GFK-Biegeträger unter quasistatischer und schwingender Beanspruchung, Internationale Tagung über verstärkte Kunststoffe, AVK Frankfurt, 1982, Seite 35-1.

[7] MEIER U., Carbon Fiber-Reinforced Polymers: Modern Materials in Bridge Engineering, Structural Engineering International 1/92, pages-12.

[8] RACKWITZ R., Kabel für Schrägseilbrücken - Theoretische Ueberlegungen, VMPA-Tagung, Qualität und Zuverlässigkeit durch Materialprüfung im Bauwesen und Maschinenbau, TU München, 1990, Seite 189.

[9] MEIER U, DEURING M., MEIER H. and SCHWEGLER G., CFRP Bonded Sheets, Developments in Civil Engineering, 42, Fiber-Reinforced-Plastic Reinforcement for Concrete Structures, Editor A. Nanni, Elsevier 1993, pages 423-434.

Steel Fibre Reinforced Concrete with Application in Bridge Repair

Application de bétons de fibres d'acier dans la réparation de ponts

Anwendung von Stahlfaserbeton in der Brückensanierung

Lubin GAO
Associate Professor
China Acad. of Railway Sciences
Beijing, China

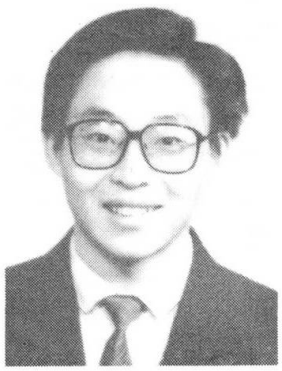

Lubin Gao, born 1965, received his Ph.D. degree in 1989. He was involved in the research of mechanics of materials and structures and now at CARS works on application of steel fibre reinforced concrete and the study and design of cable-stayed bridges.

SUMMARY

This paper presents the main experimental results of steel fibre reinforced concrete. Several practical application cases of steel fibre reinforced concrete to damaged bridge repair are introduced. It can be concluded that this new structural material has potential for being used in bridge repair.

RÉSUMÉ

L'article présente les principaux résultats expérimentaux concernant les bétons avec fibres d'acier. Plusieurs applications pratiques de tels bétons à des réparations de ponts endommagés sont présentés. Ce nouveau matériau a un potentiel d'utilisation pour la réparation des ponts.

ZUSAMMENFASSUNG

Der Beitrag stellt Forschungsergebnisse zu stahlfaserverstärktem Beton vor. Behandelt werden mehrere praktische Anwendungen in der Reparatur beschädigter Brücken. Die Möglichkeiten dieses Werkstoffs in der Brückensanierung erscheinen vielversprechend.

1. INTRODUCTION

In the past decades, steel fiber reinforced concrete has been investigated worldwide. Compared with normal concrete, steel fiber reinforced concrete has higher tensile, compressive, flexual and shear strength. Moreover, steel fiber reinforced concrete has much better ductility than normal concrete and thus its impact toughness and fracture energy rise to the extent as many times as those of normal concrete. Just because of the advantages of steel fiber reinforced concrete over normal concrete, it behaves to be one kind of much potential engineering materials to be used to special engineering such as bridge deck layment, road paving and airport runway engineering. Especially to the repair of damaged structures, steel fiber reinforced concrete behaves to be advantageous over many other engineering materials mechanically and economically.

Up till present, many existing bridges have served over 40 years. High proportion of concrete bridges, manson bridges and bridge piers have been working in the state with cracks and other kinds of damages. If these damaged structures can be suitably repaired or strengthened, they can continue to serve, and thus much finance can be saved. Otherwise, if these structures are not reasonably rehabilitated, the low safety and poor servicibility of the structures may cause a much higher loss of money and human life. In China, many highway and railway bridges at present need to be strengthened. Therefore, how to repair or reinforce these damaged bridges so as to make them work safely is a very significant research topic, which has focused much attention of research institution and administration department. With the development of the research on behavior of steel fiber reinforced concrete, steel fiber reinforced concrete has also been investigated to be applied to the repair of damaged bridges.

2. MECHANICAL BEHAVIOR

2.1 Static Strength

Static strength of steel fiber reinforced concrete may be expressed with following formulus:

$$f=f_m(1+\alpha\, l/dV_f)$$

where

f, f_m —— strength of steel fiber reinforced concrete and concrete matrix respectively

l/d —— characteristic length of steel fiber

V_f —— volumetric content of steel fiber

α —— a factor

From experiments, α is listed in Table 1.

Items	α	μ	δ
Tensile	0.72	1.03	0.14
Shear	0.55	1.01	0.10
Flexual	0.73	1.04	0.08

Table 1 Statistic value of α

Under triaxial compression, strength of steel fiber reinforced concrete is also increased.

2.2 Deformation Behavior

Figure 1 represents stress- strain curves of steel fiber reinforced concrete under uniaxial compression. The grade of concete matrix of the specimens is C35. The content of steel fiber ranges from 0. 0 to 1. 5 percent.

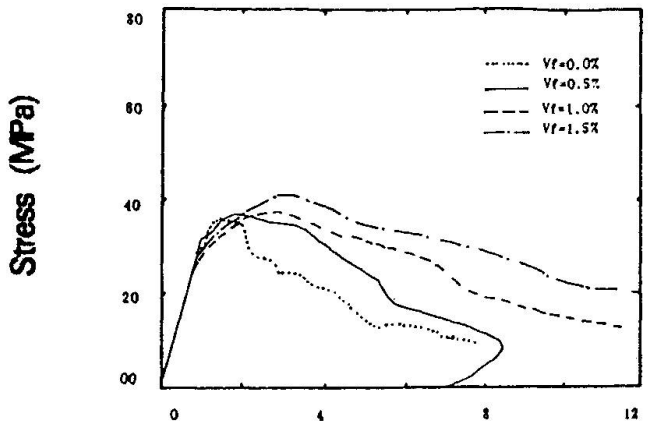

Fig.1 Stress-strain curve

From Figure 1, it can be seen that the addition of steel fiber slightly arises the compressive strength of steel fiber reinforced concrete, but post-peak cracking behavior of steel fiber reinforced concrete is highly improved with the increase of the content of steel fiber.

Therefore, the ductility of steel fiber reinforced concrete becomes much greater than that of normal concrete. The strain corresponding to the peak stress may be expressed as

$$\varepsilon_f = \varepsilon_{fm}(1+0.275l/dV_f)$$

where

ε_f, ε_{fm} —— strain corresponding to peak stress of steel fiber reinforced concrete and concrete matrix respectively

For flexual behavior of steel fiber reinforced concrete, its flexual strength and flexual failure deformation may be expressed as

$$f=f_m(1+0.509l/dV_f)$$
$$w=w_m(1+1.029l/dV_f)$$

where

f, f_m —— flexual strength of steel fiber reinforced concrete and concrete matrix respectively

w, w_m—— flexual deformation of steel fiber reinforced concrete and concrete matrix respectively

For tensile behavior, peak stress and corresponding strain can be expressed with following formulus

$$f=f_m(1+33.4V_f)$$
$$\varepsilon = \varepsilon_m(1+46.5V_f)$$

where

f, f_m —— tensile strength of steel fiber reinforced concrete and concrete matrix respectively

ε , ε_m —— tensile strain of steel fiber reinforced concrete and concrete matrix respectively

2.3 Fracture Energy and Fracture Toughness

From experiments, it can be obtained that fracture energy and fracture toughness of steel fiber reinforced concrete can be expressed as

$$G_F=G_{Fm}(1+7.788l/dV_f)$$
$$G_{IC}=G_{ICm}[1+1.997(l/dV_f)^2]$$

where

G_F, G_{Fm}—— fracture energy of steel fiber reinforced concrete and concrete matrix respectively

G_{IC}, G_{ICm} — fracture toughness of steel fiber reinforced concrete and concrete matrix respectively

Figure 2 represents load- displacement relation of steel fiber reinforced concrete under three point bending of fracure toughness test

specimens.

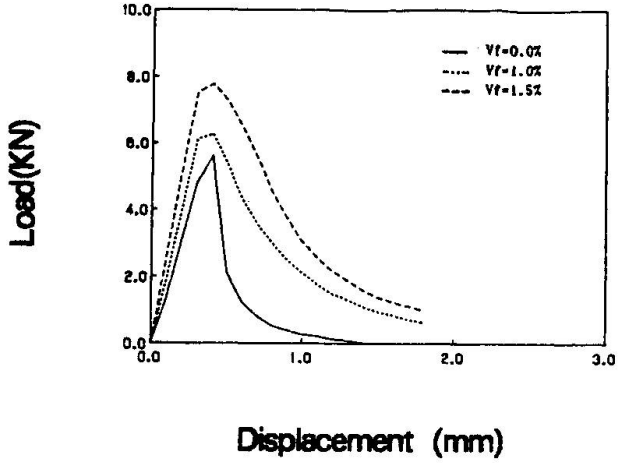

Fig. 2 Load-displacement curve

2.4 Fatigue Behavior

From experiments, fatigue behavior of steel fiber reinforced concrete is much better than that of normal concrete. Under uniaxial compressive fatigue, fatigue life of steel fiber reinforced concrete may be elongated by 20 percent of that of normal concrete. Under flexual fatigue, fatigue life of steel fiber reinforced concrete can reach 1 to 7 times of that of normal concrete. S- N relation of steel fiber reinforced concrete under flexual fatigue can be described with

$$S=A-B\log N$$
$$A=0.894+15.7V_f$$
$$B=0.051+1.5V_f$$

Based on the experimental results discussed above, it can be assumed that steel fiber reinforced concrete may be one kind of effective materials to damaged bridge repair.

3. APPLICATION TO BRIDGE REPAIR

3.1 Yanjia River Bridge

Yanjia river bridge, constructed in 1907, with the length of 92m, is a railway bridge situated near Dalian City, Liaoning Province on the

railway line from Changchun to Dalian. It consists of 3 spans of steel girders. The height of bridge piers is 20.6m. The bridge is situated in the earthquake region. Because of long time service, its manson piers appeared many cracks. When trains passed the bridge, it vibrated with large amplitude. Transport administration department asked to strengthen the piers of the bridge. From 1985 to 1986, the repair project was worked out. Total amount of 650 cubic meters of steel fiber reinforced concrete and 60 tons of steel fiber were used in the project

After the repair, vibration amplitude of bridge pier No.1 is reduced to 0.29mm from previous 1.22mm, and the amplitude of pier No.2 is reduced to 0.3mm from 1.06mm.

3.2 Fengtai Crossing Bridge

Fengtai crossing bridge is a frame structure bridge with the span of 14 .9+17.5+17.5+14.9, situated at Fengtai, Beijing. During construction, serious cracks appeared on the walls. According to the engineering requirement, steel fiber reinforced concrete was selected to be applied to the bridge repair. From September to Octomber, 1990, the repair work was completed within only one month. More than 600 cubic meters of steel fiber reinforced concrete and 80 tons of steel fiber were used. The service state of this bridge after repair behaves very satisfactory.

3.3 Santaizi River Bridge

Santaizi river bridge was built in 1940's, situated on the railway line from Shenyang to Shanhaiguan. Reinforced concrete girders deteriorated very seriously. In 1987, under the condition of not stopping traffic, steel fiber reinforced concrete was used to repair the concrete girders.

4. CONCLUSION

Steel fiber reinforced concrete has good physical and mechanical behavior. Therefore, it can be efficiently applied to damaged bridge repair. Many practical applications of steel fiber reinforced concrete have also proved this conclusion.

REFERENCES

1. CHENG Q. G., ZHANG L., GAO Lubin, Constitutive Relation and Fatigue Damage of Steel Fiber Reinforced Concrete, China Academy of Railway Sciences, Beijing, 1991
2. GAO Lubin, Constitutive Theory for Concrete, Southwest Jiaotong Uni-Versity Publishing House, 1993

Improved Corrosion Protection for Parallel Cables of Cable-Stayed Bridges

Amélioration de la protection contre la corrosion des câbles porteurs de ponts haubanés

Verbesserter Korrosionsschutz für Parallelkabel von Schrägseilbrücken

Bernd E. REINER
Technical Advisor
Sika Chemie GmbH
Stuttgart, Germany

Bernd E. Reiner, born in 1946, was trained in applied chemistry and specialises in corrosion protection and protective coatings for steel, galvanised surfaces and concrete structures, in particular bridges and railway structures. He is responsible for coatings technology transfer within the Sika group.

SUMMARY

The paper gives an overview of cable failures, corrosion protection developments and current practice, outlining the need for high-performance protective measures when parallel wire stay cables are exposed to high stress. It then describes the development of corrosion inhibitive, flexible grouts with superior performance, permitting cable duct injection before installation or even in the workshop in order to arrive at higher long-term protection levels and ease of installation.

RÉSUMÉ

L'article fait état des désordres dus à des câbles défectueux, mentionne l'historique et les pratiques courantes de protection contre la corrosion en soulignant la nécessité de réaliser une protection à haute performance dans le cas des câbles porteurs (à fils parallèles) soumis à de fortes contraintes. Il décrit ensuite le développement et les performances des coulis flexibles permettant une injection dans la gaine des câbles avant leur mise en place ou même en atelier, afin de parvenir à de hauts niveaux de protection à long terme et conserver une mise en oeuvre facile.

ZUSAMMENFASSUNG

Der Artikel gibt eine Übersicht von Schäden an Brückenseilen und deren Ursachen. Die historische Entwicklung des Korrosionsschutzes und heutige Praxis werden zudem gezeigt. Die Notwendigkeit besonders hochwertiger Schutzmassnahmen im Falle von Paralleldrahtbündeln für hochbeanspruchte Schrägkabel wird besonders herausgestellt. Anschliessend wird die Entwicklung und Anwendung flexibler Füllmassen mit aktiver Korrosionsschutzwirkung und überragendem technischen Leistungsvermögen beschrieben, die bereits unter kontrollierten Bedingungen im Werk injiziert werden können und somit die Sicherheit erhöhen und den Einbau erleichtern.

1. INTRODUCTION

A number of spectacular shortcomings and failures of cables on stayed bridges over the last couples of years have sincerely alarmed the engineering community. The article "Cables in Trouble" [1] and subsequent publications in numerous countries resulted in a world-wide wave of most alarming damage reports becoming public knowledge. A typical example is Germany's "Koehlbrand" bridge in Hamburg, where 25 broken wires were detected in 1976 on a routine inspection, i. e. only 2 years after opening of the bridge. As a consequence, all cables had to be exchanged in 1978, costing more than US$ 10 mio at the time.

1.1 Causes

A very thorough survey on causes of damage and a comprehensive list of current methods (by design and selection of materials) for corrosion prevention is contained in the Saul/Svensson publication "On the corrosion protection of stay cables" [2].

There is a multitude of causes and a variety of corrosive effects involved, the main ones being:

- "conventional" atmospheric corrosion caused by presence of electrolyte and oxygen, accelerated by corrosion stimulators as present in industrial or marine atmosphere, namely chlorides and sulphates. Higher concentrations of chlorides, e.g. deriving from de-icing salts, are known to cause severe pitting.

- stress corrosion cracking/fatigue corrosion caused by the much higher dynamic stresses compared to conventional suspension bridges. There are still disputes amongst metallurgists whether certain high tensile steels may be more susceptible to this type of corrosion than mild steel.

- corrosion caused by contact of different metals/alloys in moist, salty conditions (bimetallic corrosion).

2. CLOSED COIL CABLES

2.1 Previously employed Protective Methods

There is a long reference record of reliable long-term protective systems for Locked Coil Cables of conventional suspension bridges. However, the majority of them cannot be employed anymore these days for environmental reasons as they were often based on red lead combinations (practically non-degradable and known to cause blood diseases) or contained zinc chromate (considered carcinogenous). Furthermore, many of them - as one learned the hard way - cannot cope with the stresses occuring on large stay bridges as these materials tend to embrittle in the long run.

2.2 Current Practice

Important improvements have been made in the design an manufacture of the cables themselves, e.g. by reducing the alloy content of copper, sulphur and phosphor, thus also increasing fatigue strength or by employing more sophisticated hot dip galvanizing methods with better controlled pre-treatment and thickness.
Modern protective systems are usually based on polyurethane combinations, using flake pigments in the outer coatings to arrive at maximum UV, water vapour and oxygen diffusion resistence ("barrier principle") [3]. The German Federal Department of Transport recently published a very complex draft standard on supply and testing requirements for coatings, sealants and injection resins for cables [4]. Typical (and clearly defined) requirements of the cured materials include flexibility (bending test), permanent elongation ability, vapour diffusion resistance, adhesion on new and old galvanized surfaces after artificial ageing, resistance to salt spray, simultaneous action of condensed water and sulphur dioxide, oil resistence, intercoat adhesion and compatibility with other substances found on/in cables. Weathering tests, pinhole detection and dynamic exposure (pulsating load) form also part of the approval procedure. This Standard should inevitably lead to much longer life and maintenance cycles.

Bridge Cables - Corrosion Protection in Germany

System	Function	Parallel cables	Locked coil
2K-Epoxy	Primer for steel and galvanized surfaces		+
2K-PUR solventfree	Low viscosity injection material	+	
2K-PUR solventfree	Sealant (flexible grout)	+	+
2K-PUR high-solid	High-build flexible protective coating		+
2K-PUR	Topcoat, UV-resistant, flexible	+	+

According to Technical terms of delivery "TL-KOR-Seile", Bundesministerium für Verkehr.(Department of Transport)

3. PARALLEL WIRE CABLES

These cables consist of a bundle of straight or slightly twisted wires (diameter 7mm or 1/4 in.), connected to steel anchor heads. This type of stay cable was originally developed from post-tensioning systems and was introduced in the early sixties. General requirements for these cables were published in the USA in 1986 [5].

3.1. Previously employed Protective Systems

The outer protective shell consists normally of UV-resistant Polyethylene or stainless steel ducts which are filled with a cementitious grout injection after erection. The grout is destined to provide active corrosion protection by its high alkalinity. Whereas the PE ducts (sometimes wrapped with PVC-tape) present a reasonable reference record (see [2]), the grout - although perfectly ok on smaller bridges - presented problems on some large bridges due to its weight (density) during application and its relative brittleness in the dynamic exposure, leading to cracking and water ingress.

3.2 Current Practice

The most widespread practice for protection are shop-fabricated cables incorporated in PE ducts. This permits optimum quality control during fabrication and exactly predetermined length. They are transported to site on coils, i.e. relatively well protected from the environment, and then injected with grout after installation. Whilst the performance of the cementitious grout can be considerably improved by incorporating appropriate admixtures reducing shrinkage, easing injection and increasing flexibility, injection on site is a lengthy, tricky process which may require extensive scaffolding in case of a larger bridge. Although the right admixtures (e.g. plasticizers and retarders) would permit large injection shots, this is in practice limited by the pressure resistance of the ducts as one does not only have to overcome friction but also the hydrostatic pressure in the inclined duct.
In addition to the standard protection, i.e. PE duct and grout, other protective layers were sometimes used, e.g. epoxi-coated wires (Quincy bridge, Illinois/USA) [6], directly PE extruded wires (Kemijoki River bridge, Finnland and Annacis Bridge, Vancouver/Canada). Galvanized wires were also used but should not be used in direct contact with alkaline grout to avoid reaction and possible hydrogene embrittlement, so that an additional polyester coating was employed at the Meiko-Nishi Bridge in Japan.

4. CONCLUSIONS

It is obvious that completely shop-fabricated cables offer considerable advantages with regards to optimum fabrication and injection conditions and in particular with regards to installation time and procedure on site. This was successfully achieved with a number of bridges already, using injection materials of permanently plastic consistency like grease (Tähtiniemi Bridge, Finnland) or petroleum jelly (Annacis Bridge, Vancouver). However, considering that sun radiation on a black PE duct may easily raise temperature above +70°C (158°F), such materials tend to become liquid and may leak out, presenting - apart from the loss of corrosion protection at the top - a considerable risk of environmental pollution. Field tests using nitrogene gaz filling to cut out moisture (as recently demonstrated on a Rhine bridge in Germany) were technically successful but proved to be excessively expensive, requiring permanent monitoring.
It is obvious from the above, that non-thermoplastic, permanently flexible injection materials offers evident advantages over the other solutions presented. In 5 years research work, the Japanese Yokohama Rubber Company developed a Polybutadiene Polyurethane Compound which was used for cable injection of the Iwakuro-jima and Hisuishi-jima cable stay bridges of the Honshu-Shikoku link in 1986/87, however injected on site [7]. This solution is said to work perfectly well but proved to be very expensive, required the use of stainless steel ducts due to the flammable nature of the injection material and relied exclusively on its imperviousness to water, i.e. offered no active corrosion protection.

5. CONSEQUENCES

In 1982, the German Sika subsidiary began research work in the same direction, resulting in a 2-pack, flexible, solvent-free polyurethane combination incorporating corrosion inhibitors. In 1985, 50 tons were successfully employed for the corrosion protection of 15 m long, prestressed parallel wire rock anchors on a large hydroelectric site in Bulgaria. 4 more similar projects followed during the next 2 years, including a nuclear power station.

Until 1987, following a performance specification by the legendary bridge designers Leonhardt, Andrae & Partner, Stuttgart, the injection material, now named Icosit KC 320, was further optimized and subsequently used for the first time on a cable stay bridge in Pforzheim/Germany. After some more applications in the field and extensive full scale tests in the workshops of one of the most renown cable manufacturers in Switzerland, injecting cables, rolling them on a coil and leaving them in this condition for some weeks before unrolling and testing, the product was fully released. In 1989, stay cables were manufactured and injected with the flexible Polyurethane at the workshops of Messrs. Spanstaal in Utrecht/Netherlands. The cables were subsequently rolled on coils, shipped to England and installed at the Connaught Swing Bridge, London Docklands. Already in 1986, the material had undergone extensive corrosion tests, including salt spray, and proved its outstanding performance [8]. As corrosion protection does not only rely on the displacement of humidity but also on the active effect of the hydrophobic corrosion inhibitors embedded into the polyurethane matrix, the protection effect is also achieved in case of larger movements and even in case of cracks in the PE ducts (which are quite often reported in literature [2]). The pot-life limit of 30 - 60 minutes permits large injection shots.

Viscosity Development at 20°C

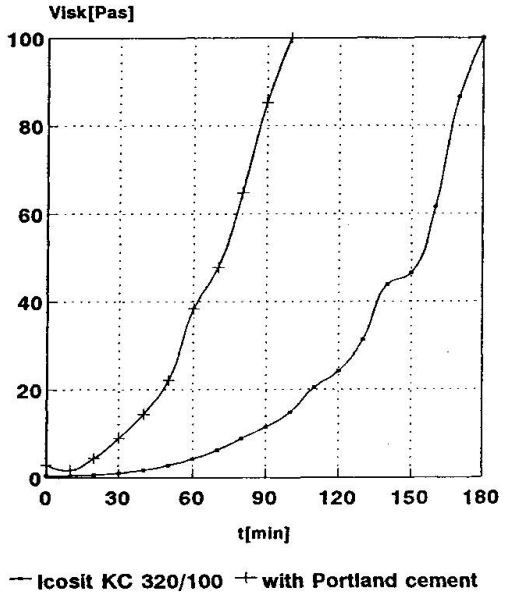

Curing progression at 20 C

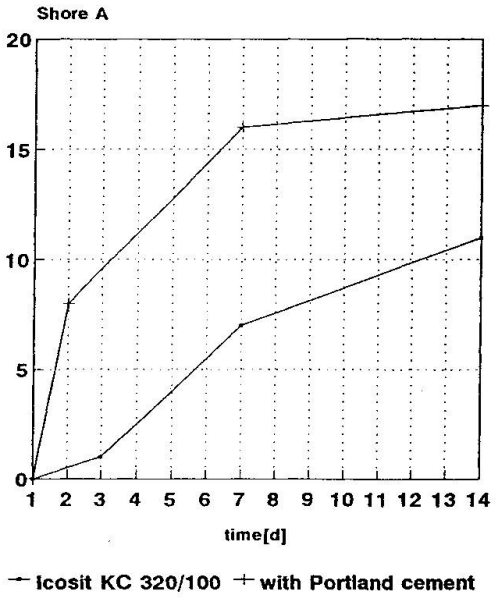

Optimum economy can be achieved by mixing the injection material up to a proportion of 1:1 by weight with Portland cement. Laboratory comparison tests (1000 hours salt spray) proved that the alkalinity and the affinity of the cement to steel provided an even better adhesion and maximum corrosion protection, in fact considerably superior to all other systems tested.

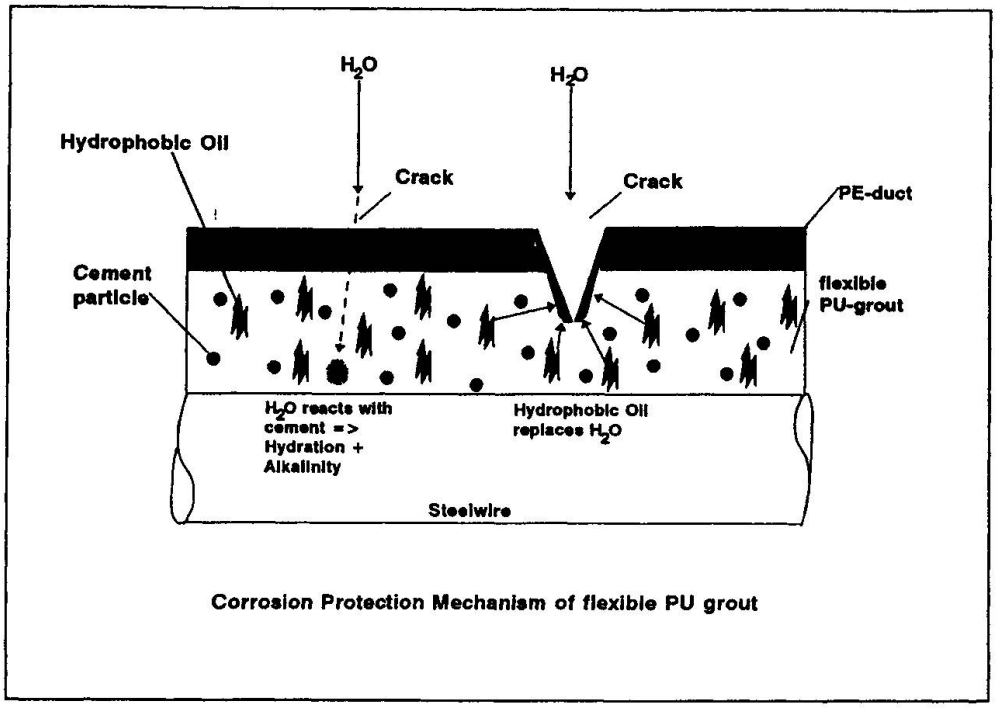

Corrosion Protection Mechanism of flexible PU grout

In case of long, thick parallel cables, workshop injection and transport on coils might sometimes not be possible. However, a competitive advantage will still be gained by injecting the cables on site before installation, as long as they are laid out on the bridge ramps. This avoids the erection of extensive scaffolding as normally necessary for injection of the cable ducts after installation.
The use of the corrosion-inhibitive, flexible polyurethane grout does undoubtedly increase the safety factor of parallel stay cable corrosion protection considerably, particularly where high dynamic stresses and corrosive environments are concerned. From the ecological point of view, the cured polyurethane grout can be regarded as inert.

BIBLIOGRAPHY:

1. WATSON S. C./STAFFORD D.: Cables in Trouble. Civil Engineering, April 1988, pp. 38-41
2. SAUL R./SVENSSON H. S., On the Corrosion Protection of Stay Cables. Stahlbau 6/1990, pp. 165-176. Wire Rope News and Sling Technology. August 1991, pp. 14-29
3. FUNKE, Prof. Dr. W.: Recent discoveries on the working principle of active pigments and the barrier principle. Lechler Chemie Symposium 1984
4. Bundesanstalt fuer Strassenwesen, Germany, TL-KOR-Seile. draft standard 20.07.1994
5. Post tensioning Institute Ad Hoc Commitee on Cable-Stayed Bridges, Recommendations for Stay Cable Design and Testing. USA, Jan. 1986
6. KULICKY, J. M./WALDNER, H. E./PRICKET, J. E.: Design of the Cable-Stayed Mississippi River Bridge at Quincy, Illinois. Transportation Research Council, Record 950, pp. 35-50
7. KOBAYASHI, Dr. T./KATO, Y./MORI, T.: High Polymer Type Anticorrosion Materials for Cables, Bangalore, India, Oct. 1988
8. FUNKE, Prof. Dr. W.: Expert opinion on the corrosion protective effect of a polyurethane/oil combination as injection material for parallel wires, Istitut fuer Technische Chemie, Universität Stuttgart, 18.9.86 (unpublished)

Mechanical Model for Lifespan Analysis of Bridges

Modèles mécaniques pour l'étude de la durée de vie des ponts

Mechanisches Modell für die Lebensdauer von Brücken

Carmelo MAJORANA
Researcher
Universita di Padova
Padova, Italy

Anna SAETTA
Researcher
I.U.A.V.
Venezia, Italy

Roberto SCOTTA
Ph.D. Student
Universita di Padova
Padova, Italy

Renato VITALIANI
Associate Professor
Universita di Padova
Padova, Italy

SUMMARY

A computational procedure for the evaluation of material damage under changes of loads, actions and as a result of aggressive chemicals, is presented. The proposed approach is based on a numerical formulation to analyse thermal, hygrometrical and chemical effects, to simulate the ion diffusion into the porous material and then to determine the mechanical behaviour of the damaged material. Structural life span is finally estimated through the effects of chemical and mechanical processes affecting both concrete and steel. Numerical examples are shown.

RÉSUMÉ

Une méthode de calcul pour évaluer les dégâts aux matériaux soumis à des variations de charges, d'actions et d'agents chimiques diffus, est présentée. L'approche est basée sur une formulation numérique des effets thermiques, hygrométriques et chimiques, en simulant la diffusion d'ions dans le matériau poreux et en déterminant le comportement mécanique du matériau endommagé. La durée de vie de l'édifice est évaluée au moyen des effets des procédés chimiques et mécaniques combinés agissant sur le béton et l'acier. Des exemples numériques sont donnés.

ZUSAMMENFASSUNG

Eine Berechnungsmethode zur Bewertung der Schäden an den Materialien, die verschiedenen Belastungen, Einflüssen und weitverbreiteten chemischen Stoffen ausgesetzt sind, wird dargestellt, um schliesslich die Lebensdauer der Brücken und Bauten im allgemeinen zu bewerten. Der vorgeführte Versuch gründet sich auf eine zahlenmässige Formulierung, die aufgestellt wurde um die thermischen, hygrometrischen und chemischen Auswirkungen zu analysieren, indem eine Diffusion von Ionen im porösen Material simuliert wird, um danach das mechanische Verhalten des Materialschadens zu ermitteln. Zuletzt wird die Lebensdauer der Bauten geschätzt, die sich aus den Auswirkungen der Vereinigung von chemischen und mechanischen Vorgängen ergeben, die auf Stahlbeton und Stahl einwirken. Es werden numerische Beispiele gezeigt.

1. INTRODUCTION

The evaluation of mechanical and durability performance of bridges and building structures is a relevant goal in civil engineering. Together with mechanical and thermal actions, main causes of deterioration of concrete structures are steel corrosion, induced by the action of chloride and carbonation, and concrete damage due to its reaction with calcium chloride and sulphates salts. For this purpose, a computational analysis of the stress state in connection with thermal, humidity and chemical species changes, is carried out in this paper with the aim of estimating lifespan extension of structures. The development of suitable algorithms based on the finite element method has been performed in view of producing efficient procedures for the analysis of bridges and structures. The evolutions of humidity, temperature and contaminant concentrations are considered through partially coupled diffusive mechanisms; chemical effects are analyzed studying in particular calcium chloride or sulphate ions diffusion. Then the mechanical effects are evaluated in terms of stresses, strains and material damage.

The temperature and humidity fields are described generalizing a formulation presented in [1,2], to take into account saturated-unsaturated behaviour (see Ref. [3]), within the framework of a purely diffusive model. More complete formulations considering the whole humidity range, together with phase changes, like evaporation is developed in [4].

The evolution of the chemical species, like e.g. chlorides, sulphates, carbon dioxide, etc., into a porous medium exposed to a contaminant environment, is a complex phenomenon involving various factors such as the gas or ion diffusion and the ion flux due to the solution permeation through the material [5]. One of the main new features of this paper is to take into account the dependence of the chemical species diffusivity on the damaging of the material.

As far as the mechanical aspects are concerned, in Ref. [6] viscoelastic models including isotropic damage effects have been considered, substituting in the stress-strain relationship expressed as a Stieltjes integral, different definitions of the standard relation based on the concept of the so called effective stress as in [7], or different definitions of the relaxation or creep functions to take into account material damaging [8]. Here account is taken also of anisotropic damage as in [9] and its coupling with viscosity [10] to better model the time transient behavior of concrete. The mechanical aspect of the problem is strictly linked to the diffusive one since the chemical reaction between cement hydrates and diffusing species modifies the mechanical behaviour of the material as shown in [11]. Moreover both the sulphate and the calcium chloride attacks appear macroscopically through swelling and cracking of the original material.

The space discretization of the model is carried out using the finite element method and solved numerically. The transient numerical simulation allows to analyze the evolution of the temperature, relative humidity, ions concentration, damage parameter, stresses and strains.

The knowledge of the above behaviour allows to draw a durability evaluation in terms of residual actual load capacity of the investigated structure compared with the external applied loads. The proposed tool also allows the forecasting of the expected service-life time of structures in whatever different aggressive environment.

2. GOVERNING EQUATIONS

The governing equation of moisture flow is derived following the lines of References [2,3]. It is assumed that the various phases of water in each pore (vapour, capillary water and adsorbed water) are in thermodynamic equilibrium with each other [2] and with the solid skeleton.

Non isothermal moisture flow is governed by a nonlinear parabolic equation of diffusive type as reported in [1,2,3]. The energy transport through the concrete is governed by a similar nonlinear parabolic equation. Both equations are used here, as explained below, being the complete formulation given in Refs. [3,12].

The flow of chemical species through concrete, coupled with non isothermal moisture one, is described by the following relationship:

$$\frac{\partial C}{\partial t} = \mathrm{div}(D_c \cdot \nabla C) + \frac{C}{\alpha} \cdot \frac{\partial w}{\partial t} \tag{1}$$

where the first term of the R.H.S. represents the diffusion mechanism and the second one takes into account the ions dragged by water flux [5]. In eq.(1) C is the diffusive species concentration (e.g. chloride, sulphate); w is the moisture content, D_c is the actual diffusivity coefficient of the material and α is a binding coefficient. The diffusivity of aggressive species $D_c = \beta \cdot D_{c,ref}$ is assumed to be dependent on pore humidity, temperature and degree of cement hydration through $D_{c,ref}$ described in [5]. To consider the damaging effect of the chemical pollutants, such diffusivity is assumed increasing with the parameter β which is defined as follows:

$$\beta = \chi + (1-\chi) \Big/ \left[1 + \left(2 \cdot C/C_f\right)^4\right] \tag{2}$$

where χ is the ratio between the residual strength corresponding to $C=C_f$ (i.e. the reference concentration of the diffusing species for which the degradation process attains its maximum effect) and the initial strength. χ parameter is related to the material characteristics and the aggressive agent (in particular $\chi=1$ for undamaged material).

The time transient boundary conditions associated to non isothermal, moisture and ion diffusion equations may be either of the following types: prescribed humidities, temperatures, and chemical concentrations or prescribed water vapour flows, heat flows and flux of species concentration. For the ion transport analysis, a more realistic boundary condition able to reproduce the ion deposition rate from the external environment and the natural washing effect of rains, can be used [5].

The equilibrium equations can be written once suitable hypotheses on mechanical behaviour are posed. Here, a formulation based on viscoleasticity coupled with damage is considered. The geometrically nonlinear approach has to be adopted because if anisotropic models are taken into account, the principal directions of damage rotate during the process. Hence the variables which control the evolution of damage (true strains), rotate also and must be referred to evolving geometrical configurations even if strains remain small. Here we consider such situations with small strains, hence the heat and mass transfer formulation stated before within a linearized geometrical framework can be considered sufficiently accurate.

The viscoelastic constitutive relationship taking into account damage effects presented in [6] is written using the second (symmetric) Piola-Kirchhoff stress tensor $\underline{S}$ and the associated Lagrangian strains. Elastic damage at finite strains is incorporated in the procedure, reducing the free energy by the factor $\|(\underline{1} - \underline{d})\|$, where $\underline{d}$ is the damage tensor. In the particular case of isotropic damage behaviour, the process is controlled by a scalar variable $d \in [0,1]$. As in the above paper, the damage model is based here on the maximum strain concept [7].

The diffusion of sulphates salts and calcium chlorides affects the cementitious materials inducing a reduction of their mechanical strengths [11]. Therefore in the numerical algorithm the initial elastic Young modulus of the material is reduced according to the parameter β, eq.(2). Damage tensor is also affected by β parameter as follows: $\underline{d} = \underline{d} + (1- \beta)(\underline{1}-\underline{d})$. The physical justification can be found in [11]. As stated before, the value of parameter χ depends mainly on the material characteristics and the type of chemical attack. Typically the value of the reference concentration C_f varies within the range 4-8% in weight of cement content. For OPC paste specimens with w/c ratio 0.35, immersed in 30% $CaCl_2$ solution, assuming $\chi=0.25$ and $C_f=6\%$ a good fitting with the experimental data reported by Collepardi in [11] was achieved, as shown in fig. 1a.

Taking into account the constitutive relation, a new form of the equation of motion is obtained, as shown in [12]. The space discretization by means of finite element technique is reported in the

same Reference. After solving the resulting system of algebraic equations, the strains can be calculated. The stresses are then obtained by the standard procedure for viscoelasticity with damage [13]. The procedures were implemented in the finite element code DAMVIS.

3 - NUMERICAL COMPUTATIONS

The numerical simulation of a typical bridge cross-section was performed to check the evolution of the humidity, thermal, chloride, stress, strain and damage fields during construction. The building up time was divided into 75 time steps of variable size (maximum time = 6 years). Since the procedure takes into account construction phases, it was assumed as completely built-up at time t = 180 days from the beginning of the simulation. The boundary conditions for humidity and temperature were assumed constant during all the period, respectively $R.H.$ = 50% and T = 20 °C. As far as the chloride diffusion is concerned, the effect of calcium chloride in reducing the mechanical characteristics of the concrete was considered. After 200 days from the beginning of the simulation, a chloride deposition rate on upper surface of bridge, with a sinusoidal trend during the winter period (maximum value 10 g/mq/day), constantly equal to zero during the summer period, was used. A constant washing away effect and the contribution of a upper bituminous layer 2 cm thick in reducing the chloride penetration was also considered. The typical chloride concentration curves along a vertical section of the bridge slab are drawn in fig. 1b. The maximum surface concentration is reached at the end of the winter period when the external deposition stops; the washing away effect produces the drop of the surface concentration that reaches its minimum at the end of the summer period. The chosen value of the parameters for chemical analysis can be found in [5].

With the finite element mesh shown in fig. 2a the time transients of relative humidities, temperatures (including generation of heat of hydration), diffusion of chemical species, and the corresponding stresses and strains in the viscoelastic damaging material were found. In figs. 2b,c,d,e,f are shown at time 6 years the relative humidities, max. principal stresses without chloride, damage without chlorides, max. principal stresses with chlorides and damage with chlorides. The complex stress state found is the result of competing effects of contractive (like shrinkage) or expansive (thermal and chemical) types. Damage is concentrated where chemical attack occurs and shrinkage (although smoothed by creep effects) gives rise to high local strains.

4. CONCLUSIONS

The presented model allows a realistic evaluation of the stress-strain states in multiphase materials like concrete in several engineering situations. The model incorporates diffusive thermal, hygral and ionic species fields, coupled with the mechanical one. The latter is strictly connected to the previous ones and embodies viscoelasticity coupled with damage to simulate a typical time transient behaviour of concrete accounting for material degradation. The feasibility of the finite element formulation here adopted has been shown in complex structures such as a bridge section, giving a picture of the stresses and strains developed in the domain of interest during an assigned time transient. Further efforts are under development in improving the damage model including itself the chemical attacks action and moreover to better justfy experimentally the parameters used in the numerical analysis.

5. REFERENCES

1. Bazant, Z.P., "Mathematical modeling of creep and shrinkage of concrete", J.Wiley & Sons, 1988.
2. Bazant, Z.P., Najjar, L.J., "Nonlinear water diffusion in nonsaturated concrete", Materials and Structures, RILEM, Paris, Vol. 5, n. 25, 1972, pp. 3-20.
3. Schrefler, B., Simoni, L., Majorana, C., "A general model for the mechanics of saturated unsaturated porous materials", Materials and Structures, Paris, n. 22, 1989, pp. 323-334.
4. Baggio, P., Majorana, C., Schrefler, B., "Thermohygrometric and mechanical analysis of concrete by a finite element method", 8th Int. Conf. on Num. Meth. in Thermal Problems, Swansea, U.K., july 11th-16th, 1993.
5. Saetta, A., Scotta, R., Vitaliani, R., "The numerical analysis of chloride penetration in concrete", ACI Material Journal, Vol. 90, n. 5, 1993, pp. 441-451.
6. Majorana, C.E., "Influence of damage in thermohygrometric and mechanical behaviour of the continuum", Giornale del Genio Civile, Vol. 7-9, 1989, pp. 211-236, (in italian).
7. Lemaitre, J., Chaboche, J.L., Mecanique des materiaux solides, Dunod, Paris, 1988.
8. Bazant, Z.P., Prasannan, S., "Solidification theory for concrete creep. II - verification and application, Journal of Engineering Mechanics, Vol. 115, N. 8, 1989, pp. 1704-1725.
9. Ramtani, S., "Contribution a la modelisation du comportment multiaxial du béton endommagé avec description du caractére unilatéral", Thèse de doctorat présentée a l'Université Pierre et Marie Curie, Paris, 1990.
10. Kachanov, L.M., "Introduction to continuum damage mechanics", Mechanics of elastic stability, ed. H.H.E. Leipholz e G. Oravas, Martinus Nijhoff Publishers, Dordrecht 1986.
11. Collepardi, M., Coppola, L., Monosi, S., "Chemical attack of calcium chloride on the portland cement paste", Il Cemento, n. 2, pp. 97-104, 1989.
12. Majorana, C.E., Vitaliani, R., "Finite element modeling of creep and shrinkage of concrete including damage effects", Proc. 5th Int. RILEM Symposium Creep and Shrinkage of Concrete, no. 22, Barcelona, RILEM, Sept. 6-9, 1993, pp. 421-426.
13. Majorana, C.E., Vitaliani, R., "Numerical modeling of creep and shrinkage of concrete by finite element method", 2nd Int. Conf. on Computer Aided Design in Concrete Structures, SCI-C, Zell-Am-See, Austria, 4th-6th april 1990, pp. 773-784.

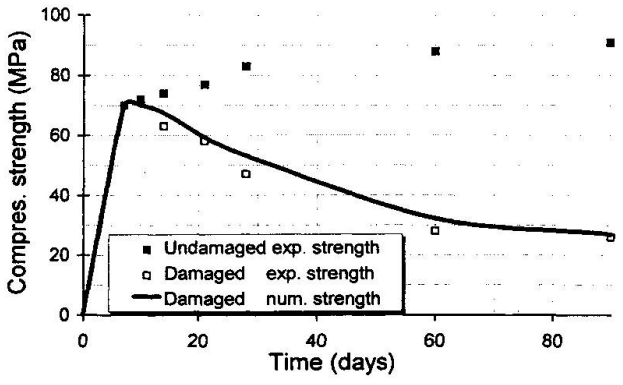

Fig. 1a: numerical simulation of strength decrease of OPC cement paste specimens immersed in a 10% $CaCl_2$ solution (experimental data by Collepardi [11]).

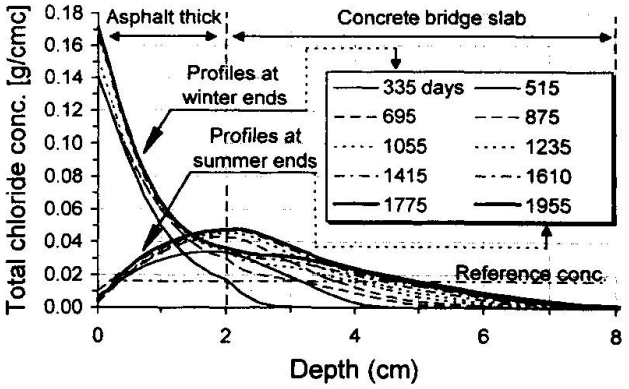

Fig. 1b: chloride concentration profiles along a vertical section of the bridge slab at various time.

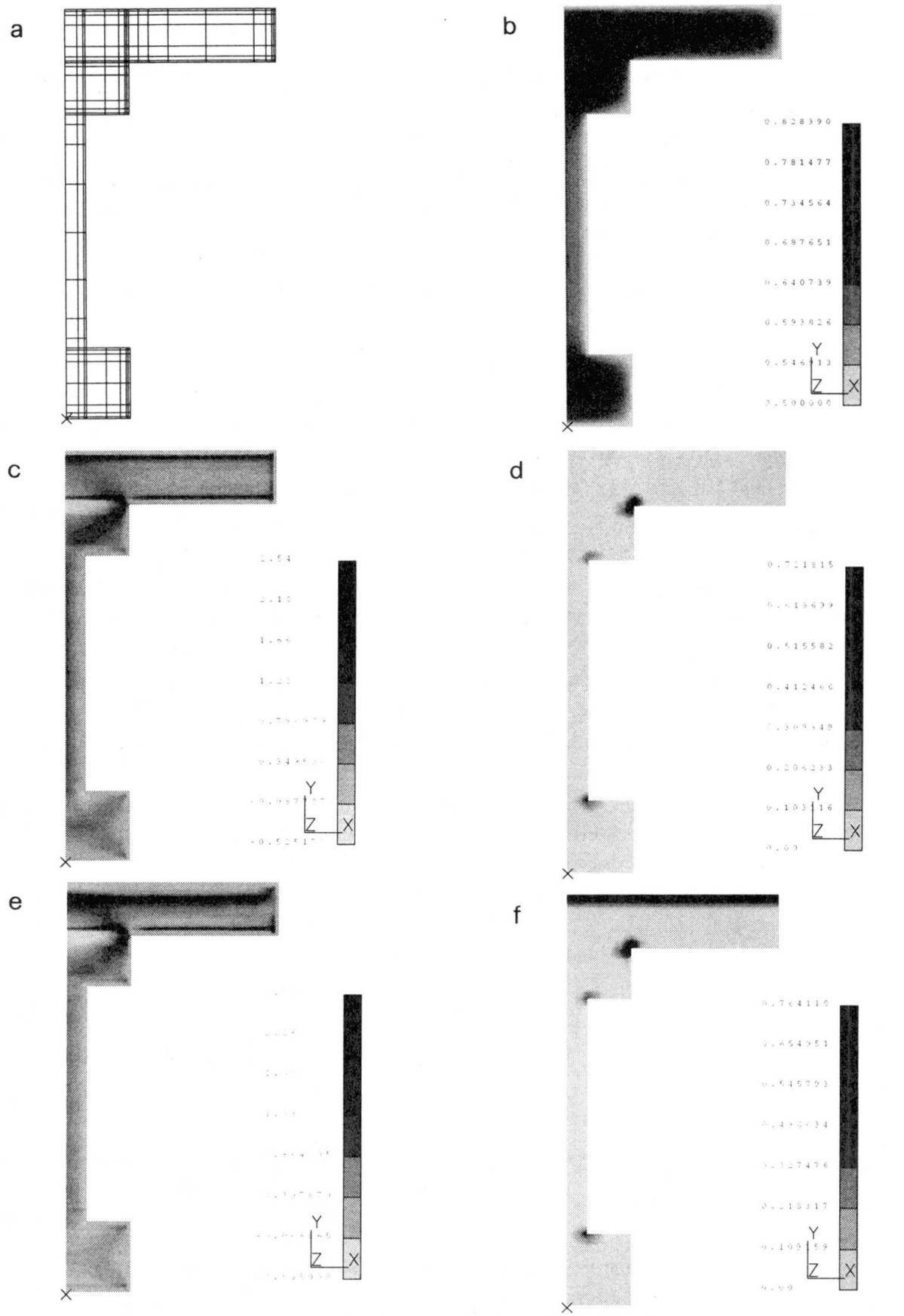

Fig. 2: a)half bridge cross-section used in the numerical analysis; b) relative humidities at time 6 years; c) max. principal stresses without chlorides at time 6 y.; d) damage without chlorides at time 6 y.; e) max. principal stresses with chlorides at time 6 y.; f) damage with chlorides at time 6 y.

New Approach in the Ultimate Life Calculation for Cracked Concrete

Nouvelle méthode d'évaluation de la durée de service de structures en béton armé

Eine neue Methode zur Bemessung von Stahlbetonkonstruktionen im gerissenen Zustand

Dubravka BJEGOVIC
Dr. Eng.
University of Zagreb
Zagreb, Croatia

Vedrana KRSTIC
Civil Engineer
Rutgers University
Piscataway, NJ, USA

Dunja MIKULIC
Dr. Eng.
University of Zagreb
Zagreb, Croatia

Jure RADIC
Prof. Dr.
University of Zagreb
Zagreb, Croatia

Vinko CANDRLIC
Dr. Eng.
University of Zagreb
Zagreb, Croatia

SUMMARY

The paper describes a new proposal for the design of reinforced concrete structures in an aggressive environment. The procedure takes into account the real condition of concrete section cracking under dead and live loads and special durable loads. In this way the least possible probability of structural damage resulting from the effect of special durable loads, can be provided for already in the design phase.

RÉSUMÉ

L'article propose une nouvelle méthode pour le projet de constructions en béton armé dans un environnement agressif. La procédure prend en compte l'état réel de la fissuration du béton sous charges permanentes et variables et sous charges spéciales durables. Cette méthode permet de prévoir, déjà lors de l'établissement du projet, les dommages structuraux les moins probables qui proviennent de l'effet de charges spéciales durables.

ZUSAMMENFASSUNG

Eine neue Methode zur Bemessung von Stahlbetonkonstruktionen in aggressiver Umgebung wird beschrieben. Das Verfahren zieht in Betracht reelle Verhältnisse von Stahlbetonquerschnitten im gerissenen Zustand unter ständigen Verkehrslasten und speziellen Dauerlasten (Umgebungseinflüssen). Die kleinstmögliche Wahrscheinlichkeit von strukturellen Schäden kann so schon in der Projektphase gesichert werden.

1. INTRODUCTION

The fulfillment of the crack limitation criteria frequently results in considerable increase of reinforcement necessary for ultimate limit state design, as well as other criteria of serviceability limit state. However, the manifestation of cracks greater than obtained by the calculations and prescribed, cannot be completely eliminated. Therefore, this paper proposes to introduce the new criterion of the serviceability limit state instead of the cracking limit state. In this way, other numerous factors of reinforced structure durability could be considered.

Such additional durability factors are proposed to be called "special durable loads" [1]. As special durable loads increase material degradation, especially reinforcement corrosion, the new criterion is proposed to be called "the criterion of corrosion limit state" [1].

According to the corrosion limit state it is necessary to prove that the calculated service life t_c is higher or at least equal to the designed life t_p:

$$t_o + t_1 = t_c > t_p \qquad /1/$$

where:

t_o is period of initiation of reinforcement corrosion in concrete,

t_1 is period of propagation of reinforcement corrosion in concrete [2].

2. PERIOD OF INITIATION AND PERIOD OF PROPAGATION REINFORCEMENT CORROSION PROCESS IN CONCRETE

The period of initiation of reinforcement corrosion in concrete stimulated by chlorides (structures in marine environment or structures on roads where the surfaces are strewed with salt for defrosting in the conditions of continental winters), can be determined by diffusion analysis of chlor ions in reinforced concrete cross-sections. The time necessary for the concentration of chlor ions to reach the critical value C_{cr} on the level of reinforcement should be calculated as follows:

$$C(c, t_o) = C_{cr} = 0.4\% \text{ [3]}. \qquad /2/$$

The continuous diffusion process of chlor ions for time-varying diffusion coefficients and the initial concentration of chlor ions is most appropriately expressed by the following experimental formula [1]:

$$C(x,t) = \left[C_o + k(t-1)\right]\left(1 - \operatorname{erf}\frac{x}{2\sqrt{\tau}}\right) + k\left[\left(1+\frac{x^2}{2\tau_1}\right)\left(1 - \operatorname{erf}\frac{x}{2\sqrt{\tau_1}}\right) - \frac{x}{\sqrt{\pi\cdot\tau_1}}e^{-\frac{x^2}{4\tau_1}}\right], \quad 0 \le C_o \le C_{max}, \qquad /3/$$

while after reaching the maximum starting concentration $C_o = C_{max}$ the following expression is valid:

$$C(x,t) = C_o\left(1 - \operatorname{erf}\frac{x}{2\sqrt{\tau}}\right), \quad C_o = C_{max} \qquad /4/$$

where:

C_o is initial concentration of chlor ions,

C_{max} is maximum concentration of chlor ions [1, 4],

k is the coefficient of linear increase of initial concentration [1, 5],

τ is the substitution by which variation of D_{Cl} with time [4] is being taken into account,

$\tau_1 = \tau(t = 1)$.

The period of propagation of reinforcement corrosion in concrete (t_1) can be defined from the expression for the corrosion rate [6], which is modified by the introduction of the coefficient of corrosion current density (p) and of the safety coefficient (γ) [1]. The coefficient of increase of corrosion current density takes into account the influence of sulphates, carbonation and real cracking of concrete section under the live and dead load, on the rate of reduction of the reinforcement area.

The safety coefficient takes into account the contribution of qualitative probability factors of failure probability of the bearing capacity of cross-section where the corrosion process has already started. By introducing these coefficients the formula for corrosion rate [6] takes the following form[1]:

$$\phi(t)=\phi_i - \gamma(0.023 \cdot p \cdot i_{corr} \cdot t) \qquad /5/$$

where:

$\phi(t)$ is the reinforcement diameter in time t (mm),
ϕ_i is the initial reinforcement diameter in time t = 0 (mm),
0.023 is transformation constant ($\mu A/cm^2$) in (mm/year),
i_{corr} is corrosion rate density ($\mu A/cm^2$),
p is coefficient of corrosion rate density increase,
γ is safety coefficient calculated on the basis of fuzzy sets theory [1].

From the condition of equalization of reinforcement diameter in the period of corrosion process propagation (t_1), with the limiting value $\phi_u = 0.9 \cdot \phi_i$ [1, 7], the final period of corrosion process development is determined by the formula:

$$\phi(t_1) = \phi_i - \gamma(0.023 \cdot p \cdot i_{corr} \cdot t_1) = \phi_u = 0.9 \cdot \phi_i \Rightarrow t_1 = \frac{0.1 \cdot \phi_i}{\gamma(0.023 \cdot p \cdot i_{corr})} . \qquad /6/$$

3. THE EXAMPLE OF CALCULATION ACCORDING TO THE CORROSION LIMIT STATE CRITERION

The complete calculation procedure, according to the corrosion limit state criterion, will be shown on the example of the flange of box-type concrete arch of new Maslenica bridge (Fig. 1).

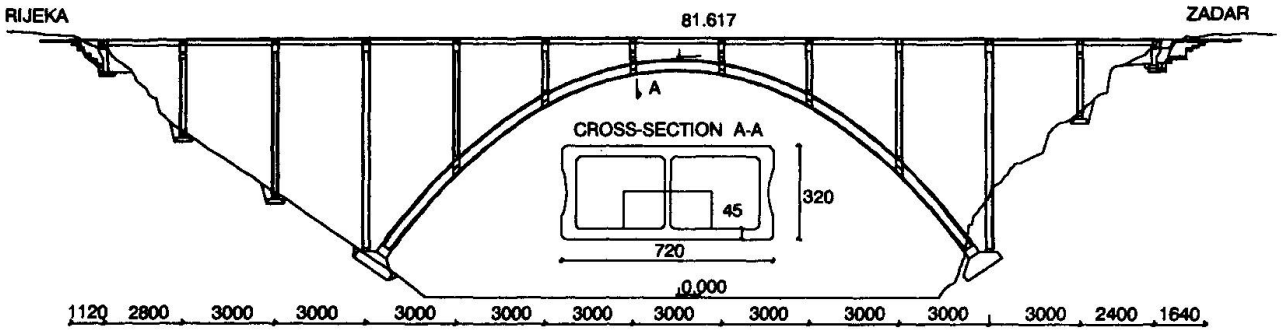

Fig. 1 Arch cross-section and longitudinal layout of new Maslenica bridge

By the dimensioning the flange in the transverse direction, according to the limit state design, the necessary reinforcement has been determined as:
$A_s = 7.3\ cm^2/m'$, and calculated crack width under the dead and live loads $w_k = 0.26$ mm [1].

As the structure is located in the aggressive marine environment and as the owner prescribed the life of 100 years, the crack width in concrete is limited to 0.1 mm. The calculations, taking into consideration the criteria of limit cracking condition, resulted in almost 100% increase of reinforcement quantity, compared to the required one from the ultimate limit state design: A_s ($w \leq 0.1$ mm) = $14.0\ cm^2/m'$.

In order to avoid such an increase, the cross-section will be designed according to the corrosion limit state criterion, which permits the real concrete cracking under the dead and live loads only. Due to marine environment, chlorides can be taken as special durable loads so that the period of corrosion initiation is calculated by the analysis of chlor ions diffusion process (formula /3/ and /4/) and under the following assumptions:

- w/c = 0.45,
- c = 5.0 cm,
- C_o (t=0) = 0 ,
- k = 0.2 for structures at 50 - 250 m from the sea [1],
- C_{max} = 7.64% [4],
- cement with slag addition, D_{01} = 0.3 [1],
- crack width w = 0.26 mm, D_{02} = 1.08 [1], $D_o = D_{01} \cdot D_{02}$ = 0.324 [1],

and t_o = 17 years (Fig. 2).

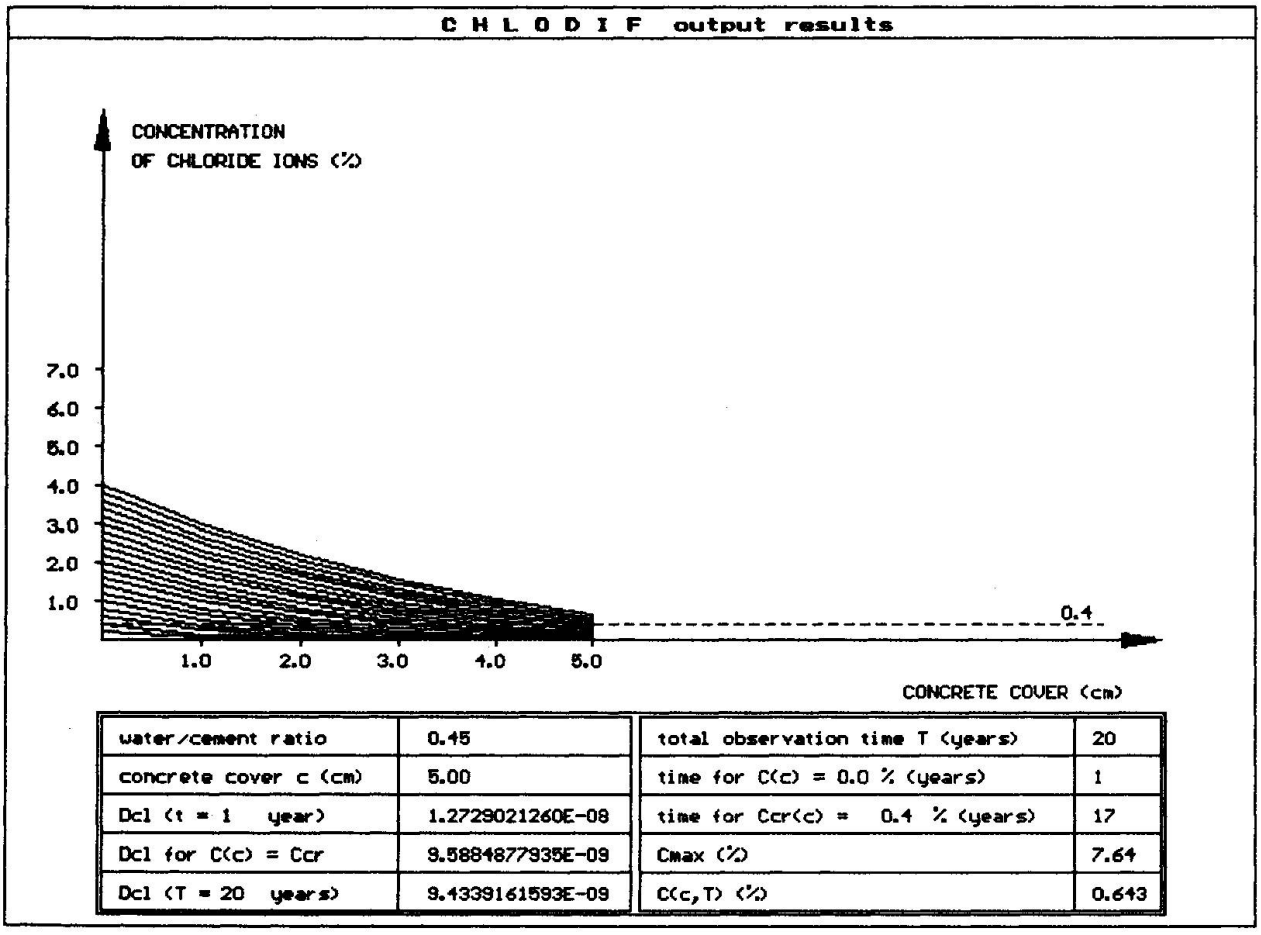

water/cement ratio	0.45	total observation time T (years)	20
concrete cover c (cm)	5.00	time for C(c) = 0.0 % (years)	1
Dcl (t = 1 year)	1.2729021260E-08	time for Ccr(c) = 0.4 % (years)	17
Dcl for C(c) = Ccr	9.5884877935E-09	Cmax (%)	7.64
Dcl (T = 20 years)	9.4339161593E-09	C(c,T) (%)	0.643

Fig. 2. Analysis of chlor ions diffusion process to the period t_o

The period of corrosion progress, propagation time t_1 with parameters [1]:
i_{corr} = 0.5 μA/cm², p = 2.37, γ = 1.2, according to the formula /6/ is t = 36.7 years. Calculated life of the arch element is than t_c = 17 + 36.7 = 53.7 years, which is far less than prescribed t_p = 100 years.

The problem is solved in such a way that the necessary value of the initial diffusion coefficient $D_{Cl} = 2.34 \cdot 10^{-9}$ cm²/s (prior $D_{Cl} = 1.27 \cdot 10^{-8}$ cm²/s, Fig. 2), is read from the nomogram (Fig. 3.) [4, 1], elaborated for the concrete cover thickness c = 5 cm and prescribed period t_o = 64 years.

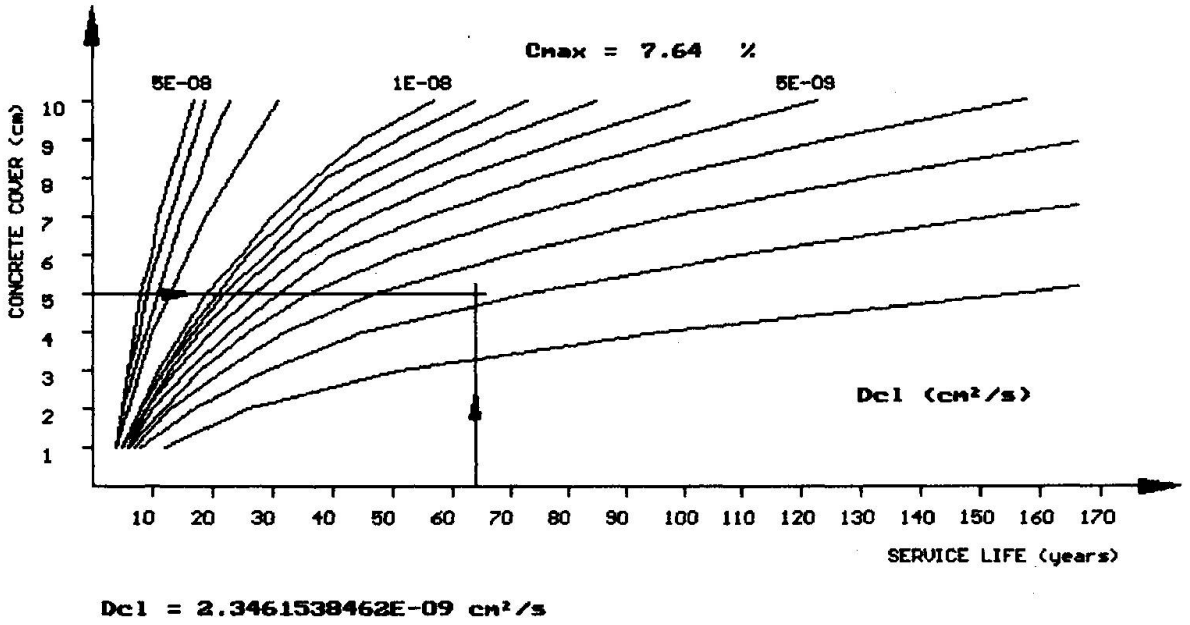

Fig. 3. C-D-c-t nomogram

As it is impossible to fulfill the criteria of the service life of 100 years [8] by above mentioned procedures (the only one remained possibility [8] of water-cement ratio reduction at w/c = 0.4 decreases value of the diffusion coefficient to $D_{Cl} = 8.08 \cdot 10^{-9}$ [1]), it is proposed to apply the mobile corrosion inhibitors [9, 10] in the form of admixtures during concreting or in the form of surface coats, which will in their activation time stop the corrosion process (Table 1, [1]).

t (years)	ACTIVITY
0	Finishing of construction (structural element)
21	Applying of mobile corrosion inhibitors in the form of surface coats
37	Activation of corrosion inhibitors
39	Reaching of critical chlorine ion concentration on reinforcement
64	Stopping of corrosion inhibitors activity, starting of corrosion process
100	Fulfillment of the criterion of corrosion limit state

Table 1 Time schedule of structure maintenance

4. CONCLUSION

The proposed new method is based on supplementing the existing design procedure according cracking limit state design with corrosion limit state design under the conditions of simultaneous action of dead and live loads and special durable loads.

Dimensioning to the corrosion limit state design yields initiation and propagation time for reinforcement corrosion process. This procedure, applied in design phase, frequently results in less reinforcement steel than obtained from standard cracking limit state calculation.

Acknowledgment

The authors wish to acknowledge Mr Zlatko Šavor for useful advices during the preparation of this paper.

REFERENCES:

1. V. Krstić: Numerical Model of Durability Calculation for Reinforced Concrete Structures, Magisterium, Faculty of Civil Engineering University of Zagreb, Zagreb 1994. (in Croatian);
2. K. Tuutti: Service Life of Structures with Regard to Corrosion of Embeded Steel, ACI SP 65-13, International Conference on Performance of Comcrete in Marine Environment, Canada, August 1980, pp 223-236;
3. Croatian Code on Concrete and Reinforced Concrete, 1987;
4. D.Bjegović, V. Krstić, D.Mikulić, V. Ukrainczyk: C-D-c-t Diagrams for Practical Design of Concrete Durability Parameters, Cement and Concrete Research, vol. 25. No. 1. 1995. pp. 187-196;
5. K. Takewaka, S. Mastumoto: Quality and Cover Thickness of Concrete Based on the Estimation of Chloride Penetration in Marine Environments, ACI SP 109-117, Concrete in Marine Environment, Detroit (USA), 1988. pp. 381-400;
6. C. Andrade, C. Alonso, J.A. Gonzales, J. Rodriguez: Remaining Service Life of Corroding Structures, IABSE Symposium on Durability of Structures, Lisabon (Portugal) pp. 359-364;
7. C. Andrade, C. Alonso, J.A. Gonzales: An Initial Effort to Use the Corrosion Rate Measurements for Estimating Rebar Durability, ASTM Symposium on Corrosion Rate of Reinforcements in Concrete, Baltimore (USA), June 1988 pp. 29-37;
8. V. Ukrainczyk, D. Bjegović, D. Mikulić, Z. Rak, V. Krstić; Special Tender Condition for Maslenica Concrete Arch Bridge, Croatian Roads Authority, Zagreb 1993;
9. D. Bjegović, L. Sipos, V. Ukrainczyk, B. Mikšić; Diffusion of the MCI 2020 and MCI 2000 Corrosion Inhibitors into Concrete, International Conference on Corrosion and Corrosion Protection of Steel in Concrete, Sheffield, UK, 1994. Vol 2. pp. 865-878;
10. SHRP-S-666: Concrete Bridge Protection and Rehabilitation: Chemical and Physical Techniques (Corrosion Inhibitors and Polymers), National Research Council, Washington DC, 1993. 248 pp.

Behaviour and Durability of Concrete with Regards to Cycle and Time Dependent Effects

Comportement et durabilité du béton compte tenu des effets des cycles et du temps

Eigenschaften und Dauerhaftigkeit von Beton mit Rücksicht auf die von Perioden und Zeit abhängigen Effekte

Maria SZERSZEN
Adjunct Professor
Univ. of Technology
Cracow, Poland

Jean-François DESTREBECQ
Lecturer
Université Blaise Pascal
Clermont-Ferrand, France

Krzysztof DYDUCH
Professor
Univ. of Technology
Cracow, Poland

SUMMARY
The paper presents the main results of a research programme devoted to the problem of plain concrete subjected to cyclic stress, including both analytical and experimental investigations. Two mechanical approaches are proposed to allow for both cycle dependent and time dependent effects, the latter being more significant at high levels of loading. Based on the theory of damage, they provide a prediction of the durability of plain concrete subjected to cyclic loads. A constitutive law is proposed that accounts for the behaviour of concrete as observed during the tests up to failure point.

RÉSUMÉ
L'article présente les principaux résultats d'un programme de recherche portant sur le problème du béton soumis à des chargements cycliques, selon un double aspect analytique et expérimental. Deux approches mécaniques sont présentées pour rendre compte des effets des cycles et de ceux du temps, ces derniers étant réellement significatifs pour les niveaux élevés de chargement. Basées sur la théorie du dommage, elles fournissent une prédiction de la durabilité du béton soumis à des charges cycliques. Une formulation est ensuite proposée pour rendre compte du comportement du béton observé au cours des tests jusqu'à la rupture.

ZUSAMMENFASSUNG
Diese Arbeit präsentiert die Hauptergebnisse des Prüfungsprogrammes, das den Beton unter wiederholten Spannungen betrifft, mit sowohl analytischen wie auch experimentellen Prüfungen. Zwei mechanische Annäherungen werden präsentiert, um die von den Perioden und der Zeit abhängigen Effekte zu berücksichtigen. Der Einfluss der Zeit, besonders bei hohen Spannungen, wurde untersucht. Auf der Bruchtheorie basierend, ermöglichen sie, die Dauerhaftigkeit von Beton unter wiederholten Spannungen abzuschätzen. Eine konstitutive Gleichung wurde präsentiert, die das Verhalten des Betons, wie es bei der Prüfungen bis zu dem Bruchpunkt beobachtet wurde, berücksichtigt.

1. INTRODUCTION

During their service life, concrete structures can have to withstand accidental overloadings, which are likely to induce cyclic stresses. Such are the effects of seismic actions for example. For low levels of loading, the cyclic failure of concrete depends mainly on the extreme values of the loading stress. For maximum stress over 75% of the static strength, the influence of the cycle features (period, shape) is more obvious, and has been reported by several authors.

A reliable knowledge of the behaviour of their constitutive materials is required to predict the carrying ability of concrete structures subjected to variable loadings. The paper aims to present the main results of a research programme devoted to this specific problem. Test results are reported for 32 plain concrete samples subjected to cyclic compression, the maximum stress ranging between 65% and 90% of the static strength. Based on the test evidences, an analytic approach is proposed, that allows for both time dependant and cycle dependant damage. Then, the theory of damaging viscoplasticity is used to set up a constitutive law that accounts for the decrease of the longitudinal modulus and for the irrecoverable strain which develops up to failure point.

2. EXPERIMENTAL INVESTIGATIONS

Cylinders of diameter 8 cm and height 16 cm, made from ordinary concrete of broken granite gravel and Portland cement (strength class 35) were subjected to axial cyclic compression. The specimens were prepared in three batches from the same mixture, and stored under similar conditions. For all specimens, the age at testing time was about 7 months. A mechanical testing system (MTS) bed was used to conduct the tests. The axial load was transmitted to the sample ends through two steel plates. A spherical joint was used on the upper part of the press. The form of the loading cycle was sinusoidal. The cyclic load was adjusted for each sample, according to its actual compressive strength f_c, estimated from volumetric strain measurement at the beginning of the test [1]. The minimum stress σ_{min} was about equal to $0.1\, f_c$ for all samples. The maximum stress σ_{max} was chosen between $0.65\, f_c$ and $0.90\, f_c$. The tests were conducted up to failure point with a frequency of 10 Hz.

Table 1 : Summary of data for the cyclic tests.

sample †	f_c [MPa]	$\frac{\sigma_{max}}{f_c}$	$\frac{\sigma_{min}}{f_c}$	N_r [cycles]
24/3	*42.5	.90	.12	10
09/5	38.8	.87	.10	210
14/5	42.4	.85	.10	110
07/5	44.2	.85	.10	247
32/3	*42.5	.82	.12	130
19/3	*42.5	.81	.11	180
35/4	32.6	.80	.10	100
16/5	49.7	.80	.10	110
01/5	45.7	.80	.05	140
17/3	*42.5	.80	.10	190
18/3	*42.5	.80	.10	220
37/4	39.6	.80	.10	360
02/5	49.1	.80	.10	4130
39/4	28.1	.80	.10	9630
10/5	38.8	.80	.10	180500
06/5	*51.1	.78	.10	17468

sample †	f_c [MPa]	$\frac{\sigma_{max}}{f_c}$	$\frac{\sigma_{min}}{f_c}$	N_r [cycles]
03/5	39.7	.775	.10	30445
26/3	39.2	.75	.10	409
21/3	47.9	.75	.10	2950
31/3	29.5	.75	.10	6650
34/4	*39.6	.75	.09	16800
11/5	*51.1	.75	.09	19060
22/3	*42.5	.72	.10	4040
27/3	40.9	.70	.10	300
29/3	41.4	.70	.10	420
30/3	39.8	.70	.10	2610
28/3	41.8	.70	.10	70050
12/5	*51.1	.70	.09	231680
13/5	*51.1	.69	.08	216370
33/4	*39.6	.67	.09	761530
15/5	*51.1	.66	.08	661280
25/3	*42.5	.65	.08	93610

† *sample/batch numbers ;* * *mean value measured from six* $\Phi 8/16$ *cm cylinders.*

Two induction gauges 80 mm long were fixed opposite to each other on each cylinder. The level of the loading force, the longitudinal displacement given by the two gauges, the number

of applied cycles and the loading frequency were monitored during the test. The density of measurement points was 10 per loading cycle. The data were recorded over 50 cycles for each 1000 cycles (each 350 cycles at the beginning and the end of the test duration).

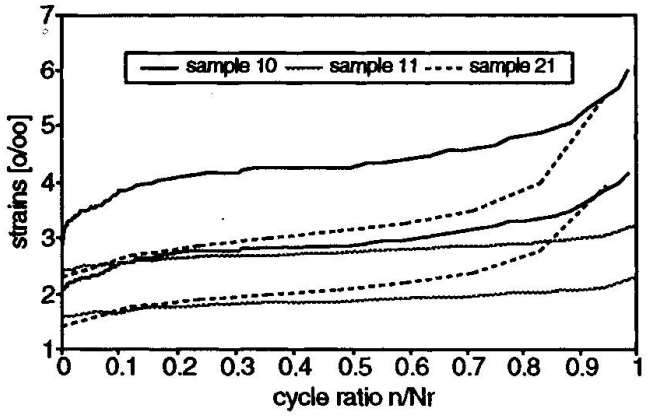

Fig.1 Maximum and minimum values of the longitudinal strains in terms of cycle ratio to failure.

Table 1 shows the ultimate compressive strength, the extreme levels of the cyclic stress and the number N_r of cycles at failure point for each sample. For most of the specimens, the measured longitudinal strains follow a S-shaped relationship in a strain *versus* cycle ratio to failure diagram. Typical curves are presented on Fig.1 for three samples (for each of them, the two curves show ϵ_{min} and ϵ_{max} corresponding to σ_{min} and σ_{max} respectively). Such curves suggest that the process of damage which leads to the failure is not only cycle dependant. The S-shape of the curves indicates the coexistence of creep damage which is a time related phenomenon depending on the stress level. As a matter of fact, the damage of plain concrete originates from the microcracks which develop during the loading. Authors have observed an increase of the microcracking in concrete samples subjected to either sustained or cylic high level loadings [2].

3. ANALYSIS OF DAMAGE IN PLAIN CONCRETE

3.1 Pure fatigue damage

Miner's law provides a simple way to allow for the rate of cycle dependant damage. In accordance with this law, the damage factor D_n accumulates in a linear way in terms of cycle ratio to failure :

$$dD_n = \frac{dn}{N_f} \quad \text{where} \quad dn = \frac{dt}{T} \qquad \Longleftrightarrow \qquad \dot{D}_n = \frac{1}{N_f T} \tag{1}$$

where T denotes the period of the loading cycle. The number N_f of cycles corresponding to pure fatigue failure can be derived from Aas-Jakobsen's formula :

$$\frac{\sigma_{max}}{f_c} = 1 - 0.0685 \left(1 - \frac{\sigma_{min}}{\sigma_{max}}\right) \log N_f \tag{2}$$

According to Tepfers and Kutti [3], this relationship applies for $\sigma_{max} \leq 0.75\, f_c \div 0.80\, f_c$.

3.2 Creep damage

For higher levels of loading, the number of cycles at failure proves to be more sensitive to the features of the cyclic stress (period, shape of the cycle). In the case of a static load maintained at a constant level, the process of damage causes the failure after a delay which depends on the level of loading. Rabotnov's law is a convenient way to express the rate of creep damage D_t at any time t. It can be written as follows :

$$\dot{D}_t(t) = \frac{\beta}{r+1} \left(\frac{\sigma}{f_c}\right)^k (1 - D_t)^{-r} \tag{3}$$

where β, k and r are material coefficients.

3.3 Total damage

One way to express that the behaviour of concrete is both cycle and time dependant is to assume the rate of total damage to be a linear combination of pure fatigue damage and creep damage :

$$\dot{D} = \phi_n \dot{D}_n + \phi_t \dot{D}_t \qquad \forall t \geq 0 \tag{4}$$

where ϕ_t and ϕ_n are two coupling coefficients. According to Eq.1 and Eq.3, the rate of pure fatigue damage keeps constant for identically repeated cycles, but the rate of creep damage at a given stress depends on the r value (constant rate for $r = 0$).

4. DURABILITY OF PLAIN CONCRETE UNDER CYCLIC LOADING

4.1 First method

Eq.3 can be easily integrated in the case of a constant stress σ. The failure is supposed to occur after a period of time t_u, corresponding to $D_t = 1$:

$$t_u(\sigma) = \frac{1}{\beta}\left(\frac{\sigma}{f_c}\right)^{-k} \tag{5}$$

The values of k and β coefficients have been calibrated from test results reported by Fouré [4] : $\beta = 3.058$, $k = 62.5$ [t_u *in sec.*].

One possible approach to account for a cyclic loading, is to assume $r = 0$ in Eq.3 and $\phi_n = 1$ in Eq.4. Under these conditions, the former equations yields :

$$\dot{D}(t) = \frac{1}{N_f T} + \frac{\phi_t}{t_{u(\sigma)}} \quad \Longrightarrow \quad D(t) = \frac{t}{N_f T} + \phi_t \int_0^t \frac{d\tau}{t_u(\sigma)} \tag{6}$$

keeping in mind that $t = nT$ (n : number of applied cycles). The failure is supposed to occur at cycle N_c, corresponding to $D = 1$. Hence :

$$\frac{1}{N_c} = \frac{1}{N_f} + \phi_t D_{t1} \qquad \text{where} \quad D_{t1} = \int_0^T \frac{dt}{t_u(\sigma)} \tag{7}$$

zone	σ_{max}	effect
A	$\leq 0.75\, f_c$	no
B	$0.75\, f_c \div 0.85\, f_c$	+
C	$\geq 0.85\, f_c$	+++

Table 2 : Influence of time on the cyclic strength of plain concrete.

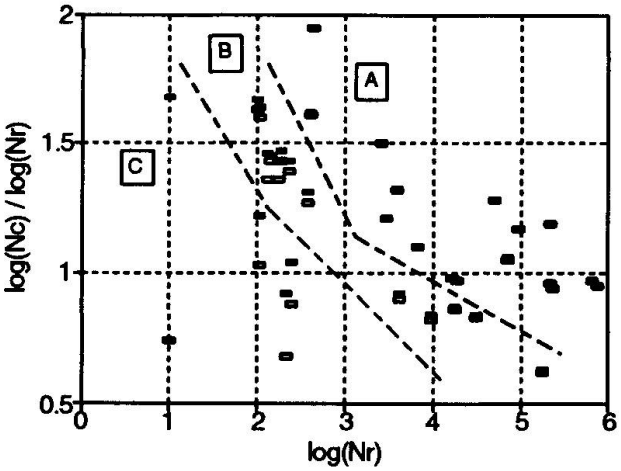

Fig.2 Comparison of computed values (Eq.7) with experimental figures (Table 1).

D_{t1} depends on the shape, the period and the level of the cyclic stress. In the case of a sinusoidal cycle, D_{t1} can be estimated as follows, s being any odd number ($s \geq 9$ for accuracy) :

$$D_{t1} = 0.469\, 10^{-18} \left(\frac{\sigma_{max}}{f_c}\right)^{62,5} \frac{T}{s} \sum_{i=1}^{s} \left[1 + \frac{\sigma_{min}}{\sigma_{max}} + \left(1 - \frac{\sigma_{min}}{\sigma_{max}}\right) \sin \frac{2\,i\,\pi}{s}\right]^{62.5} \tag{8}$$

Theoretical values N_c, computed for $\phi_t = 0$ (▪) and $\phi_t = 5000$ (▫), are compared with test results on Fig.2. The influence of time depends on the upper level of the cyclic stress. For levels lower than 75% of the compressive static strength, the influence of time vanishes, in agreement with Tepfers and Kutti's conclusions [3].

4.2 Second method

An alternative approach consists to assume that the total damage is time dependant, whatever the level of loading is. This corresponds to $\phi_n = 0$ and $\phi_t = 1$ in Eq.4. Integrating that equation gives the total damage in terms of time. Keeping in mind that $t = nT$, the number of cycles at failure is obtained for $D = 1$:

$$D(t) = 1 - \left(1 - \beta\,\Gamma^{(k)}\,t\right)^{\frac{1}{r+1}} \qquad \text{where} \quad \Gamma^{(k)} = \frac{1}{T}\int_0^T \left(\frac{\sigma(t)}{f_c}\right)^k dt \tag{9}$$

$$\text{hence :} \qquad N_r = \frac{1}{\beta\,\Gamma^{(k)}\,T} \tag{10}$$

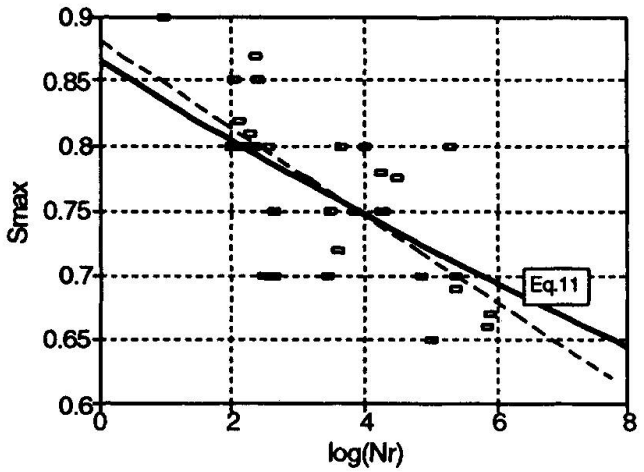

Fig.3 Representation of Eq.11 (solid line), compared with test results on a σ-N diagram.

According to Eq.10, the relationship between $\Gamma^{(k)}$ and N_r should be linear in a logarithmic scale. A linear regression, based on the mean square method, has been performed on our test results (assuming the slope to be equal to -1), in order to check this conclusion :

$$\log \Gamma^{(k)} = -\log N_r - 5.03$$

$$\Longleftrightarrow \qquad N_r = \frac{0.93\,10^{-5}}{\Gamma^{(k)}} \tag{11}$$

Expression (11) is compared with the regression line (dashed) calculated for σ_{max}/f_c in terms of $\log Nr$ for our test results on Fig.3.

5. BEHAVIOUR OF PLAIN CONCRETE UP TO CYCLIC FAILURE

The longitudinal strain has been recorded for each sample over the whole test duration. The data show a progressive decrease of the longitudinal modulus, along with the growing of a plastic strain during the test. The total strain can be expressed at any time as the sum of an elastic strain and a creep strain :

$$\epsilon(t) = \frac{\sigma(t)}{(1 - D(t))\,E_o} + \epsilon_p(t) \tag{12}$$

where E_o is the initial value of the longitudinal modulus of elasticity. The expression of the damage factor $D(t)$ can be determined from Eq.3, assuming the existence of a possible initial damage D_o :

$$D(t) = 1 - \left[(1 - D_o)^{r+1} - \beta\,\Gamma^{(k)}\,t\right]^{\frac{1}{r+1}} \tag{13}$$

The creep strain ϵ_p is supposed to develop according to Norton's law. The influence of the

state of damage on the creep rate is accounted for by considering the effective stress $\tilde{\sigma}$:

$$\dot{\epsilon}_p(t) = \left(\frac{\tilde{\sigma}(t)}{B}\right)^m \quad \text{where} \quad \tilde{\sigma}(t) = \frac{\sigma(t)}{(1 - D(t))} \tag{14}$$

where B and m are material coefficients. Integrating Eq.14, assuming the possible existence of an initial strain ϵ_o, yields :

$$\epsilon_p(t) = \epsilon_o + \left(\frac{B}{f_c}\right)^{-m} \Gamma^{(m)} \delta(t) \quad \text{where} \quad \delta(t) = \frac{1}{T}\int_0^t (1 - D(\tau))^{-m}\, d\tau \tag{15}$$

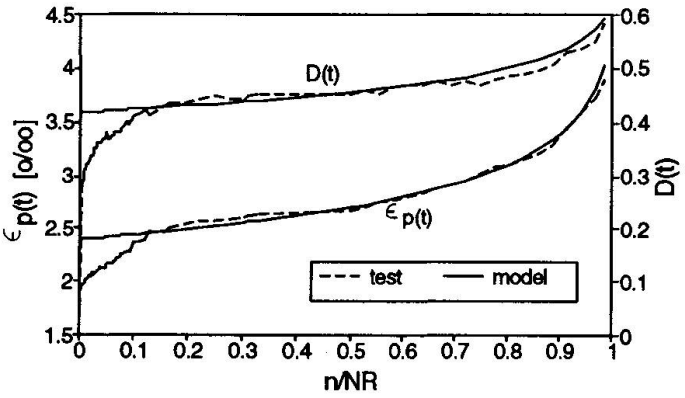

Fig.4 Theoretical and experimental values for $D(t)$ and $\epsilon_p(t)$

and $\Gamma^{(m)} = \frac{1}{T}\int_0^T \left(\frac{\sigma(t)}{f_c}\right)^m dt$

Equations (12), (13) and (15) describe the constitutive law of plain concrete subjected to high level compressive loading. In order to check the validity of these expressions, it is necessary to estimate the values of D and ϵ_p from our test results. At cycle $n = t/T$:

$$D(t) = 1 - \frac{\sigma_{max} - \sigma_{min}}{E_o\,(\epsilon_{max} - \epsilon_{min})} \tag{16}$$

$$\epsilon_p(t) = \epsilon_{max} - \frac{\sigma_{max}}{(1 - D(t))\,E_o} \tag{17}$$

Fig.4 shows a comparison of the experimental figures corresponding to the sample 10, with the values predicted from Eq.13 and Eq.15 respectively.

6. CONCLUSION

The existence of a strain flow developing at a growing rate in terms of cycle ratio to failure, allows to assume that the process of fatigue damage is a time related phenomenon. Based on this assumption, two complementary approaches are proposed to account for the durability of plain concrete subjected to cyclic compressive stress. They both allow for the failure for low as well as high levels of loading. Assuming that the strain flow can be related to damaging viscoplasticity, it is possible to explain the cyclic behaviour of plain concrete as the result of a progessive decrease of the longitudinal modulus along with the growing of a creep strain in terms of the number of cycles. Based on this assumption, the behaviour of tested samples can be accounted for with a good accuracy.

7. REFERENCES

1. DYDUCH K., SZERSZEŃ M., DESTREBECQ J-F., Experimental investigation of the fatigue strength of plain concrete under high compressive loading. Structures and Materials, 27(173), 1994, 505-509.
2. SHAH S.P., CHANDRA S., Fracture of concrete subjected to cyclic and sustained loading. ACI Journal, 61(10), 1970, 816-824.
3. TEPFERS R., KUTTI T., Fatigue strength of plain, ordinary, and lightweight concrete. ACI Journal, 76(5), 1979, 635-652.
4. FOURÉ B., Résistance potentielle à long terme du béton soumis à une contrainte soutenue. Annales ITBTP, (431), 1985, 47-63.

Reliability-Based Design of Deteriorating Bridges under Corrosion Effects

Théorie de fiabilité appliquée au dimensionnement des ponts soumis à la corrosion

Einsatz der Zuverlässigkeitstheorie bei der Bemessung korrodierender Brücken

Dan M. FRANGOPOL
Professor
University of Colorado
Boulder, CO, USA

Samer BARAKAT
Assistant Professor
Jordan Univ. of Science & Technology
Irbid, Jordan

Kai-Yung LIN
Graduate Student
University of Colorado
Boulder, CO, USA

SUMMARY

Available data suggests that corrosion may have significant effects on the reliability of highways bridges. Therefore, the design requirements for highway bridges must include consideration of corrosion. This paper presents a highway bridge reliability-based design formulation which accounts for corrosion effects on both steel and reinforced concrete bridges. The approach incorporates both time-independent constraints specified in the AASHTO bridge code and time-dependent constraints due to corrosion effects. Numerical examples illustrate the application of the proposed approach.

RÉSUMÉ

Les données actuelles laissent supposer que la corrosion a une influence significative sur la fiabilité des ponts autoroutiers. Raison pour laquelle il faut prendre en compte un tel phénomène destructif dans les exigences de calcul de ces ouvrages. L'article expose une méthode d'étude basée sur la théorie de la fiabilité, qui tient compte des effets corrosifs aussi bien sur les ponts métalliques que sur ceux en béton armé. Ce mode opératoire inclut tant les sollicitations ne dépendant pas du temps et spécifiées par la norme AASHTO applicable aux ponts, que celles dépendant du temps et résultant de l'influence de la corrosion. Des exemples numériques illustrent l'utilisation de la méthode proposée.

ZUSAMMENFASSUNG

Vorhandene Daten deuten auf den grossen Einfluss, den Korrosion auf die Zuverlässigkeit von Autobahnbrücken hat. Deshalb müssen die Bemessungsanforderungen die Berücksichtigung der Korrosion einschliessen. Der Beitrag stellt eine Entwurfsregel für Stahl- wie auch Stahlbetonbrücken auf Grundlage der Zuverlässigkeitstheorie vor. Eingeschlossen sind sowohl zeitunabhängige Nebenbedingungen nach der AASHTO-Brückennorm als auch zeitabhängige infolge Korrosionsauswirkungen. Numerische Beispiele illustrieren die Anwendung des vorgeschlagenen Ansatzes.

1. INTRODUCTION

In the past two decades, deterioration in highway bridges has received increased attention as a cause of strength reduction and possible collapse [1-3]. In fact, several recent bridge failures have been attributed to various material degradation processes. Corrosion in steel and reinforced concrete bridges appears to be one of the most important degradation mechanisms in determining the service life of these structures. As pointed out by Kulicki *et al* [1] "the estimated cost of repairing corrosion-damaged bridges in the United States is staggering". At present, however, there are no established procedures for taking into account corrosion effects in the design of highway bridges. This paper presents a highway bridge design formulation which accounts for corrosion effects in both steel and reinforced concrete bridges. The approach incorporates both time-independent (reserve) constraints specified in the AASHTO bridge code [4] and time-dependent (residual) constraints due to corrosion effects.

2. CORROSION

The effects of corrosion on steel and/or concrete highway bridges can vary dramatically depending on the environment, location, and amount of deterioration.

For steel bridges, Kayser [2] and Kulicki *et al* [1] described various forms of corrosion, including uniform corrosion, pitting, galvanic corrosion, and stress corrosion. In this paper uniform corrosion is considered. On steel bridges this type of corrosion can be identified easily. It consists of many small pits joined together [1]. From the collected data on uniform corrosion penetration in steel coupons in different environments, Townsend and Zocolola [5] fitted time-corrosion penetration curves to a power function

$$C(t) = At^B \tag{1}$$

where C(t) is the average corrosion penetration determined from weight loss, A and B are regression coefficients whose value depend on the type of steel and the type of environment [3], and t is the time in years. A coefficient α may also be introduced to take into account modeling uncertainty [6]. In this case the corrosion penetration is given as

$$C(t) = \alpha At^B \tag{2}$$

For concrete bridges, corrosion of the reinforcement due to carbonation and chloride is considered herein. Once corrosion of reinforcement is initiated it is assumed to be propagated as uniform corrosion (i.e., all bars are assumed to become corroded with the same penetration rate at the same time) [7,8]. The total flexural reinforcement area in a cross section of a reinforced concrete beam as a function of time is

$$A_s(t) = \begin{cases} n\pi d^2/4 & \text{for} \quad t \leq t_0 \\ n\pi[d - 2\nu(t - t_0)]^2/4 & \text{for} \quad t > t_0 \end{cases} \tag{3}$$

where d is the diameter of a single bar, n is the number of reinforcement bars (i.e., all bars are assumed to have the same diameter), t_0 is the time of corrosion initiation, and ν is the rate of corrosion. The shear reinforcement area in a cross-section of a reinforced concrete beam placed in a corrosive environment can be also defined as a function of time [9].

3. RELIABILITY-BASED DESIGN INCLUDING CORROSION

For composite steel bridges, corrosion will cause a reduction in the cross-sectional area of the lower flange and the web and a reduction in the geometric bending properties of the section. This reduction will decrease the tensile capacity of the lower flange and reduce the ultimate moment capacities of the section. Similarly, for concrete bridges corrosion of reinforcement will reduce both the bending and shear capacities.

Under corrosion, the formulation of the design problem in a reliability-based design format is almost identical to that of the time invariant model [10]. In order to include the corrosion effects in the formulation, the two additional regression coefficients A and B in Eq.(1) should be considered to describe the corrosion model for a given environment. Using the time-variant reliability-based context, the design formulation of steel and/or concrete bridges under corrosion is as follows:

$$\text{Minimize} \qquad C(\mathbf{X}, \mathbf{Y}, \mathbf{Z}, t) \tag{4}$$

such that :

$$\beta_i(t) \geq \beta_i^*(t) \qquad i = 1, 2, \ldots, m \tag{5}$$

$$g_j(t) \leq 0 \qquad j = 1, 2, \ldots, n \tag{6}$$

$$\beta_{system,k}(t) \geq \beta^*_{system,k}(t) \qquad k = 1, 2, \ldots, s \tag{7}$$

where C = cost function, $\mathbf{X}$ = vector of design variables, $\mathbf{Y}$ = vector of design parameters, $\mathbf{Z}$ = vector of parameters defining the corrosion process, t = time, $\beta_i(t)$ = reliability index with respect to limit state i, $\beta_i^*(t)$ = allowable value of β_i, $g_j(t)$ = performance function such that $g_j(t) \leq 0$ is the safe state, $\beta_{system,k}(t)$ = system reliability index, and $\beta^*_{system,k}(t)$ = allowable value of $\beta_{system,k}(t)$.

The reliability-based design formulation (4)-(7) is general and allows flexibility in choosing the cost function C, the design variables $\mathbf{X}$, the reliability-based constraints (5) and (7), and the performance constraints (6). The nonlinear programming problem (4)-(7) is solved by linking the general purpose deterministic optimization software ADS [11] with the structural reliability analysis software RELTRAN [12]. The time-dependent reliability indices $\beta_i(t)$ and $\beta_{system}(t)$ are defined as:

$$\beta_i(t) = -\Phi^{-1}(P_{f_i}(t)) \tag{8}$$

$$\beta_{system}(t) = -\Phi^{-1}(P_{f_{system}}(t)) \tag{9}$$

where $P_{f_i}(t)$ = probability of occurrence of limit state i at time t, and $P_{f_{system}}(t)$ = system failure probability at time t. $P_{f_{system}}(t)$ is computed considering all limit states as a series system as the average of Ditlevsen's bounds [13] at time t.

4. RESULTS

To illustrate the applications of the proposed reliability-based design approach to steel and reinforced concrete bridges under corrosion effects, two numerical examples are considered herein.

First, a simply supported 24.40 m, composite, welded, hybrid, stiffened plate girder of a multi-girder bridge exposed to corrosion is designed according to AASHTO [4]. There are 22 design variables, X_1 to X_{22}, 13 design parameters, Y_1 to Y_{13}, and two parameters defining the corrosion process [10],[14]. Nine deterministic design variables are considered independent (see Fig. 1), and eight design parameters and two parameters A and B defining the corrosion process (see Fig. 2,[2]) are considered random variables [10]. The time-dependent reliability-based design problem (4)-(7) is solved considering the steel weight as the objective to be minimized. Fig. 3 shows results of time-dependent reliability-based design. The least-weight required to maintain the same target reliability level increases with both time of exposure to corrosion and required reliability level. Fig. 4 shows the effects of the number of girders on the time-dependent

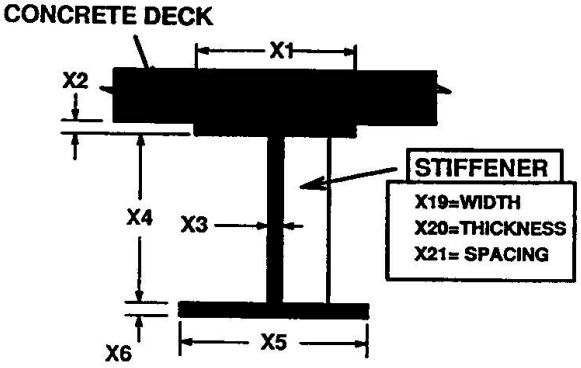

Fig. 1 Independent design variables of a steel plate girder

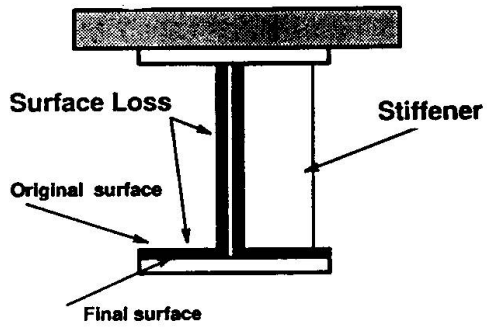

Fig. 2 Surface loss due to corrosion [2]

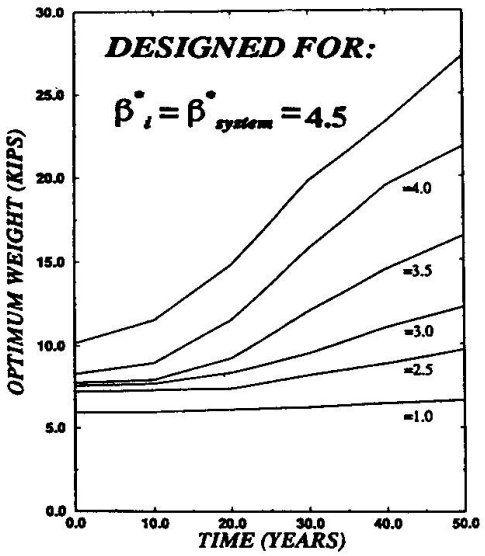

Fig. 3 Optimum girder weight vs. time; 1 kip = 4.45 kN

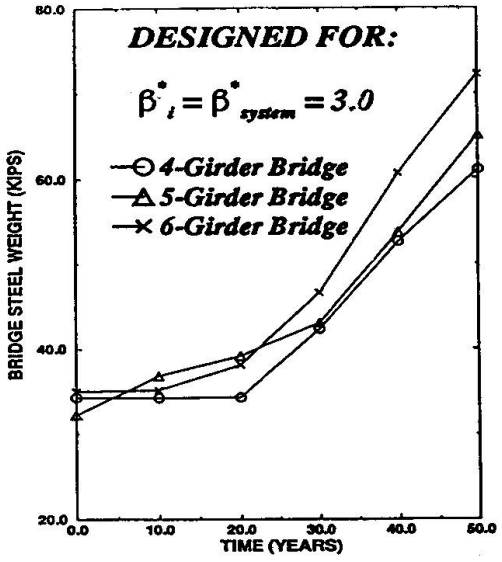

Fig. 4 Optimum bridge weight vs. time; effect of number of girders

reliability-based design of a 24.40-m span bridge. It is interesting to observe that the five-girder bridge (girder spacing = S= 2.45 m) is the best solution for the first four years, and after that the four-girder bridge (S= 3.05 m) becomes the least-weight design. The six-girder bridge (S=1.85 m) is never the optimum solution.

Second, a reinforced concrete T beam of 18.30 m span, simply supported multi-girder bridge is design according to AASHTO [4]. In this case, there are 21 design variables, X_1 to X_{21}, 12 design parameters, Y_1 to Y_{12}, and one deterministic parameter ν defining the corrosion process [9]. Nine deterministic design variables are considered independent (see Fig. 5), and eight design parameters are considered random. The time-dependent reliability-based design problem is solved considering the minimum cost as the objective. The cost is taken as $C = C_{con} + C_{st}$, where C_{st}= cost of steel and C_{con} = cost of concrete. Fig. 6 plots the optimum cost of an individual reinforced concrete T beam of the bridge versus time of exposure to corrosion for different corrosion rates. In this figure, the corrosion initiation time is t_0=3 years, the assumed ratio between the unit cost of steel to concrete is 50 (i.e., C_S/C_C=50), and the allowable reliability indices are $\beta_i^*=\beta_{system}^*$=3.0. The optimum beam cost required to maintain an imposed target reliability level increases with both exposure time and corrosion rate.

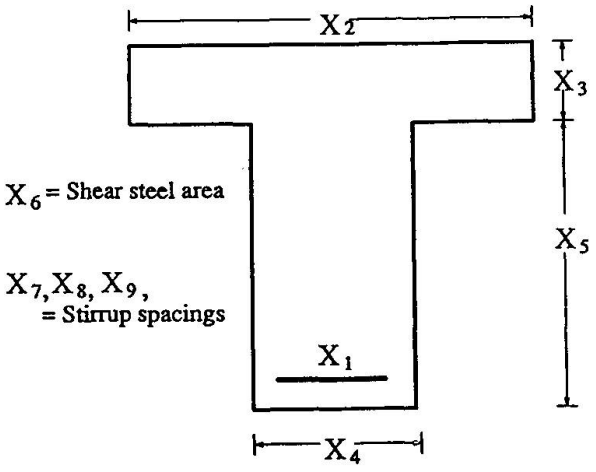

Fig. 5 Independent design variables of a reinforced concrete T beam

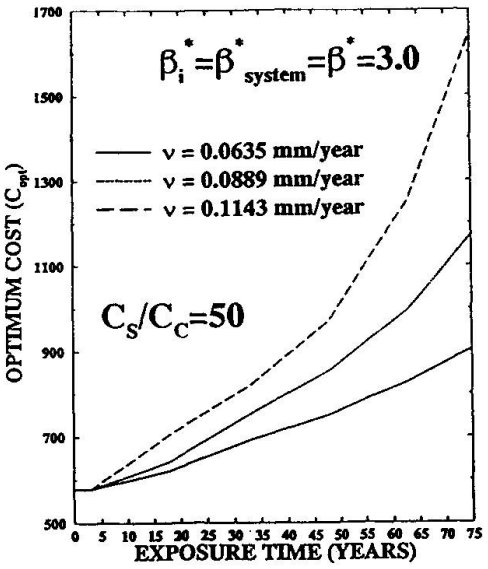

Fig. 6 Optimum beam cost vs. time for different corrosion rates

5. CONCLUSIONS

The proposed reliability-based design model capable of including deterioration constraints has permitted a reexamination of performance requirements of steel and reinforced concrete bridges. The limit state functions considered in the proposed reliability-based design approach are time-dependent. They consider explicitly the environmental effects due to corrosion. Other time-dependent effects, such as fatigue, and accidents, such as collision, need to be incorporated in reliability-based design of highway bridges. More research in this area is needed.

REFERENCES

1. KULICKI, J.M., PRUCZ, Z., SORGENFREI, D.F., and MERTZ, D.R.," Guidelines for Evaluating Corrosion Effects in Existing Steel Bridges," Report 333, NCHRP, Washington, D.C., 1990.

2. KAYSER, J.R., The Effects of Corrosion on the Reliability of Steel Girder Bridges, Ph.D. Thesis, Dept. of Civil Eng., Univ. of Michigan, Ann Arbor, Mich., 1988.

3. ALBRECHT, P., and NAEEMI, A.H., Performance of Weathering Steel in Bridges, Report 272, NCHRP, Washington, D.C., 1984.

4. STANDARD SPECIFICATIONS FOR HIGHWAY BRIDGES, AASHTO, 13th & 14th eds., Washington, D.C., 1983 & 1989.

5. TOWNSEND, H.E., and ZOCCOLA, J.C., Eight Year Atmospheric Corrosion Performance of Weathering Steel in Industrial, Rural and Marine Environments, Special Technical Publication 767, ASTM, Pittsburgh, Penn., 1982.

6. CHAKRAVORTY, M., FRANGOPOL, D.M., MOSHER, R.L. and PYTTE, J.E., Time-Dependent Reliability of Rock-Anchored Structures, Reliability Engineering & System Safety (in press), 1995.

7. MORI, Y. and ELLINGWOOD, B., Methodology for Reliability Based Condition Assessment, NUREG/CR-6052, ORNL/Sub/93-SD684, Dept. of Civil Engineering, Johns Hopkins Univ., Baltimore, Maryland, 1993.

8. SØRENSEN, J.D. and THOFT-CHRISTENSEN, P., Inspection Strategies for Concrete Bridges, Proceedings of the Conference on Reliability and Optimization of Structural Systems, London, Sept. 1988.

9. LIN, K-Y., Reliability-Based Design of Concrete Bridges, Ph.D. Thesis, Dept. of Civil Eng., Univ. of Colo., Boulder, Colo., 1995 (in progress).

10. HENDAWI, S., Structural System Reliability with Applications to Bridge Analysis, Design and Optimization, Ph.D. Thesis, Dept. of Civil Eng., Univ. of Colo., Boulder, Colo., 1994.

11. VANDERPLAATS, G.N., ADS- A Fortran Program for Automated Design Synthesis: Version 1.10, Engineering Design Optimization Inc., Santa Barbara, Calif., 1986.

12. LEE, Y-H., HENDAWI, S., and FRANGOPOL, D.M., RELTRAN - A Structural Reliability Analysis Program: Version 2.0, Report No. CU/SR-93/6, Dept. of Civil Eng., Univ. of Colo., Boulder, Colo., 1994.

13. DITLEVSEN, O., Narrow Reliability Bounds for Structural Systems, Journal of Structural Mechanics, 7, 1979.

14. FRANGOPOL, D.M. and HENDAWI, S., Incorporation of Corrosion Effects in Reliability-Based Optimization of Composite Hybrid Plate Girders, Structural Safety, 16(1+2), 1994.

Improving the Durability of Precast Concrete Bridges

Amélioration de la durabilité des ponts en béton préfabriqués

Verbesserung der Dauerhaftigkeit von vorfabrizierten Betonbrücken

Tomasz SIWOWSKI
Dr. Eng.
University of Technology
Rzeszow, Poland

Tomasz Siwowski, born in 1961, received his civil engineering degree in 1985 and Ph.D. degree in 1994 at Rzeszow University of Technology. He was involved in design as well as in supervision, evaluation and rehabilitation of bridges. Presently he is engaged in the research works on fatigue and service life of steel bridges.

SUMMARY

Prefabricated road bridges have been constructed in Poland for over 35 years. During this long period about 20 various types of precast concrete bridge beams have been designed and implemented. The experience gained from inspection and maintenance indicates that this kind of structure has very low durability. The paper presents some general methods of repair and rehabilitation of prefabricated bridges. In addition a case study on the rehabilitation of a typical precast structure in Poland is described..

RÉSUMÉ

Les ponts-routes préfabriqués sont construits en Pologne depuis 35 ans. Plus de vingt différents types de poutres préfabriquées ont été développés durant cette période. Les résultats d'inspection et de contrôle des ponts préfabriqués indiquent que ces types de construction sont peu résistants. Cet exposé présente les principes de réparation et de consolidation des ponts préfabriqués. Un exemple typique de reconstruction est présenté.

ZUSAMMENFASSUNG

Die vorfabrizierten Brücken werden in Polen seit über 35 Jahren gebaut. In diesem Zeitraum waren im Brückenbau über 20 verschiedene Typen von vorfabrizierten Balken projektiert und eingeführt worden. Die bei den Brückenüberwachungen gesammelten Erfahrungen zeigen aber, dass die Bauwerke sehr niedrige Festigkeiten haben. In dem Artikel werden ein paar allgemeine Reparatur- und Sanierungweisen der vorfabrizierten Brücken dargestellt und ein Beispiel der Instandsetzung einer in Polen typischen vorfabrizierten Brücke beschrieben.

1. INTRODUCTION

The construction of fully prefabricated bridges has been the predominant technology of concrete road bridge building in Poland. Bridges with precast concrete beams constitute 18% the whole number of all polish bridges and 67% the number of concrete ones, constructed in 1956 - 1990. Generally, in polish public road network there are about 5300 precast concrete bridges [1].
A general tendency to industrialize bridge construction led to working out and practical application of over 20 different systems of precast bridges. Regarding to the span length there have been constructed bridges with following types of precast beams:
- reinforced - up to 15 m,
- prestressed pre-tensioned - up to 24 m,
- prestressed post-tensioned - up to 36 m.

Most of the above-mentioned bridge systems are fully prefabricated with minimum of cast-in-place concrete. Multispan structures have been constructed as a row of simply supported beams with many expansion joints. Analysis of the precast bridges deteriorations showed, that the bad state of their repair results from unsatisfactory construction, poor quality of used materials and faulty design solutions. Due to low durability of precast spans these bridges need now urgent rehabilitation.
The paper presents the most typical damages of polish prefabricated bridges and some basic ways of their rehabilitation with a case study of the typical reconstruction.

2. TYPICAL DAMAGES OF PRECAST CONCRETE BRIDGES

The basic reasons of precast bridge damages are mainly:
- inadequate transverse stiffness of the span, causing destruction of longitudinal joints between precast beams,
- poor quality of the superstructure fitting, i.e., waterproofing, expansion joints, gulleys, sidewalks,
- poor quality of both precast and cast-in-place concrete, causing not adequate rebars protection from aggressive environment.

The superstructures built of the precast beams are very leaky. Most of the longitudinal cast-in-place joints between beams, poor quality transverse expansion joints, too thin deck slabs and the sidewalks made of loose, separate elements provide good conditions for seepage through the deck causing their corrosion.
Unsatisfactory transverse stiffness is usually responsible for damaging the joints between the prefabricated elements. Due to service load the deflection of the beams is so extensive that the poor quality cast-in-place concrete in the joints gets damaged and the waterproofing ripped. Longitudinal joints became loose due to vibrations caused by dynamic load. The water gets through and causes extensive corrosion of the beams.
Widely used domestic expansion joints are leak and not satisfactorily anchored in the structure. The parts of the structure next to expansion joints and those under them become affected. The effect of leaking expansion joints is also corrosion of the areas where cables are anchored and destruction of the area round the span supports as well as extensive damage of the supports.
The low quality of waterproofing and its damage due to beam fluctuation caused insufficient protection for the concrete of the deck slab and the beams against the aggressive influence of water with deicing salt. The chloride attack took usually place.
Other fitting of prefabricated spans was also bad quality. For example gulleys with pipes of too small diameter were installed in the holes, either left or hammered in the concrete deck slab, when it has been precast. Such installation is not watertight and water does not flow through the gulley but through the adjacent area.

The greatest corrosion damage usually occurs along the sidewalks, exactly in the slab under them and on external beams. This results from placing water-collecting elements inside the sidewalks. There are various chambers, empty spaces for telecommunication cables and water or gas pipes, lean concrete and other porous materials as filler, which not only let water through but also hold some of it for a long time.
Another cause of the fast deterioration of the structure is poor concrete quality in both precast and cast-in-place elements. The strength grade of the concrete is usually too low. It is badly compacted, has numerous voids and losses and low corrosion resistance. This resistance is considerably reduced due to the content of fly ash commonly used in the seventies as concrete admixture. The poor quality of the concrete makes it insufficient protection for the reinforcement against the chloride attack, more so as the thickness of the concrete cover was often too small.

3. METHODS OF IMPROVING PRECAST BRIDGES DURABILITY

These defects of prefabricated bridges required, after a relatively short period (5-10 years), a major repair. Initially, the repair consisted in a reconstruction of the original state, i.e., damaged elements were removed and replaced by new ones of the same kind. However, this procedure was not effective as it only temporarily eliminated the effects, but not the main causes of the damage.
In the end of the eighties, the way of modernization of the precast bridges underwent considerable change consisting in the elimination of the faults pointed out in until now applied solutions. The main changes were the following:
- making the structure continuous - eliminating of expansion joints and changing the statical scheme greatly enhance the durability of the object,
- increasing the stiffness of spans and supports - making the structure dynamic and fatigue resistant,
- good waterproofing of the superstructure - stopping water penetration through the concrete.

Making the structure continuous aimed mainly at getting rid of faulty expansion joints as the main factor of prefabricated bridge destruction (fig.1). The first way was to join the spans in a chain by means of a flexible slab, covering a gap, shaped in the thickened deck slab of a bridge. It formed a continuous beam scheme regarding horizontal forces and thermal influence, but it was still a chain of simple - supported beams regarding live load. However, this method did not work properly. Theoretical assumption concerning the behavior of a flexible slab allowed its cracking, which really occurred. Consequently, they underwent very fast damage. Thus, they stopped being used.
Another method of eliminating expansion joints was performing full continuity of the deck slab without changing existing system of bearings. The static scheme of the structure was changed from a chain of simple - supported spans into a row of quasi - frame segments of several spans.
The technologically most complicated solution necessitating use of assembly supports was obtaining a full continuity of all spans in a continuous beam system or a frame system. A monolithic joint, shaped above the pier, made it possible to place some extra reinforcement on negative moments as well as protect and strengthen the ends of precast RC beams. The change of the static scheme enabled to upgrade the load carrying capacity of the whole structure and to achieve its considerable stiffening.
Except monolithic joints, the upgrading of span stiffness was achieved by casting, on the whole deck, a new reinforced concrete about 12 cm thick deck slab. The slab was made as composite with the existing precast elements or, possibly, with the old deck slab. It ensured the cooperation of two slabs in carrying live load, which often increased the load capacity of the bridge. In the new slab extra reinforcement was embedded, transverse and longitudinal falls were shaped and new gulleys fastened. Over the gap between the span and the abutment, the new deck slab was lengthened behind the back wall using brackets, thus eliminating expansion joints.

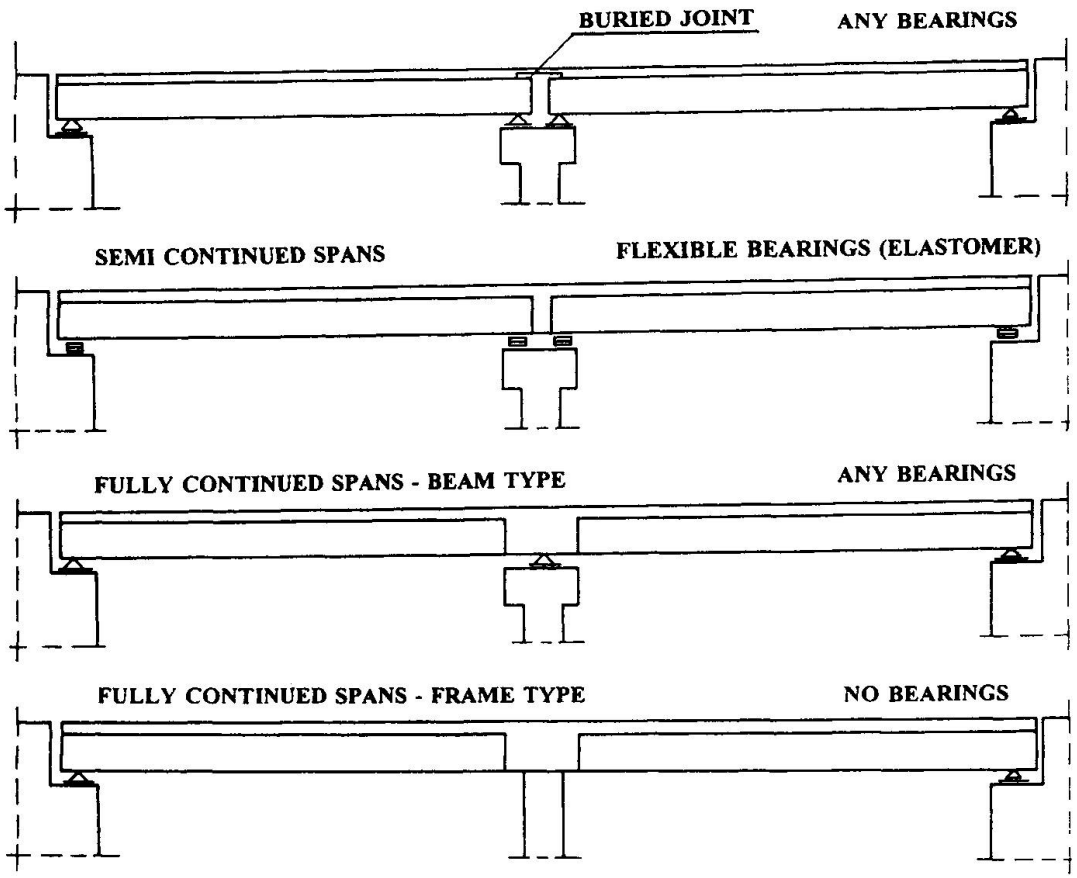

Fig.1. Methods of making continous of simply supported precast spans

The complex updating of the decks included also additional sealing of the structure. Additional waterproofing layers were put on, particularly in the curb area. The sidewalk was modernized by shaping reinforced concrete put-on slabs while all hollow bricks, openings and extra installations were removed. Besides, leakproof pavement both on the carriageway and sidewalk was laid.
Described above rehabilitation steps executed on a broad basis and up to proper quality standard restored the right condition of the structure and often upgraded its load capacity.

4. CASE STUDY OF PRECAST BRIDGE REHABILITATION

The rehabilitated bridge is a four-span structure with axially spaced supports of 16.3 m and a total length of 68.6 m, with a curbless deck of 11.0 m service width. Each span contains six beams, spaced axially at any 2.0 m. The beams support precast deck slabs of 2.0 x 3.0 x 0.12 m. The whole deck has a one sided 1.5% crossfall and a 4.0% longitudinal fall. The bridge had no draining gulleys.
The faulty structure of the spans and severe service conditions caused considerable damage of deck elements, fittings and supports. The condition of the main beams varied regarding the span and the cross-section of the beams. The areas near the supports were the most deteriorated because of the leaky expansion joints. Corrosion of the main reinforcement caused cover destruction and occurrence of considerable concrete loss and delamination. As in the beams, corrosion affected areas of the

precast deck slabs were near the leaky expansion joints. The blooms, decolorization, scalling and small concrete losses were observed. The other parts of slabs were in good repair and showed no corrosion.

The caps of piers were the most damaged elements of the bridge structure. Leaky expansion joints and also lack of efficient drainage of the pavement caused extensive and deep losses in the concrete, loosening of the cover to the level of the reinforcement, exposure of the corroding rebars, scalling on the whole surface, etc. Besides, hammerhead piers with such a wide cap form too flexible support for bridge structures. The flexibility could easily be felt when heavy lorries were crossing the bridge.

The main rehabilitation stages were the following:

- making continuity of spans by joining them with piers in a frame,
- introduction of changes in the cross-section of the bridge,
- covering of the whole superstructure with a reinforced concrete slab,
- extending the deck slab beyond the back walls of the abutments.

The main goal of making continuity of spans was the upgrading the longitudinal and transverse rigidity of the structure and the elimination of expansion joints, which meant sealing the structure. Concrete cast-in-place joints over the piers create a frame structure. A strongly reinforced joint of considerable size stiffens also the cap of the pier (fig.2).

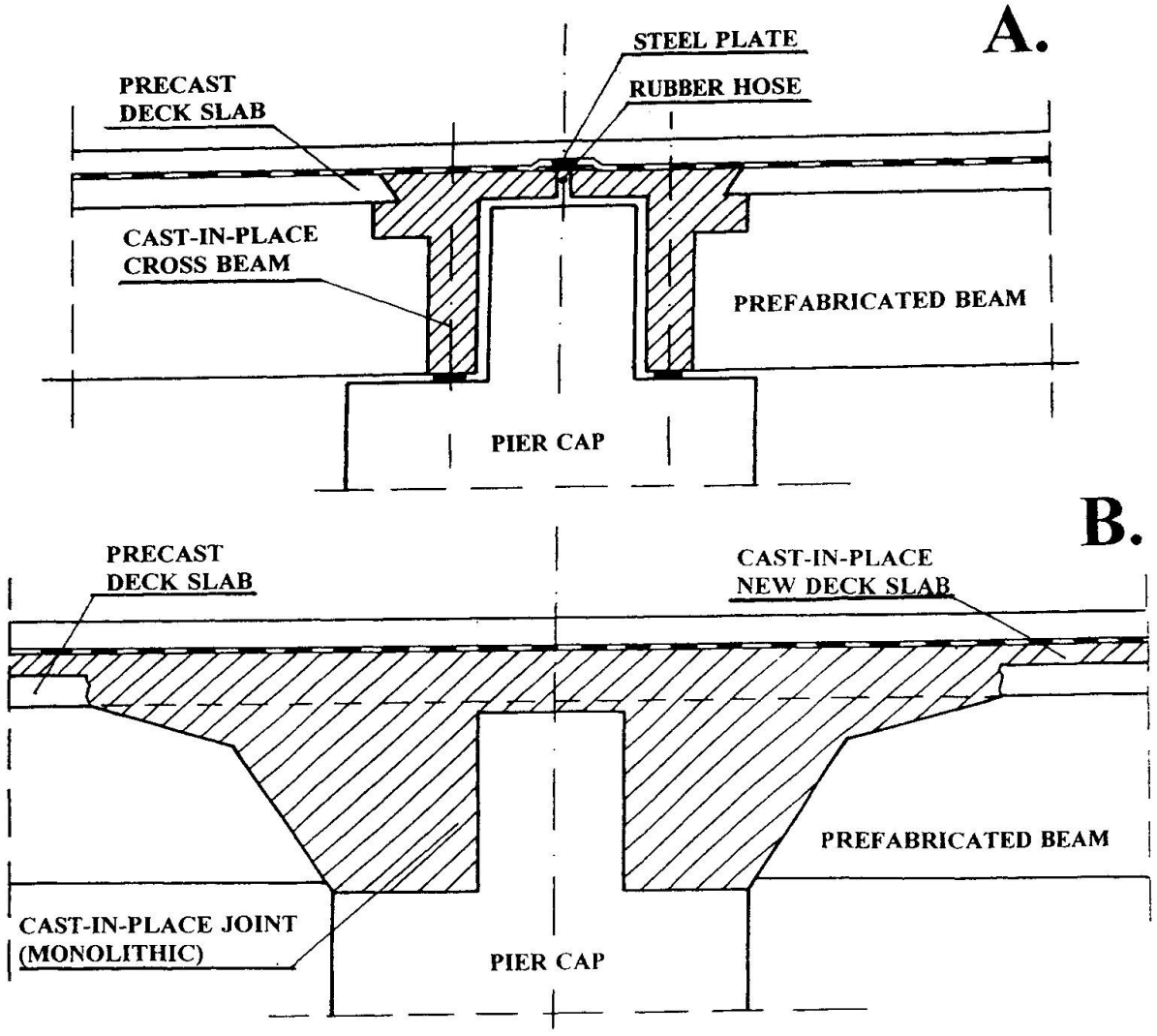

Fig.2. Modernization of the supporting area of piers:
a) before reconstruction; b) after reconstruction.

Curbless cross-section was replaced by new one with curbs separating pedestrian lanes from those for the traffic. Total structure and service width does not change. Sidewalk was designed as reinforced concrete put-on slab separated from the carriageway by stone curbs. All hollows, pipes and empty chambers were removed.
The new deck slab was composite with the hitherto existing one by means of special steel studs. The new slab sealed the deck, increased the load capacity of the span and enabled to properly anchor rebars of the joints over the piers.
To eliminate expansion joints over the abutments, the deck slab was extended beyond the back walls of the abutments. Besides, end cross beams were made which grasped the ends of the main beams over the bearing seat of the abutment.

5. CONCLUSIONS

The most important condition of long service life and high durability of concrete road bridges is the suitable protection of the structure from the influence of aggressive environment. For precast bridges it can be obtained by eliminating of expansion joints, applying of effective waterproofing and drainage and increasing the transverse stiffness of the span.
The unproven design of many prefabricated bridges, poor quality of construction and materials and mass construction of such objects caused the bad state of repair of many bridges in Poland. It is estimating, that more than 30% of the precast bridges require the fast repair or strengthening. To work out methods of their rehabilitation and restore their service value became an exigency. The presented method, which has been set up at several construction sites, seems to be the most effective.

REFERENCES

1. **BILISZCZUK J., MACHELSKI C., MALISZKIEWICZ P., MISTEWICZ M.,** Typowe uszkodzenia betonowych mostów prefabrykowanych (Typical damages in polish prefabricated bridges), Drogownictwo, April 1994 (in polish).

Monitoring and Evaluation of Bridges

Surveillance et évaluation des ponts

Überwachung und Beurteilung von Brücken

Ladislav FRYBA
Professor
Inst. of Theoretical & Applied Mech.
Prague, Czech Republic

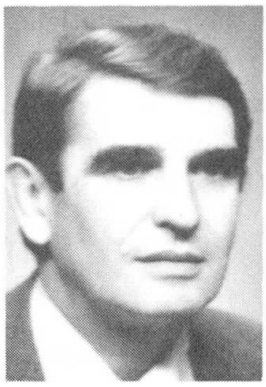

Ladislav Fryba, born 1929, studied civil engineering at the Technical University Prague. He is involved in the research of bridges and President of the Czech Society for Mechanics. Since 1984 he is at the Institute of Theoretical and Applied Mechanics of the Czech Academy of Sciences.

Miros PIRNER
Professor
Inst. of Theoretical & Applied Mech.
Prague, Czech Republic

Miros Pirner, born 1928, received his civil engineering degree from Technical University Prague 1952. He has worked as assistant professor and as researcher. Since 1990 he is director of the Institute of Theoretical and Applied Mechanics of Czech Academy of Sciences.

SUMMARY

Monitoring of stresses provides the stress spectra, i.e. number and distribution of stress cycles in steel bridges subjected to traffic loads. Identification together with modal analysis after dynamic tests recognises the deterioration of the state of bridges as reflected in diminishing of natural frequencies and in deformations of modes of natural vibrations.

RÉSUMÉ

L'enregistrement des contraintes fournit les spectres des contraintes, c'est-à-dire le nombre et la distribution des cycles de contraintes dans les ponts métalliques sous charges de trafic. L'identification et l'analyse modale après les essais dynamiques reconnaissent les dommages aux ponts, qui se manifestent par une diminution des fréquences propres et des déformations des modes de vibration naturelle.

ZUSAMMENFASSUNG

Die Überwachung der Spannungen ergibt ein Spannungsspektrum, d.h. die Anzahl und die Verteilung der Spannungen in den Stahlbrücken unter Verkehrslasten. Die Identifikation und modale Analyse nach den dynamischen Versuchen lassen die Brückenbeschädigungen erkennen, welche sich durch die Verkleinerung der Eigenfrequenzen und der Deformationen der Eigenschwingungsformen ausdrücken.

1. INTRODUCTION

Monitoring is a process where some characteristics of the structure (deflections, strains, stresses, etc.) are recorded during a certain time (hours, days, months, years, etc.). On the other hand, identification is a process where the real properties of the structure are discovered from the response of the structure.

Several methods have been developped for both processes mentioned above and some of them, that were applied to bridges, will be referred in the present paper.

2. MONITORING OF STRESSES

Most of railway and highway bridges are subjected to irregular traffic loads that are more or less of the random character and they may be idealized by a stochastic process randomly variable in space and time. As the life of bridges is long (80 to 120 years) the knowledge of the current and expected strengths in bridges is very important for the estimation of their life, fatigue, maintenance, inspection intervals etc.

Therefore, the stresses were recorded in 5 railway and 3 highway bridges and the obtained stress-time records were evaluated using the rain-flow counting method [1]. The method supposes that the fatigue of steel structures depends first of all on the stress ranges (two stress ranges = one stress cycle), [2] :

$$\Delta\sigma = \sigma_{max} - \sigma_{min} \tag{1}$$

where σ_{max} or σ_{min} is a local maximum or minimum, respectively.

In such a way, the stochastic stress-time records are transformed into simple stress ranges and/or stress cycles. The rain-flow method supposes that the fatigue damage due to small stress ranges may be added to the fatigue damage due to big stress ranges without respect to their time sequence.

The result of counting is a histogram of frequency of stress ranges which is called stress spectrum. An example is shown in the Fig. 1. The stress spectra possess the following properties (for details see [3]) :

- — both static and dynamic components of the response of bridges are included,
- — a great number of cycles of small stress ranges appears (dynamic components) while the great stress ranges are rare (static components),
- — the stress spectra depend on the intensity and composition of traffic loads,
- — they depend on the shape and on the length of influence line of the investigated bridge element,
- — they do not depend on any hypothesis of fatigue damage nor on Wöhler curve,
- — the spectra possess large dispersions.

The statistical evaluation of results and the regression analysis provided an empirical formula for the number n_i of stress ranges in the i-th class per year :

$$n_i = aT^b L^c \lambda_i^d \mathrm{e}^{ks} \tag{2}$$

where the following designation has been used :

T – number of heavy vehicles per 24 hours (devided by 500) for highway bridges, or
– mass of all trains on the given line per year for railway bridges (in million of tons),

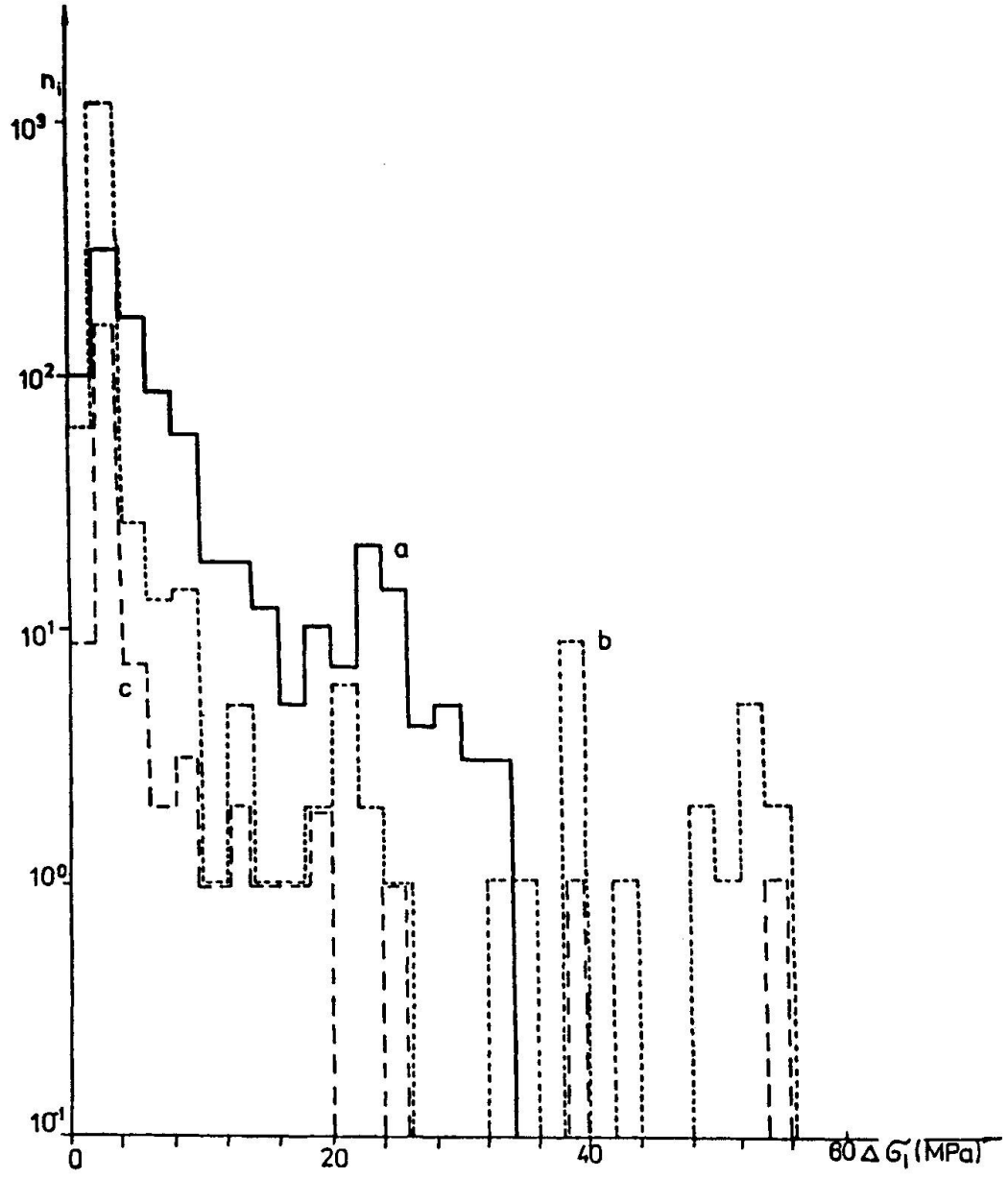

Fig. 1 Stress spectrum in the main girder of a steel railway bridge, L = 30 m
a) daily traffic, 65 trains,
b) 10 runs of a very heavy train,
c) one run of a very heavy train

L - length of influence line of the investigated element (in metres),

$\lambda_i = \Delta\sigma_i/\Delta\sigma_s = 0,1; 0,2; ...; 0,9; 1$ - dimensionless stress ranges, $\Delta\sigma_s$ - greatest stress range in the investigated bridge element due to standard life load multiplied by the standard dynamic impact factor,

a, b, c, d - regression coefficients (3) and (4),

s - standard deviation of measured data,

$k = 1,65$ - coefficient ascertaining the 95% reliability.

The experiments [3] have brought the following data :
for highway bridges :

$$\begin{array}{llllll} a = 13,099 & b = 1 & c = -0,461 \\ d = -5,208 & s = 0,930 & k = 1,65 \end{array} \quad (3)$$

for railway bridges :

$$\begin{array}{llllll} a = 17,742 & b = 0,860 & c = -0,354 \\ d = -4,464 & s = 1,323 & k = 1,65 \end{array} \quad (4)$$

The obtained statistical data have been applied to the design of bridges for fatigue and to the estimation of inspection intervals, see [3].

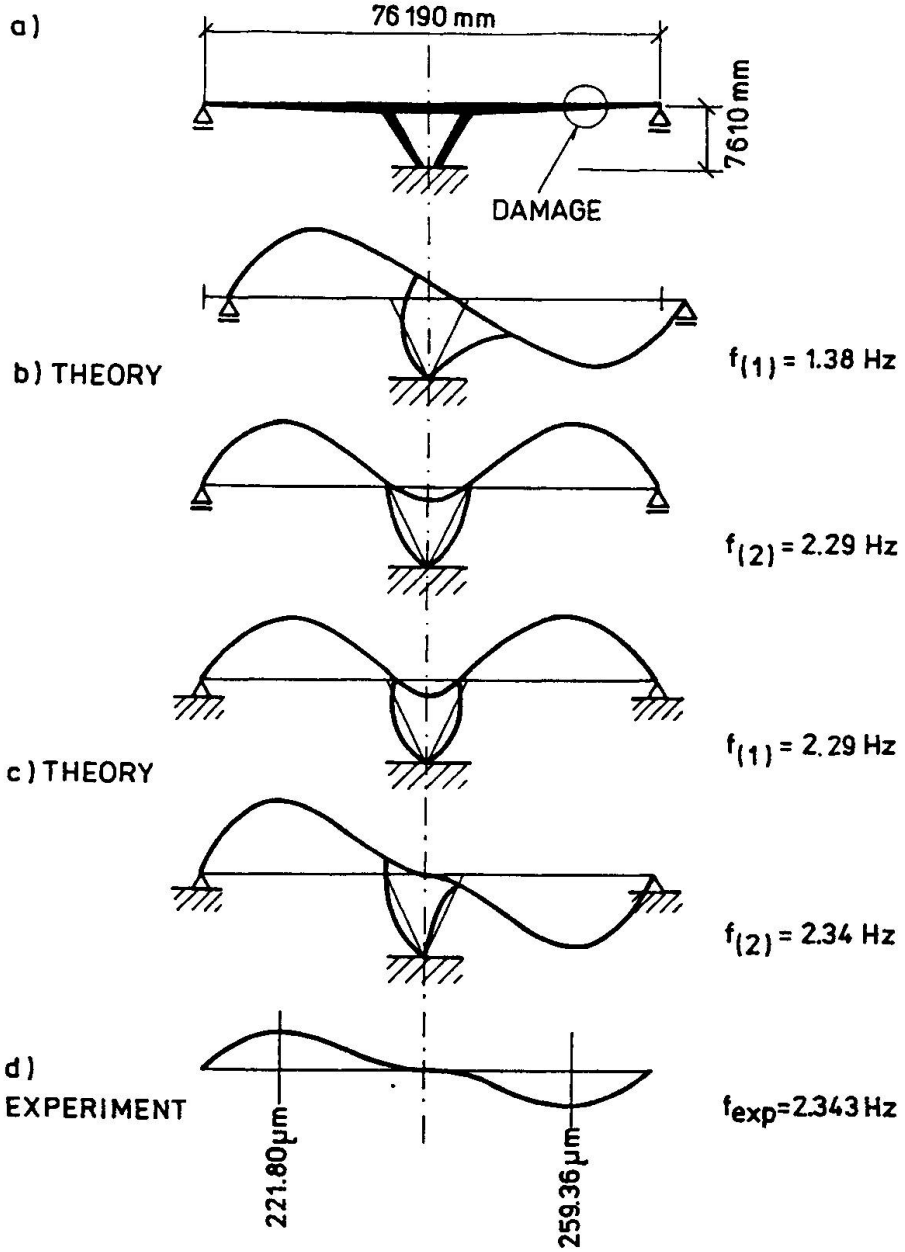

Fig. 2 Prestressed concrete highway bridge of length 76,19 m
a) scheme of the bridge,
b) theoretical modes of natural vibration of the bridge with moving bearings,
c) theoretical modes of natural vibration of the bridge with blocked bearings,
d) experimental mode of natural vibration

3. IDENTIFICATION

A special identification method was developped for bridges [4]. It is based on dynamic tests where the bridge is loaded by a periodic exciter. (An other possibility of loading would be an impact by a load or by a rocket motor, or a moving vehicle. However, the last types of loading are less convenient than an exciter because they excite more harmonics.)

The identification of a damage and of incorrect function of bearings is shown in Fig. 2 as an example. It represents a prestressed concrete highway bridge which was damaged by peeled off concrete. The excitation by a harmonic force provided the measured frequency $f_{exp} = 2{,}343$ Hz (Fig. 2d) that did not correspond to the theoretical calculations (Fig. 2b). It was discovered that the bearings were blocked after 20 years traffic. The new theoretical model gave the value 2,34 Hz (Fig. 2c) that is in good agreement with the measured value 2,343 Hz (Fig. 2d). Even the mode of natural vibration is similar.

Moreover, the experimental excited mode discovered the place of damage (peeled off concrete, Fig. 2a) where the amplitude was higher (+29%) than on opposite side of the bridge.

4. EFFECT OF DAMAGES

An other important question is the investigation of the deterioration of a bridge and of the location of a damage. This is possible using the repeated identification.

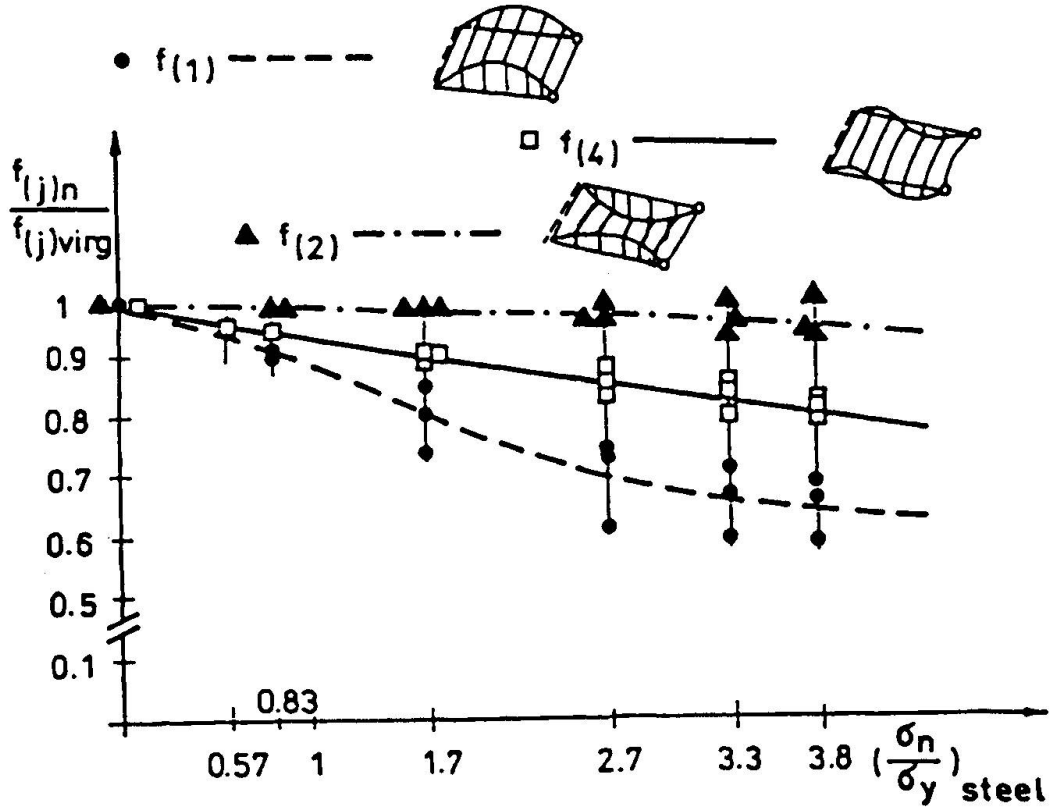

Fig. 3 Natural frequencies of 3 unloaded plates as a function of static loading :
$f_{(j)n}$ – j-th natural frequency after the n-th load step,
$f_{(j)virg}$ – j-th natural frequency before loading (in virginal state),
σ_n – real stress in steel bars after the n-th load step,
σ_y – yield stress of steel

As experiment, three rectangular concrete plates reinforced by a double net 6ø6 mm/m were produced; dimensions 1,5x2 m, thickness 50 mm, hinged supported along the short side and

two pendulum bearings at the corners of the opposite side. The plates were loaded at their centres in steps by 1,25; 2,5; 4; 5 and 5,7 kN. The static load acted for 4 minutes on the plate and between every two loads the cracks in concrete and dynamic response of unloaded plate were measured. For dynamic testing an electrodynamic exciter was applied. The response was measured in 35 points.

It has shown (Fig. 3) that the repeated loading affects the cracks in concrete, natural frequencies and modes of natural vibration. The cracks diminish the natural frequencies, especially $f_{(1)}$ while the frequency $f_{(2)}$, corresponding to the torsion, was hardly affected. The diminishing in frequencies amounted to 30-40% for $f_{(1)}$, 0,5-7% for $f_{(2)}$, 17-23% for $f_{(3)}$ and 17-20% for $f_{(4)}$ after the fifth load 5,7 kN.

The values $(\sigma_n/\sigma_y)_{steel}$ = 0,57; 0,83; 1; 1,7; 2,7; 3,3 and 3,8 correspond to the applied static forces 0,86; 1,25 (maximum life load); 1,5; 2,5; 4; 5 and 5,7 kN, respectively in the Fig 3. The energy necessary for the excitation of the response diminishes with the increasing deterioration of plates. The sequence of this conclusion is the increasing dynamic yielding with increasing load.

5. CONCLUSIONS

Monitoring of stresses in bridges for a longer period presents valuable data necessary for the estimation of their fatigue life. It has appeared that both static and dynamic stress ranges and their distribution are very important.

The repeated monitoring could recognize the damages and their location in bridges. Of course, it means the repetition of experiments several times in intervals, say 10 years, under the same conditions including the identification of the original state before traffic (virginal state). A series of such tests may identify the damages and their location. Corresponding criteria for the changes in the natural frequencies and for deformations of modes of natural vibration should be developped in the future.

REFERENCES

1. DOWLING, N.E., Fatigue Failure Predictions for complicated Stress-Strain Histories. J. Mater., 7 (1972), No. 1, pp.71–87.
2. FISHER, J.M., Fatigue and Fracture in Steel Bridges. John Wiley and Sons, New York, 1984.
3. FRÝBA, L., Dynamics of Railway Bridges. Thomas Telford, London, 1995.
4. PIRNER, M., Identification of Bridges following from Dynamic Tests. Proceeding Czech-US Bridge Conference, Prague, 1994, pp.219-227.

Deterioration in Fatigue Detected by Acoustic Emission Technique

Étude du comportement à la fatigue au moyen d'émissions acoustiques

Untersuchung des Ermüdungsverhaltens durch Schallemissionsmessungen

György L. BALAZS
Associate Professor
Techn. Univ. of Budapest
Budapest, Hungary

Christian U. GROSSE
Scientific Assistant
Univ. of Stuttgart,
Stuttgart, Germany

Rainer KOCH
Head of Concrete Div.
Otto-Graf-Institute
Stuttgart, Germany

György L. Balazs is an associate professor of civil engineering at the Technical University of Budapest and a research associate at the Otto-Graf-Institute in Stuttgart. He has been active in experimental research on bond and cracking in concrete.

Christian U. Grosse graduated in Geophysics at the University of Karlsruhe in Germany. After four years at the Otto-Graf-Institute in Stuttgart he works now at the Institute of Structural Materials. He has a special interest on non-destructive testing and ultrasonic techniques.

Rainer Koch is head of the Concrete Structures Division of the Otto-Graf-Institute. He graduated in civil engineering and made his Ph.D. at the Stuttgart University. His main fields of interest are experimental and theoretical studies on structural concrete, shear, cracking and bond behaviour.

SUMMARY

The acoustic emission technique was used to investigate the progress of local damage on steel-concrete interactions subjected to repeated loading. The accumulation of internal damages detected by this technique gives a clear indication on the failure process and the subsequent failure. The damage accumulation, defined as the cumulative acoustic emission amplitudes, resulted in a similar tendency to the cyclic creep of bond.

RÉSUMÉ

La technique d'émission acoustique est appliquée pour examiner l'évolution des dommages locaux au contact acier-béton causés par des charges répétées. L'accumulation des dommages internes détectés par la technique d'émission acoustique permet d'observer le processus et la nature de la défaillance. L'accumulation des dommages, défini par les amplitudes cumulatives, indique un comportement ressemblant au fluage cyclique de l'adhérence.

ZUSAMMENFASSUNG

Mit Hilfe der Schallemissions-Technik wurde das Ermüdungsverhalten des Verbundes zwischen Stahl und Beton im Hinblick auf die lokale Schädigung untersucht. Diese Analyse liefert dabei wertvolle Hinweise über das Entstehen von inneren Schäden, den Schadensprozess sowie schliesslich über das Versagen des Bauteils. Das Schadenswachstum, ausgedrückt durch die Summenamplitude der Schallemissionen, zeigt dabei ein paralleles Verhalten zum zyklischen Kriechen des Verbundes.

1. INTRODUCTION

Repeated loads produce a progressive deterioration of the materials indicated by increasing deformations and decreasing stiffness. The deterioration is caused by internal damages.

We experimentally studied the failure process of the steel-concrete interaction under repeated loading by simultaneous registration of the acoustic emission (AE) signals and the bond-slip behavior.

Detection and evaluation of AE signals developed considerably [1,2,3] and it seems to be a very promising technique for the analysis of internal damages and their accumulation. The parallel registration of AE signals and the bond-slip behavior provided two sets of independent measurements for comparison.

Interactional (bond) stresses are associated with slip in reinforced concrete members over the steel-concrete interface indicating micro-cracking [4] and micro-crushing [5] in the concrete surrounding the reinforcing bars. Repeated loads induce an increase in slip indicating the progressive local damages without an increase in the load level.

2. EXPERIMENTATION

The specimen was a special pull-out specimen (Fig.1) had a rather short bond length of 20 mm (two rib distances) to minimize the number of sources producing local damages. The high yield (f_y=500 N/mm^2) deformed reinforcing bars of 16 mm diameter were placed centrically into the concrete cubes of 100 mm sides and had a relative rib area of 0.065. The rib pattern consisted of moonshape ribs and two longitudinal ribs.

This type of specimen provided a possibility for the registration of the entire deterioration process from the beginning of loading to the fatigue failure.

Mix proportions of concrete were 1 : 2.82 : 2.22 : 2.37 by weight of Portland cement, fine aggregate (0 to 2 mm), medium size aggregate (2 to 8 mm) and coarse aggregate (8 to 16 mm). The specimens were fog-cured at a temperature of 20°C for 7 days and then were kept in laboratory conditions. The mean compressive strength at testing measured on three cubes of 150 mm sides was 34.9 N/mm^2.

The specimens were tested in a servo-hydraulic machine [6]. The tensile force acted on the reinforcing bar and the specimen was supported by a steel plate (Fig.1). The slip was measured by an LVDT of 1 μm sensitivity at the unloaded end of the specimen.

For the recording of AE signals a transient recorder with eight channels was used with a sampling rate of 1 MHz and an internal storing facility of 256 kWord for each channel (1 Word = 2 Byte). Using only the internal memory, 243 events could be recorded with a length of 1 kWord each. The amplitude resolution of each A/D-converter was 12 bits. The signals were recorded by eight piezo-transducers, coupled to the five sides of the specimens. Six had a so-called broadband characteristic type UPE by GEOTRON and 8694 by KISTLER; two transducers operated in resonance type 8612 by KISTLER with a main frequency of about 20 kHz. They were amplified by an eight-channel preamplifier with a gain between 0 and 100 dB. We carefully paid attention to the electric decoupling of the AE monitoring system to prevent the recordings being effected by the noise of the servo-hydraulic machine.

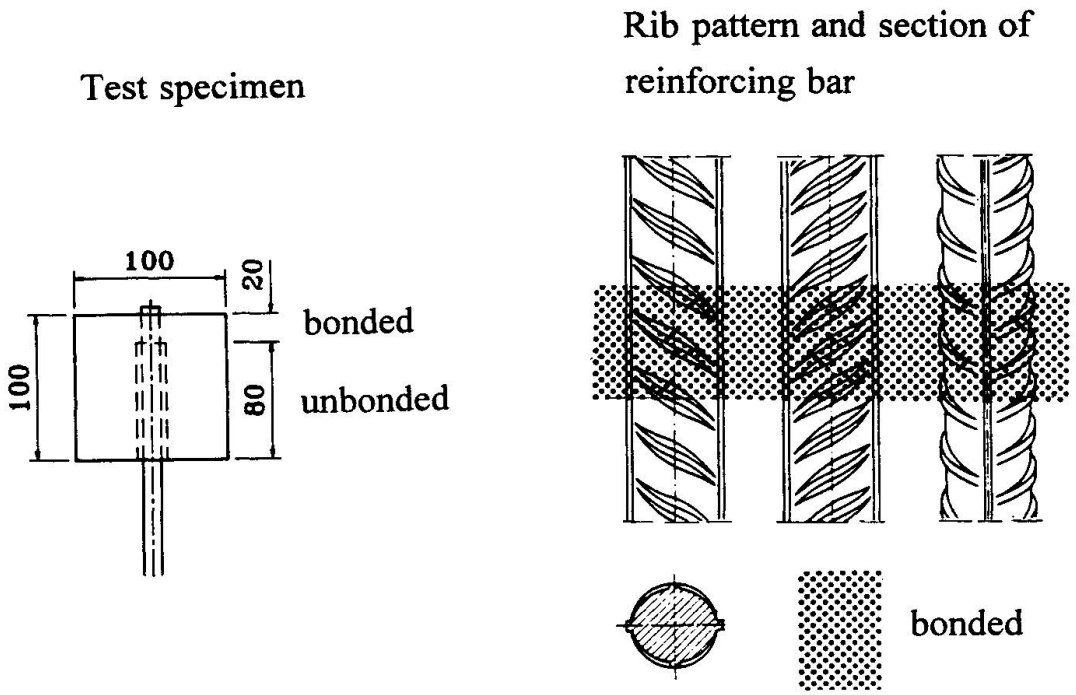

Fig.1 Test specimen and rib pattern of tested reinforcing bar

3. DETERIORATION IN FATIGUE

The results of six deformation controlled monotonic pull-out tests together with the comparison of AE signal patterns using the coherence spectrum analysis based on the fast Fourier transforms of the signals are discussed in Ref. [6].

Three typical results of the six fatigue tests are presented in Figs.2 to 4 applying one, two or four blocks of constant amplitude cyclic load. The frequency of repeated loading 4 s^{-1}. The load levels are given in percentage values, i.e. the maximum value of repeated load ($\tau_{b,max}$) related to the monotonic bond strength (τ_{bu}) measured on an average 15.4 N/mm^2. The minimum value of repeated load ($\tau_{b,min}$) was 10 percent of the maximum value.

The upper parts of Figs.2 to 4 indicate the load histories as well as the registered AE amplitudes as bar graphs. The amplitudes are given in relative values of the maximum peak-to-peak-values of the signals (denoted as PA sum per time unit) and are summed in 10 or 15 s intervals. The bottom parts of the same figures indicate the *accumulated damage* as the accumulated sum of the AE amplitudes with bar graphs as a function of the time (called Cumulative PA) together with the simultaneously measured slip versus time (number of load cycles) relationships.

Most of the AE signals were registered by applying the initial monotonic load up to the mean value of cyclic load, then at the beginning of the cyclic load or at an increase in the cyclic load level and preceeding the pull-out failure. However, signals were also detected during a block of constant amplitude cyclic load.

From the comparison of bottom figures in Fig.2 to 4 it is seen that the internal damage accumulation, defined as the cumulative AE peak amplitudes indicate a similar tendency to the cyclic creep of bond given as a slip versus time relationship.

Nevertheless, the internal damage accumulates rather linear in a block of constant amplitude cyclic loading following a transitional period after reaching the cyclic load level and accelerates preceeding the failure.

4. CONCLUSIONS

The internal damage accumulation under repeated loading was experimentally studied on the steel-concrete interaction using the AE technique with simultaneous registration of the bond slip.

Most of the AE signals were registered by applying the initial monotonic load up to the mean value of cyclic load, then at the beginning of the cyclic load or at an increase in the cyclic load level and preceeding the pull-out failure. However, signals were also detected during a block of constant amplitude cyclic load.

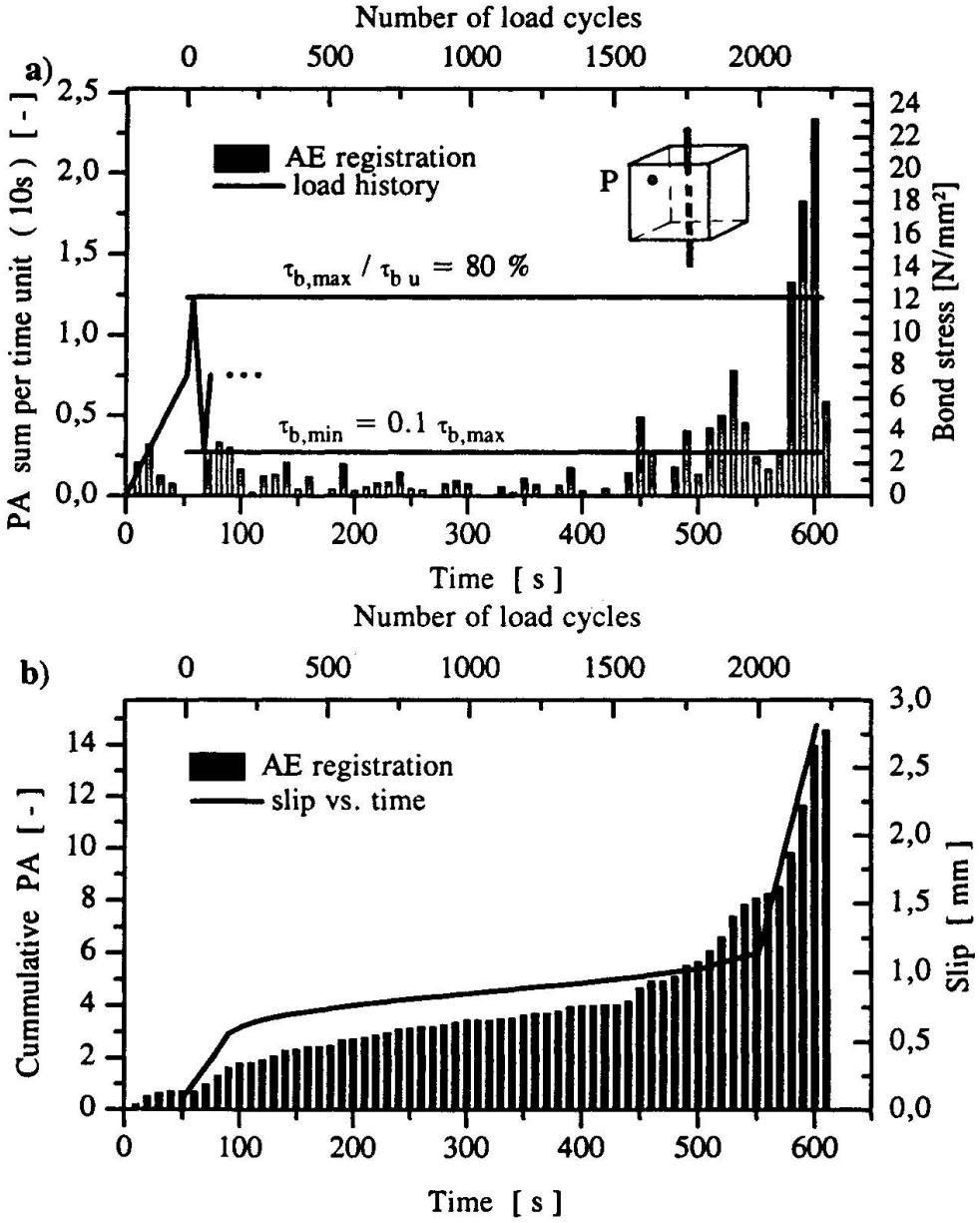

Fig.2 Cyclic pull-out test with *one load level* to pull-out failure (P: piesotransducer)
a) PA sums in 10 sec intervals and τ_b vs. time b) Cum. PA vs. time

5. ACKNOWLEDGEMENTS

The financial support of the reseach project from the German Science Community (DFG) is greatly acknowledged

6. REFERENCES

1. STEARNS, D.S., Digital Signal Analysis. Hayden Book company, 1975.
2. GROSSE, C. U., REINHARDT, H.-W., Lokalisierung von Schallemissions-Signalen in Stahlbeton bei Pull-Out-Tests. Proceedings of the 10-th Colloquium on Acoustic Emission in Jena, Germany, DGZfP, 1994.
3. GROSSE, C.U., REINHARDT, H.-W., BALÁZS, G.L., Acoustic Emission Data from Pull-Out Tests of Reinforced Concrete Analysed with Respect to Passive US-Tomograpy.

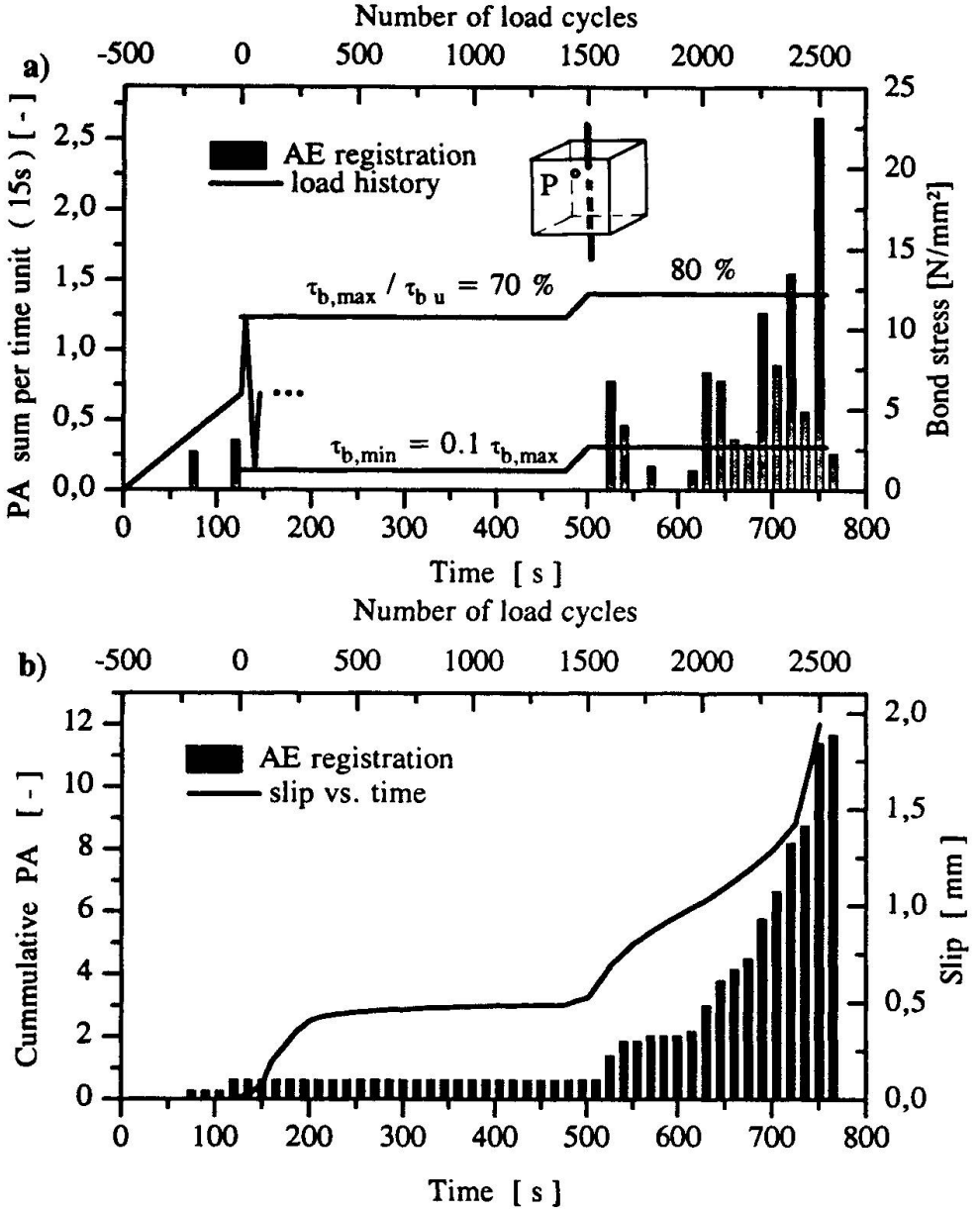

Fig.3 Cyclic pull-out test with *two load levels* to pull-out failure
a) PA sums in 15 sec intervals and τ_b vs. time b) Cum. PA vs. time

Proceedings of the 11-th Symposium on Acoustical Imaging in Laguna Beach, California, Plenum Press, 1995 (in printing)
4. GOTO, Y., OTSUKA, K., Studies on Internal Cracks Formed in Around Deformed Tension Bars. ACI Journal, April 1971.
5. GAMBAROVA, P., GIURIANI, E., Fracture Mechanics of Bond in Reinforced Concrete. Discussion, Journal of Structural Engineering ASCE, May 1985.
6. BALÁZS, G.L., GROSSE, C.U., KOCH, R., REINHARDT, H.W., Acoustic Emission Monotoring on Steel-Concrete Interaction. Otto-Graf Journal, 1993.

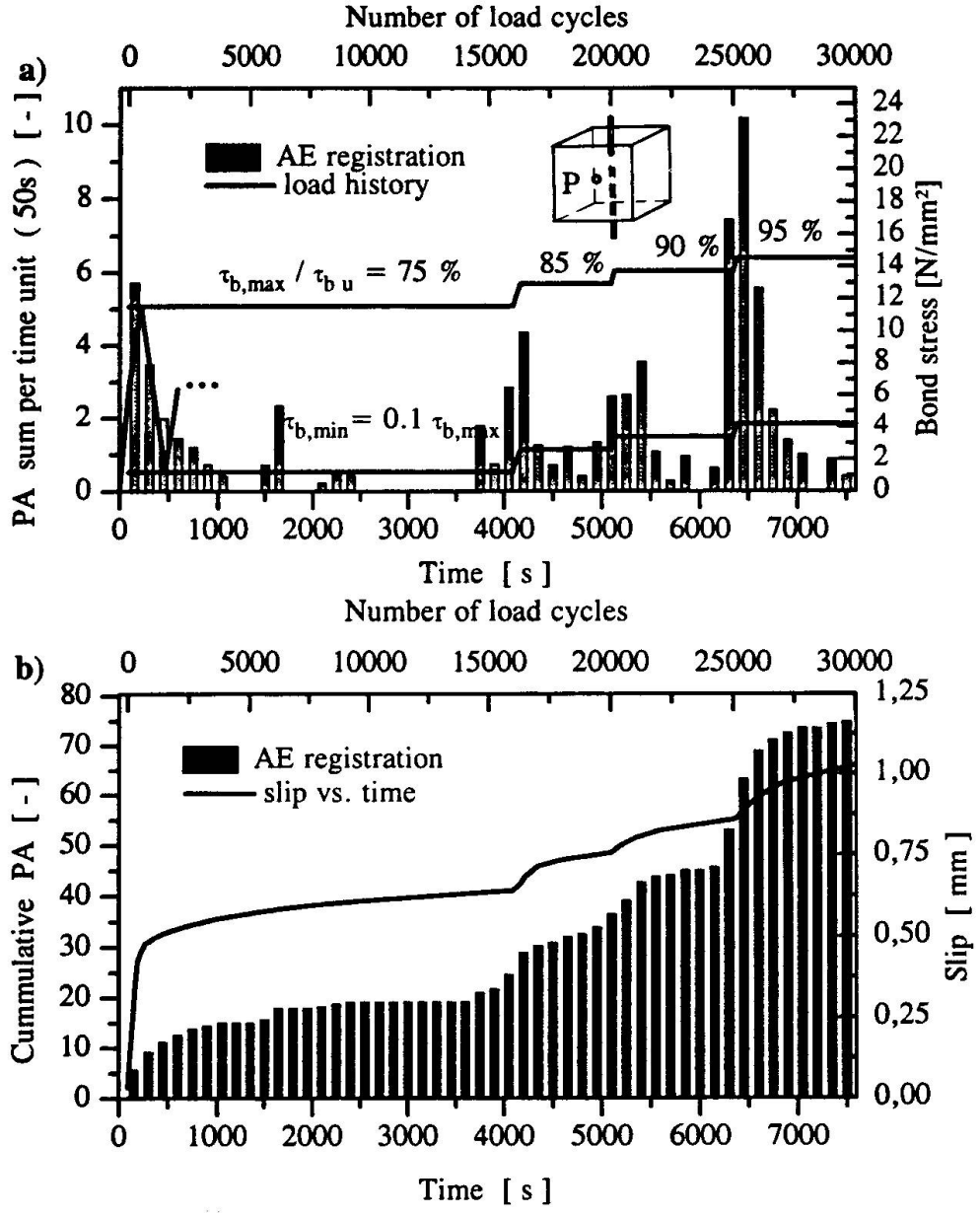

Fig.4 Cyclic pull-out test with *four load levels*
a) PA sums in 50 sec intervals and τ_b vs. time b) Cum. PA vs. time

Preventive Maintenance Methods for Fatigue Damage of Bridges

Maintenance préventive pour éviter les dommages par fatigue des ponts

Vorbeugende Instandhaltungsmassnahmen bei Ermüdungsschäden von Brücken

Shigeru NAITO
Assistant Chief
Central Japan Railway Co.
Tokyo, Japan

Makoto ABE
Managing Director
BMC Corporation
Chiba, Japan

Ichiro SUGIMOTO
Researcher
Japan Railway Techn. Res. Inst.
Tokyo, Japan

Hidehiko ABE
Professor
Ashikaga Inst. of Technology
Tochigi, Japan

SUMMARY

Fatigue damage is a problem with steel bridges, especially those of the Tokaido bullet train line, where the train traffic is very heavy. This situation requires measures for prevention and prediction of cracks, because they may propagate rapidly. The prediction method used for the bridges of Shinkansen are discussed.

RÉSUMÉ

Les dommages par fatigue sont un problème des ponts métalliques. C'est en particulier le cas des ponts de la ligne du train à grande vitesse Shinkansen dont le trafic ferroviaire est considérable. Cela exige des mesures de prévention et de prévision, car les fissures se propagent rapidement. Le présent document expose la méthode de prévision utilisée pour le réseau ferroviaire japonais.

ZUSAMMENFASSUNG

Ermüdungsschäden in Form von Rissen sind bei Stahlbrücken ein grosses Problem, insbesondere bei denen der Tokaido Shinkansen-Linie, und erfordern daher entsprechende Massnahmen zur Vorbeugung und Voraussage. Beschrieben werden die von den Bahngesellschaften in Japan eingesetzten Vorsorgemassnahmen.

1. INTRODUCTION

Fatigue is likely to become a problem on lines which pass a large number of trains or are submitted to high working stress, since the number of trains and their speeds are expected to rise. Then the traditional corrective method of bridge maintenance after damage has occurred due to fatigue will be inadequate to keep the steel bridge in sound condition and introduction of a preventive one implementing the technology of damage prediction will be mandatory. In this paper, the past practice of fatigue estimation in steel railway bridges is reviewed and referring to the latest progress in the related studies and development of new technologies, a new method of estimating the service life of steel railway bridges is proposed.

2. FATIGUE ANALYSIS AND ITEMS STUDIED

Steel bridges in service should be examined for fatigue according to the following scheme:

2.1 Observation of Fatigue Damage Already in Evidence

(1) Evaluation of soundness concerning a revealed fatigue crack
(2) Investigation into the cause of a revealed fatigue crack(load-bearing capacity of structural member, stress behavior,study of displacement).

2.2 Prediction of Fatigue Damage

(1) Inspection of fatigue limit
(2) Prediction of fatigue crack occurrence and extent
(3) Estimation of residual service life of a cracked structural member.

2.3 Estimation of Service Life (residual life) of a Structure.

Here, the method of predicting the fatigue damages is described.

3. EVALUATIONS TO PREDICT FATIGUE DAMAGE

Meanwhile, fatigue damage may be predicted in terms of "fatigue limit" or "degree of fatigue damage. To see if a fatigue damage is likely to happen, an inspection is made for "fatigue limit". On the other hand, an inspection for "degree of fatigue damage" is done when, during inspection for "fatigue limit", the maximum stress range exceeds the fatigue limit; and it is made for predicting the occurrence timing of fatigue damage. For analysis of the degree of fatigue damage, the method by "cumulative damage" and one by "fracture mechanics" are available.
Only the method by the accumulation fatigue damage is shown. Fig.1 shows assessment of fatigue damage in steel railway bridges.

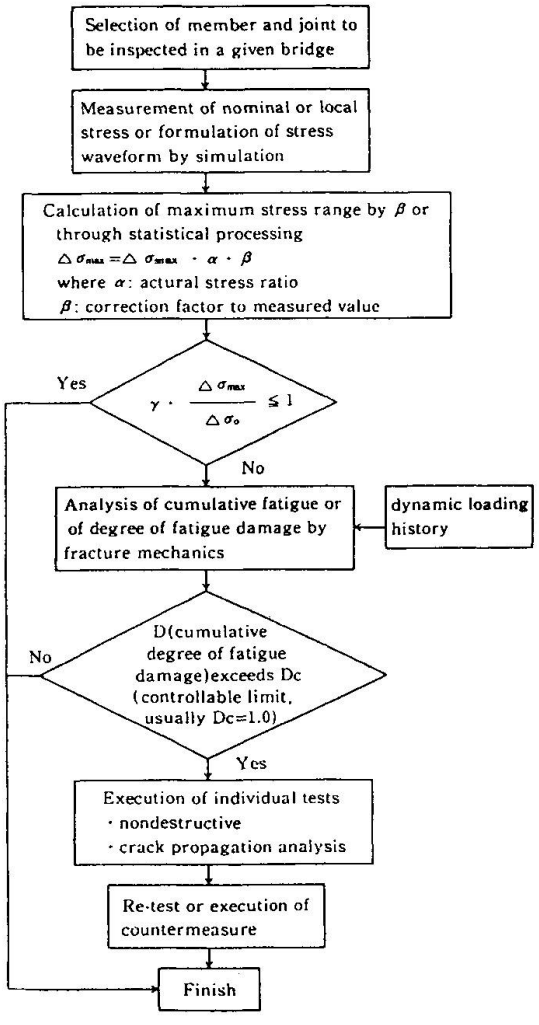

Fig.1 Assessment of fatigue damage

3.1 Assessment for Fatigue Limit

A problem with a structural member as to whether it will raise a fatigue concern in future may be approached from the theory of the so-called "fatigue limit" that the member, such as a joint, will not develop a fatigue failure unless the limit of stress range (fatigue limit) corresponding to a definite vibrational stress of the joint is surpassed, that is, using the following condition:

$$\gamma \cdot \frac{\Delta\sigma_{max}}{\Delta\sigma_0} \leq 1 \qquad (1)$$

with $\Delta\sigma_{max} = \Delta\sigma_{smax} \cdot \alpha \cdot \beta$ α,β : modified factor

where $\Delta\sigma_{smax}$: maximum stress range simulated or measured
$\Delta\sigma_0$: stress range as fatigue limit

The value of $\Delta\sigma_0$ is taken from Table 1 giving the new design standard.[1] The safety factor of a structure is determined in accordance with redundancy, importance and degree of inspection of the structure. In the case of railway bridges, a rather large value is assigned to redundancy and importance, while a rather small value is assigned to degree of inspection, considering that a periodic inspection is mandatory. Thus in the present practice assuming that good balance is assured among these three elements, the safety factor is normally set: γ=1.0.

Rank	Stress range as fatigue limit $\Delta\sigma_0$ kgf/cm² (MPa)
A	1900 (190)
B	1550 (155)
C	1150 (115)
D	840 (84)
E	620 (62)
F	460 (46)
G	320 (32)

Table 1 Fatigue limit for joints

3.2 Analysis of the Degree of Fatigue Damage

Degree of fatigue damage due to cumulative fatigue means the degree of accumulated fatigue damage, assuming that fatigue damage of a given joint occurs when the degree of fatigue damage accumulates to 1.0 (law of linear cumulative fatigue damage). In the case of railway bridges the degree of fatigue damage is more often expressed in terms of a single train or of accumulated degree of damage to the joint. Then the degree of fatigue damage D after passage of a single train (or a single unit of working load) is given by Equation.

$$D = \sum \frac{N_{eq}}{N_1} = \frac{1}{N_1} \sum \left[\frac{\Delta\sigma_i}{\Delta\sigma_1}\right]^m \cdot n_i \qquad (2)$$

Where
$\Delta\sigma_i$, n_i : respectively stress range generated by imposition of a single unit of working load, and its repetition cycle; $\Delta\sigma_i = \Delta\sigma_{s(i)} \cdot \alpha$
$\Delta\sigma_{s(i)}$: maximum stress range determined by simulation or measurement
$\Delta\sigma_1$, N_i : standard stress range and its cycle in which a crack initiates respectively.
N_{eq} : equivalent cycle of action by a single unit of working load, as converted to $\Delta\sigma_1$.

3.3 Actual Stress Ratio α

Actual stress ratio is utilized when the stress obtained through design calculation or simulation is to be converted to "working stress" for evaluation of fatigue and it is given as a ratio between measured stress and design-calculated stress. The actual stress ratio α . α sets the following values by the "Maintenance Standards"[2] now.

Influence line length	Actual stress ratio α
≤ 10m	0.65
≥ 10m	0.75

3.4 The Factor β to Correct the Measured Value

When the measured value is employed in the evaluation of fatigue limit, it will not always occur that the maximum value of stress in the range obtained thereby falls into the maximum stress range employed in the evaluation of fatigue damage. The correction factor β is provided to allow for such circumstance. In that case, β should be determined by first measuring the long-term stress frequency and therefrom calculating the probability density function. When the probability density distribution is a normal logarithm one, the non-excess probability value 97.7% is taken as the maximum value to be used in the inspection for fatigue limit and the ratio of this value to the mean (here root cube mean) in the distribution is set as β.
Accordingly, it is assumed that the product of multiplying the mean of measured values sampled by β is the maximum stress range to be employed in the inspection for fatigue limit. Incidentally, in the case of Shinkansen, the value of β is supposed to be in the range of 1.4-1.7.[3)]

4. ESTIMATION OF SERVICE LIFE FOR STEEL RAILWAY BRIDGES

4.1 Service Life for Steel Railway Bridge

"Life" which determines the endurance of steel railway bridge is variously defined. In one definition the life of the bridge is exhausted "when a damage occurs to it, which proves economically and physically fatal to maintenance of its structural strength and function;[4),5)] and thereby the period up to this time may be deemed "physical endurance period considering the structural economy (service life)".

4.2 Basic Formula for Evaluation of Fatigue Damage in Calculation of Service Life

Also in calculation of service life, as stated earlier there are two methods of evaluating the fatigue damage: "cumulative fatigue damage" approach and "fracture mechanics" approach.

4.2.1 Evaluation of cumulative fatigue damage

In the application of the above law to the evaluation of an existing structure for its soundness about fatigue, the fatigue damage is divided into D_{pT} so far accumulated and D_{aT} expected to accumulate in future; and when the sum of the two becomes one, it is considered that fatigue failure will take place.

$$D_{pT} + D_{aT} = 1 \qquad (3)$$

For the Δσ- N diagram to be used for evaluation, the Miner law considering no fatigue limit, the modified Miner law considering no fatigue limit or the Haibach method employing a bi-linear strength line diagram for the long-life zone is available, but here "the revised Miner method with cut-off limit" proposed by Miki et al. is adopted.[6)] This method is characterized in that the limit value of stress range which does not contribute to fatigue damage even under variable amplitude stress is introduced in the revised Miner law.

4.2.2 Evaluation of Fatigue Life in the Corroded Member

Usually the designing provides for possible corrosion in the structure and, except for some members, the strength inspection pays little attention to the corroded degree. And even in the maintenance control for fatigue life a decrease in the fatigue strength due to corrosion is more often not considered, although the notched section receives attention. The reasons are that the structures are usually placed under adequate paint control; and from fatigue testing to used girders it is confirmed that supposing a fatigue crack has originated from local corrosion at depth, its propagation stops midway and in consequence the ultimate failure takes place at the smallest section.[7)] Thus as far as a actual structure is concerned, it seems that in the fatigue life evaluation we need not be concerned about any local roughness.

Therefore, the evaluation is to be made using the Δσ –N diagram considering the corrosion to a certain extent, though not all is known about the influence of corrosion, so that wrong or dangerous evaluation may not be made. (see Table 2)

kind of stress	kind of joint		strength class	two million cycle strength	gradient	remark (gauge, direction, etc)
nominal stress	flange	base metal corroded	C	125	3	stress inspected on pure section with no-cut off limit
	rivetted joint	slightly corroded	C	125	3	stress inspected on pure section
hot spot	joint with no definition of nominal stress	weld finished or good bead form	D	100	3	stress measured at hot spot and analized
		non-finished	E	80	3	

Table 2 Two million cycle strenth of joints to be employed in fatigue evaluation of girders in service

4.3 Calculation Formulas for Cumulative Fatigue

4.3.1 Cumulative Fatigue D_{pT} so far Suffered and Cumulative Fatigue D_{aT} for Calculation of Residual Life

When, against the degree of fatigue damage expressed in (2), the cycle number of each stress level of K-class so far suffered and the fatigue life (cycle) at stress $\Delta\sigma_i$ are respectively given as n_i and $_i$; and the cycle number causing equivalent damage to the joint of $N_0=2\times10^6$ cycle fatigue strength $\Delta\sigma_{fo}$ is given as N_{0eq}, the cumulative damage D_{pT} can be expressed by

$$D_{Tp}=\sum_{i=1}^{k}\frac{n_i}{N_1}=\frac{N_{oeq}}{N_0} \qquad (4)$$

where, since the equivalent cycle number N_{oeq} is

$$N_{oeq}=\sum_{i=1}^{kp} n_i\cdot\left[\frac{\Delta\sigma_i\alpha}{\Delta\sigma_{fo}}\right]^m \qquad (5)$$

D_{pt} may be rewritten as

$$D_{pT}=\frac{1}{N_0}\sum_{i=1}^{kp} n_1\cdot\left[\frac{\Delta\sigma_i\alpha}{\Delta\sigma_{fo}}\right]^m \qquad (6)$$

D_{at} may also be written similarly as follows:

$$D_{aT}=\frac{1}{N_0}\sum_{i=1}^{ka} n_1\cdot\left[\frac{\Delta\sigma_i\alpha}{\Delta\sigma_{fo}}\right]^m \qquad (7)$$

where N_0 : 2×10^6 cycles
$\Delta\sigma_i$, n_i : i-th stress range and its cycles
$\Delta\sigma_{fo}$: 2x10 cycle strength of the joint
k_p : number of modes of stress range so far suffered
k_a : number of modes of stress range to be suffered thereafter
m : coefficient determining the gradient of the Δσ– N diagram of the joint
α : actual stress ratio.

4.3.2 Calculation of Residual Life

The cumulative fatigue allowable hereafter, that is D_{at} may be derived from (3) as follows:

$$D_{aT} = 1 - D_{pT} \quad (8)$$

Otherwise, D_{aT} can be given using the residual life (Tr) as follows:
D_{aT} = (annual sum of fatigue damages to be suffered hereafter) x Tr (years) Namely,

$$D_{aT} = \frac{1}{N_0}\sum_{i=1}^{ka}\left\{n_{aeq(i)}\cdot\left[\frac{\Delta\sigma_{amax(i)}\alpha}{\Delta\sigma_{fo}}\right]^m\right\}T_r \quad (9)$$

$$n_{aeq(i)} = \sum_{i=1}^{nn}\left\{n_i\cdot\left[\frac{\Delta\sigma_i}{\Delta\sigma_{amax(i)}}\right]^m\right\}N_y \quad (10)$$

where

$\Delta\sigma_{amax(i)}$: maximum stress range generated by trains to be operated
$n_{aeq(i)}$: annual equivalent cycle of maximum stress range by each train operated
$\Delta\sigma_{(i)}, n_{(i)}$: each stress range derived from frequency analysis of variable stress generated by each running train; and its repetition cycle, respectively.
nn : number of stress range levels for frequency analysis under passage of one train
N_y : number of trains passed in a year; if not known, it is assumed that N=365 x n_{ad}
n_{ad} : number of trains passing in a day

$$T_r = N_0(1 - D_{pT}) / \sum_{i-1}^{ka}\left\{n_{aeq(i)}\cdot\left[\frac{\Delta\sigma_{amax(i)}\alpha}{\Delta\sigma_{fo}}\right]^m\right\} \quad (11)$$

4.3.3 Strength Used for Cumulative Fatigue

Girders in service may comprise ones corroded partially, ones additionally treated in the field, and ones with their nominal stress not exactly known on account of complex structure or joint profile. Various surveys are underway about these anomalies the above-given Table 2 is resorted to.

5. CONCLUDING REMARKS

To cope with fatigue damage to steel railway bridges expected to aggravate with operational speed-up and increase in the number of trains operated, the technical background of methods for evaluation of fatigue damage is reviewed. Against the fatigue damage anticipated hereafter, it would be necessary to implement the technology of predicting the occurrence and propagation of cracks, unlike the traditional practice dealing with the defect after it has been discovered. Such technology is applicable for estimating the residual life of the existing steel bridges. It is important hereafter to upgrade the precision of evaluation by building up the data on the working stress and the fatigue strength of joints. It is believed that introduction of this technology will enable efficient maintenance control and reasonable replacement planning of steel railway bridges.

REFERENCES

1. Design Standard for Railway Structure (Steel Railway Bridges and Composite Girder Railway Bridges), Maruzen Co., 1992.Oct.
2. Railway Technical Research Institute: Steel Railway Bridges Maintenance Standard, 1987.Jul.
3. Sakamoto,K., Abe,M., Sugidate.: "Fatigue Strength of Steel Railway Bridge Members under Actual Train Load" (Pt.1,Pt.2),RTRI Report, 3,10(1989), 5,5(1991)
4. Murakami,A.: Maintenance and design life : Civil Engineering Planning Symposium, 17,pp.30-36, 1983.Jun.
5. Enomoto,M.: What is life of structure of civil engineering", J.Japan Soc Civ Eng.1985.Aug.
6. Miki,C., Sakano,M.: Fatigue Crack Propagation Analysis on Fatigue Design Curves", J.Str. Eng, 36a, 1990.Mar.
7. Takena,K., Kawakami,H., Asakawa,K., Abe,M.: "Fatigue Strength of Weathered and Deteriorated Rivetted Plate-Girder", RTRI Report, 1339,1987.Feb.

Influence of Loadings on the Fracture Toughness of Older Structural Steels

Influence des charges sur la fragilité à la rupture d'anciennes structures métalliques

Lasteinfluss auf die Bruchzähigkeit älteren Baustahls

Mikael LORENTZON
Graduate Student
Luleå University
Luleå, Sweden

Mikael Lorentzon, born in 1967, received his M.Sc. degree in mechanical engineering 1992. He is now at Luleå University Dept of Solid Mechanics for research studies in fracture mechanics.

Kjell ERIKSSON
Assistant Professor
Luleå University
Luleå, Sweden

Kjell Eriksson, born in 1941, received his Ph.D. in fracture mechanics in 1975, and was with the Dept of Welding, Royal Inst. of Technology, Stockholm, Sweden, until 1989. His research field is fracture and fatigue of heavy welded steel structures.

SUMMARY

Full scale rolled wide flange beam elements taken from dismantled railway bridges, and extracted small laboratory fracture toughness specimens have been used to study the influence of quasi-static loading rates and temperature upon fracture toughness. It is found that quasi-static loading rates affect fracture toughness of older structural steels significantly both at summer and winter temperatures.

RÉSUMÉ

Des éléments de profilés laminés à larges semelles, découpés dans des ponts-rails démantelés, et de petites éprouvettes de laboratoire ont été utilisés pour étudier l'influence du taux de charge quasi-statique et de la température sur la fragilité de la rupture d'anciennes structures métalliques. Il a été constaté que la fragilité est affectée de manière significative par ce taux de charge, aussi bien à des températures estivales qu'hivernales.

ZUSAMMENFASSUNG

An herausgeschnittenen Breitflansch-Walzträgerstücken, die von demontierten Eisenbahnbrücken stammten, und aus ihnen gewonnenen kleinen Bruchmechanikproben wurde der Einfluss quasi-statischer Belastungsraten und der Temperatur auf die Bruchzähigkeit untersucht. Es zeigte sich, dass quasi-statische Belastungen die Bruchzähigkeit älteren Baustahls sowohl bei Sommer- als auch bei Wintertemperaturen signifikant beeinflusst.

1. INTRODUCTION

Most structures in service are subjected to quasi-static loading conditions. We have found experimentally that typical loading rates in railway bridges of ordinary structural steel affect fracture toughness and structural reliability. This kind of influence has not been reported widely in quantitative terms in the literature, particularly in the elastic-plastic range. Quasi-static means in this context loading rates just above the maximum rate stipulated in current fracture toughness testing standards, e.g. ASTM E813 [1], but not high enough to involve effects of inertia.

For structures in cold climate regions with winter temperatures frequently down to -30 °C and below, it is of vital importance to understand the combined effect temperature and loading rate upon fracture toughness of structural steels. The ductile-to-brittle transition of ferritic steels with decreasing temperature under static loading conditions is a well-known phenomenon.

The concept of transferability plays an important role in evaluation schemes of existing structures. The aim of fracture toughness testing is to evaluate structural reliability with respect to fracture from data obtained with small standard laboratory specimens. In this work we present experimental results from quasi-static fracture toughness testing of fatigue precracked full scale beam elements from dismantled railway bridges and of extracted Compact tension and Three point bend specimens.

2. MATERIAL

The test material comprised three broad flange I-beams. Two beams (Beam I, DIP 55 and Beam II, DIP 42 1/2) were taken from dismantled railway bridges and one St37 Class D beam (Beam III, HEB 400) was acquired directly from the manufacturer and used as reference material. Tensile properties are shown in Table I. The chemical composition of the steels are typical for carbon steels.

Table I. Tensile properties.

Beam	R_{eL} (MPa)	R_m (MPa)	A_5/A_{10} %	Z %	T (°C)
I	224	380	30	70	+ 20
II	300	480	33		- 30
III	283	442	34		+ 20
	295	470	33		- 30

3. EXPERIMENTAL

Full scale precracked 6 m long elements of Beam II and III were cooled to the testing temperature -30 °C and slowly loaded to failure in four point bending. Precracking, experimental details and the results of the static tests has been described elsewhere [2].

After static failure, one of the beam halves of each beam was precracked as above with an edge crack at its midsection and cooled to the testing temperature. The beam element was loaded to failure in three point bending at the maximum obtainable loading rate in a 10 MN servo-hydraulic closed loop testing machine. The distance between the outer supports was equal to or just above four times the beam height. During testing were recorded the load and load point displacement plus some fifteen strains, displacements and temperatures.

A series of standard Compact and Three point bend specimens were tested, except the loading rate, in accordance to ASTM E813. The laboratory specimens were machined

from the flanges of the beam elements. Specimen thickness was always equal to the full flange thickness in order to obtain the best estimate of the effective toughness of the flange material. The loading rates were based on measurements on railway bridges in service, generously provided by the Swedish National Rail Administration [3].

For materials with a considerable non-linear behaviour before fracture, it is always difficult to detect the point of initiation of stable crack growth. The standard unloading compliance technique cannot be used for the present loading rates. A scanning electron microscope was used to investigate the amount of stable crack growth preceding the final fracture on the fracture surfaces.

Fracture toughness was calculated from the area under the load-displacement curves to the maximum load using the equation for the three-point bend specimen $J_c = 2A/(Bb)$, where A is the area under the load-displacement curve, B specimen thickness and b remaining ligament. J_c is considered valid if the specimen meets the ASTM thickness requirement.

4. RESULTS

Crack lengths, loading rates and fracture toughness results for static and quasi-static testing of the beam elements II and III are summarized in Table II. The results of the static testing of the full scale beam elements are discussed in [2]. The points of interest for the present work are summarized here. The J-integral for the Beam III geometry is for convenience shown in Fig 1.

Table II. Effect of Loading rate, Full scale Beam elements, Temperature -30 °C.

Beam	Load. rate	Crack length (mm)	dσ/dt (MPa/s)	dK/dt (MPa √m/s)	Jc (kN/m)	Note
II	static	38	2	1	(>100)	Buckled
	quasi-static	78	385	220	41	Brittle
III	static	70	2	1	93	Ductile
	quasi-static	60	510	254		Brittle

The Beam II element rather buckled than failed through fracture because the crack was shallow and the beam geometry deficient towards one of the beam ends. The Beam III element failed through unstable fracture. The fracture toughness of the beam element is close to the lower limit of the scatter band of the extracted specimens.

In the quasi-static test the Beam II element failed in a very brittle manner. The fracture was fast and unstable and the fracture surfaces show all the characteristics of a brittle fracture. They are flat and normal to the nominal bending stress, there are no shear lips and chevron markings run to the point of initiation at the tip of the fatigue crack. The beam element failed at a nominal bending stress 158 MPa or 53 percent of the yield stress. The quasi-static fracture toughness is less than half of the lower limit for static testing of the extracted specimens.

In the Beam III element the loading rate was somewhat higher than in Beam II. This beam element failed also in a very brittle manner as described above. The beam halves were however free to move just enough to hit and short-circuit a data acquisition cable. Therefore no data were registered for this experiment. We are left with the impression of the laboratory staff that this beam was much more brittle than in the static test.

The static fracture toughness results obtained with extracted specimens from beam elements II and III are given in full in [2]. The static fracture toughness is typically 120 - 300 kN/m for specimens from both beams.

The influence of the loading rate upon the fracture toughness of specimens extracted from Beams II and III is shown in Fig 2. The number of specimens from Beam III (but not from Beam II) is great enough to indicate the decreasing trend of the fracture toughness with increasing loading rate. However, at some increased loading rate, which is not necessarily the same for the Beam II and III steels, the quasi-static fracture toughness is reduced to approximately 15 - 25 percent of the static fracture toughness.

The fracture toughness as a function of loading rate obtained with three point bend specimens extracted from Beam I is shown in Fig 2. Some typical load-load point displacement plots for the fracture toughness tests at -30 °C and +20 °C are compared in Figs 3.

For the specimens tested at -30 °C, the non-linear material behaviour prior to fracture was principally observed at low loading rates. The increase in loading rate from 1 to 250 MPa$\sqrt{m}$/s, caused a decrease in fracture toughness in the order of two thirds. Further increase in loading rate up to 1588 MPa$\sqrt{m}$/s gave only a minor decrease in fracture toughness.

The effect of loading rate at +20 °C is more complex. Here stable crack growth of varying extent occurred before fracture. At low loading rates the load point displacement curves were linear up to a first critical load beyond which the load continued to increase at a lower rate. In some cases a local maximum occured at this critical load after which the load begun to increase again. Unstable crack growth was principally observed at a second critical load maximum.

5. DISCUSSION

The extracted specimens from the beam elements were always made to the full thickness of the beam flanges from which they were taken. In [4] it was shown that this is necessary to obtain the best estimate of the effective toughness for a structural element of an inhomogeneous material in which the toughness varies across the thickness. This and the condition that specimen and full scale element constraints agree reasonably have been shown in [4] to be two necessary conditions for transferability under static loading.

The major reduction of toughness occur in the loading rate 1- 250 MPa$\sqrt{m}$/s. Only a minor further reduction of toughness occur for higher loading rates up to 1588 MPa $\sqrt{m}$/s. This trend is in general accordance with observations of Krabiell and Dahl [5] for steel Fe E 510 and by Yongning and Huijiu [6] for a C-Mn steel.

The effect of loading rate at +20 °C is more complex. Here stable crack growth of varying extent occurred before fracture. At low loading rates the load versus load point displacement curves were linear up to a first critical load beyond which the load continued to increase at a lower rate. In some cases a local maximum occurred at this critical load after which the load begun to increase again. Fracture occurred at a second critical load which was always greater than the first.

The first critical load is associated with the development of a plastic hinge mechanism in the specimen ligament and probably also with the onset of stable crack growth. At high loading rates the first critical load increased somewhat but beyond this point, the load decreased with increasing displacement until fracture followed.

In real structures the loading is controlled rather than displacement. If a structural element is loaded to first critical load and slightly beyond, e.g. due to a growing fatigue crack,

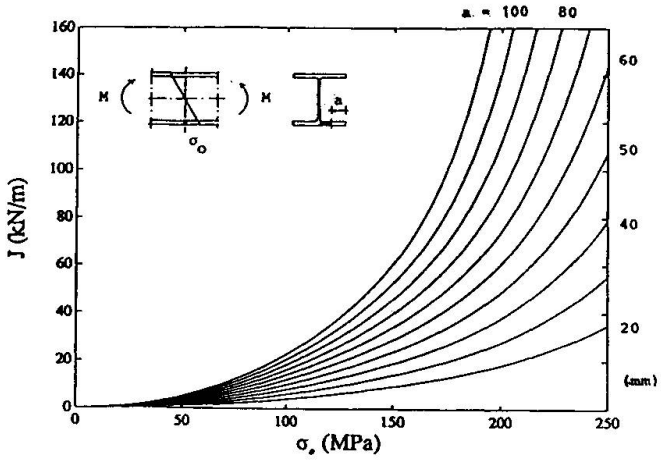

Fig.1 Crack driving force J versus nominal stress s_o for beam HEB 400.

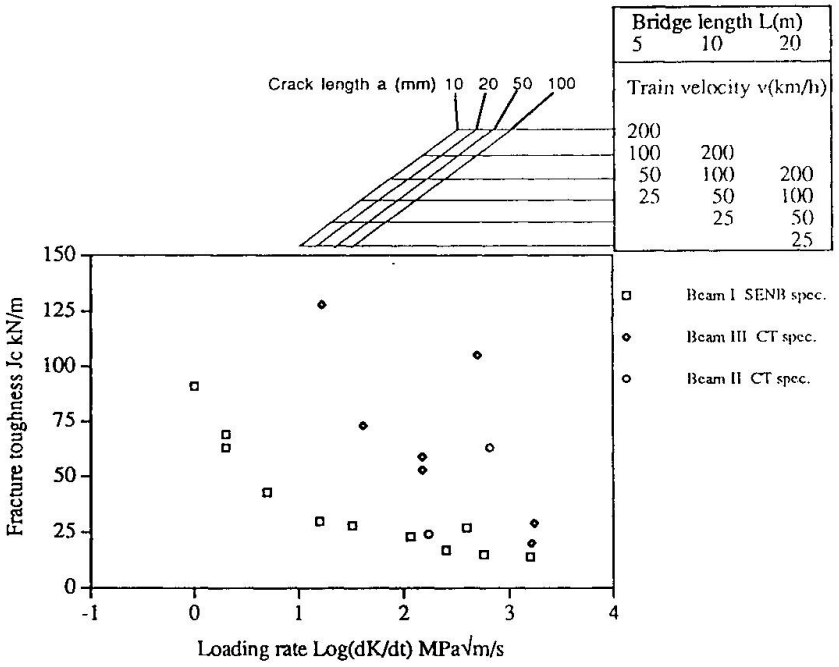

Fig.2 Comparsion of experimental results at the temperature -30 °C with loading rates in bridges.

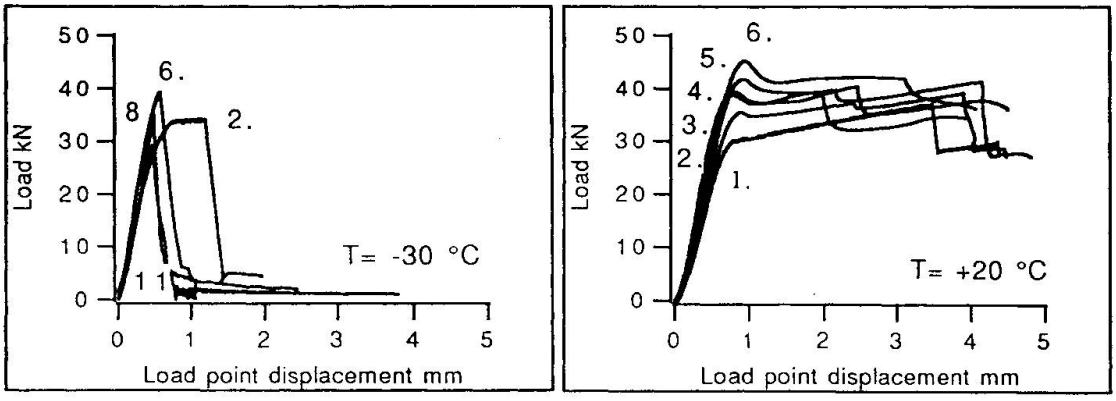

Fig.3 Load-load point displacement behaviour of fracture toughness tests at -30 and +20 °C as a function of loading rate. The loading rates at -30 °C are for **2.** 2, **6.** 33, **8.** 250 and **11.** 1588 MPa√m/s. The loading rates at +20 °C are for **1.** 2, **2.** 100, **3.** 280, **4.** 670, **5.** 1611 and **6.** 4115 MPa√m/s.

only an increased permanent deformation will occur at low loading rates. At best this will serve as the necessary warning that something unusual is going on and allow retrofit. At high loading rates, on the other hand, the situation becomes unstable at the load maximum associated with the first critical load. When this load is attained the structural element will collapse.

However, this behaviour is observed in small bend specimens while typical crack geometries in real structures are loaded in tension. The behaviour of e.g. a full scale beam element in this respect is therefore not necessarily the same. To study the transferability of this kind of behaviour is the subject of a future study.

For quasi-static loading we have in fact so far just one single data point, from Beam II, which however fit the general pattern very well. We therefore conclude that the reduction of fracture toughness due to increased loading rate in a full scale structure can be predicted from data obtained with extracted specimens. Whitout proving the contrary we assume that full thickness specimens are necessary for inhomogenous materials also in the quasi-static case.

The present results show that ordinary train speed and winter temperatures reduces fracture toughness to values that might be critical for the integrity of a structure. The results of this work also show that increased safety is obtained at low train speed not because of reduced loading but because of increased material toughness. On the other hand, increased maximum train speed means decreased safety.

Conclusions

The experimental results indicate that a) transferability in this particular case of full scale beam elements and quasi-static loading rates investigated is good enough for engineering applications and b) that the quasi-static loading rate along with temperature should be taken into account to obtain an accurate measure of fracture toughness and reliability of structures of ordinary structural steels.

References

[1] Standard test method for J_{Ic}, a Measure of Fracture Toughness, ASTM E -813 (1986) General Book of ASTM Standards, Sect. 3 American Society for Testing and Materials, Philadelphia, **1986**.

[2] ERIKSSON K., NILSSON F. and ÖBERG H., The deformation and failure of cracked broad flange beams in bending. Proceedings of the TWI Int. Conf. on ´´Shallow Crack Fracture Mechanics´´, Cambridge, **1992**.

[3] Strain measurements on railway bridges. Technical reports in Swedish. Swedish National Rail Administration, **1985-1994**.

[4] ERIKSSON K., Toughness Requirements for Older Structural Steels. IABSE Workshop, Lausanne, **1990**, pp. 95-101.

[5] KRABIELL A. and DAHL W., Influence of Strainrate and Temperature on the Tensile and Fracture Properties of Structural Steels. Advances in fracture Research. Ed. D. Francois, Proc. ICF5. Cannes, Vol. 1., **1981**, pp. 393-400.

[6] YONGNING L. and HUIJIU Z., Ductile to Brittle Fracture Transition of a Plain Carbon Steel and its Thermal Activation Model. Engineering Fracture Mechanics Vol 48, No.6, **1994**, pp. 773-782.

Load Capacity of Steel Structures with Cracked Components

Résistance des constructions métalliques avec des éléments fissurés

Tragfähigkeit von Stahlkonstruktionen mit gerissenen Gliedern

Kazimierz RYKALUK
Dr. Eng.
Technical University of Wroclaw
Wroclaw, Poland

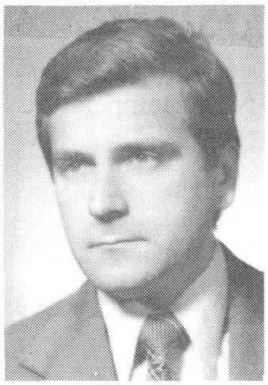

Kazimierz Rykaluk, born 1941, got his M.Sc, Ph.D. and D.Sc in civil engineering at Technical University of Wroclaw. He is Professor of Structural Steel Design and a practising consultant engineer in structural steel projects.

Andrzej CZEMPLIK
Dr. Eng.
Technical University of Wroclaw
Wroclaw, Poland

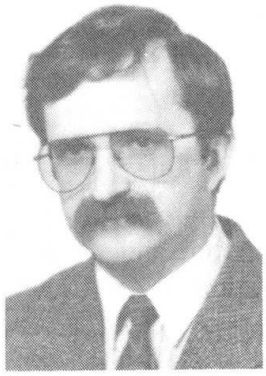

Andrzej Czemplik, born 1955. M.Sc and Ph.D. in civil engineering at Technical University of Wroclaw. Assistant Professor of Construction Technology, he is involved in technology problems of structural steel.

SUMMARY

The analysis of existing steel structures with cracked structural members is presented. The Fracture Analysis Diagram method is used in the analysis. Two components of the safety vector are considered: relative stress and stress intensity coefficient. The second component is adjusted in the analysis. Decrease of its value can be obtained by fixing the reinforcing ribs with the use of bolts and by elastic straps that fully cover the crack and which are elastically connected with a cracked member.

RÉSUMÉ

Le rapport présente l'analyse de constructions métalliques avec des éléments structuraux fissurés. La méthode de l'analyse du diagramme de la fissure est utilisée. Deux composantes du vecteur de la sécurité sont considérées: contrainte relative et coefficient de l'intensité des contraintes. La deuxième composante est ajustée dans l'analyse. La diminution de leur valeur peut être obtenue par la fixation de tôles de raidissement à l'aide de vis et par des fers plats élastiques, qui couvrent entièrement la fissure et qui sont fixés élastiquement à l'élément fissuré.

ZUSAMMENFASSUNG

Im Artikel ist die Analyse bestehender Stahlkonstruktionen mit gerissenen Konstruktionsgliedern vorgestellt. Für die Analyse wurde die Methode der Rissdiagrammanalyse angewendet. Zwei Komponenten des Sicherheitsvektors werden untersucht: Relative Spannung und der Koeffizient der Spannungsintensität. Die zweite Komponente wird in der Analyse errechnet. Die Verminderung ihres Wertes kann auf verschiedene Weisen erreicht werden. Zwei Möglichkeiten werden im Referat besprochen: die Befestigung der Verstärkungsrippen mit Schrauben einerseits und elastische Laschen, die den Riss vollkommen bedecken und mit dem gerissenen Glied elastisch verbunden sind andererseits.

1. INTRODUCTION

Brittle fractures have their origin in metallurgical discontinuities or in weld defects. The initial faults increase with the increase of monotonic load or cyclic load. Crack growth intensifies in winter seasons, when material ductility decreases. Irwin's constant K_{IC} represents the notch toughness of material and is correlated with fracture toughness measured with Charpy specimens [1]:

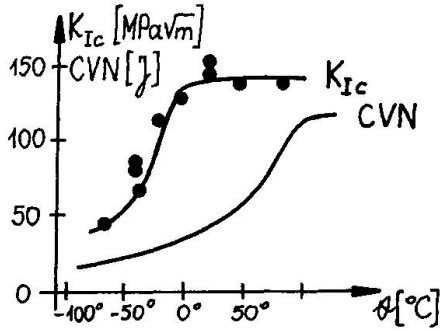

Fig.1 CVN vs. temperature and K_{IC} vs. temperature curves [2]

$$K_{IC} = \sqrt{0.22\,(CVN)^{3/2}\,E}$$

where: CVN - Charpy V-notch impact,
E - elastic modulus.

K_{IC} vs. temperature and CVN vs. temperature curves [2] are shown in Fig.1.

2. LIMIT STATES OF CRACKED COMPONENTS

The existing crack in structural component can remain unchanged if its half-length is not greater than the critical value:

$$l_{cr} = \frac{K_{IC}^2}{M \cdot \sigma^2}$$

where:

l - half-length of a crack,
M - geometrical coefficient, representing position and shape of the crack,
σ - the applied stress.

Values of M for cases shown in Fig. 2 are presented by Tada, Paris and Irwin [8]. On the basis of the critical value l_{cr} and the basic Paris equation [4]:

$$\frac{dl}{dN} = C\,(\Delta K)^m$$

the ability of survival of the cracked structural member, measured by the number of load cycles, can be determined, as:

$$N_{cr} = N + \frac{1}{C(\Delta K)^m (m-2)}\left[1 - \left(\frac{l}{l_{cr}}\right)^{\frac{m}{2}-1}\right]$$

where $\Delta K = K_{max} - K_{min} = (\sigma_{max} - \sigma_{min})\sqrt{Ml}$,
N - number of load cycles for the crack of length 2l,
C, m - material constants, proposed in [6] as $m = 3$, $C = 1.315 \times 10^{-4} / 895.4^m$.

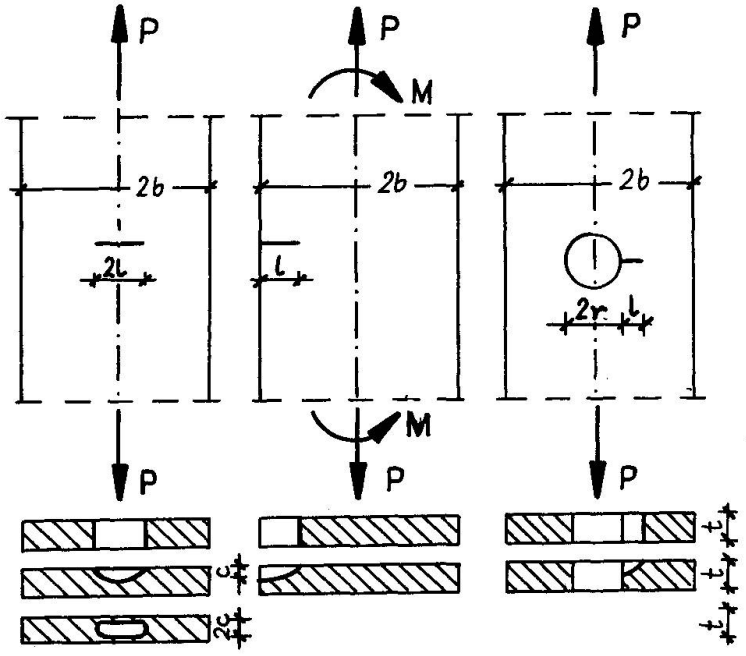

Fig.2 Characteristic cracks types

Further, for the case shown in Fig. 2a the two ways of safety improving are presented. Fitness for purpose second level criterion is suggested for load capacity analysis [6]:

$$K_r = S_r\left[\frac{8}{\pi^2}\ln\sec\left(\frac{\pi}{2}S_r\right)\right]^{-0.5}$$

where:
$K_r = n_k K_I / K_{IC}$, $K_I = \sigma\sqrt{\pi l}$,
$S_r = n_\sigma \sigma / \sigma_e$,
$\sigma_e = 0.5\,(\sigma_y + \sigma_u)$,
σ_y - material yield strength,
σ_u - ultimate strength,
n_k, n_σ - safety coefficient for brittle and ductile fracture, respectively.

While safety coefficient n_σ for ductile fracture are fixed in specifications of many countries, value of the coefficient n_k is still under intensive investigation, nowadays. Many authors usually assume, that $n_k \geq 2$.

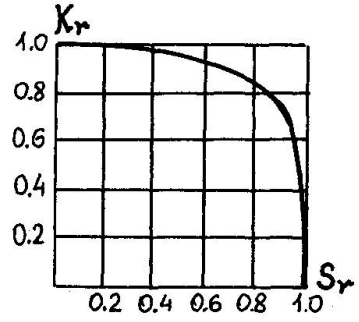

Fig.3 Limit capacity curve

In case of elements too thin for plane-strain behavior, i.e. when

$$\beta_t = \frac{(K_{IC}/\sigma_y)^2}{t} < 0.4$$

instead of K_{IC}, the following alternate value should be used in calculations:

$$K_C = K_{IC}\sqrt{1+1.4\beta_t^2}.$$

The idea of suggested methods of strengthening is to decrease the stress intensity coefficient K_{IC} to such an extend that the capacity of the structure would be described by parameters K_r and S_r which are below the limit capacity curve (Fig.3).

3. STRENGTHENING METHODS

3.1 Method I

In the first method, strengthening of cracked structural member is recommended by drilling of two relieving holes on the axis which is perpendicular to the axis of the crack (Fig. 4). Moreover, two steel straps connected with the cracked member symmetrically on its both sides, as shown in Fig.4

are recommended. This method is far more safe than popular drilling two holes through two tips of the crack. It should be noted, that drilling just two holes is not secure method of strengthening. In such a case there is a danger that the crack propagation can be initiated by the following factors:

- additional mechanical energy yielded during drilling,
- careless drilling, crack tip can be beyond the drilled hole, in the stress concentration zone.

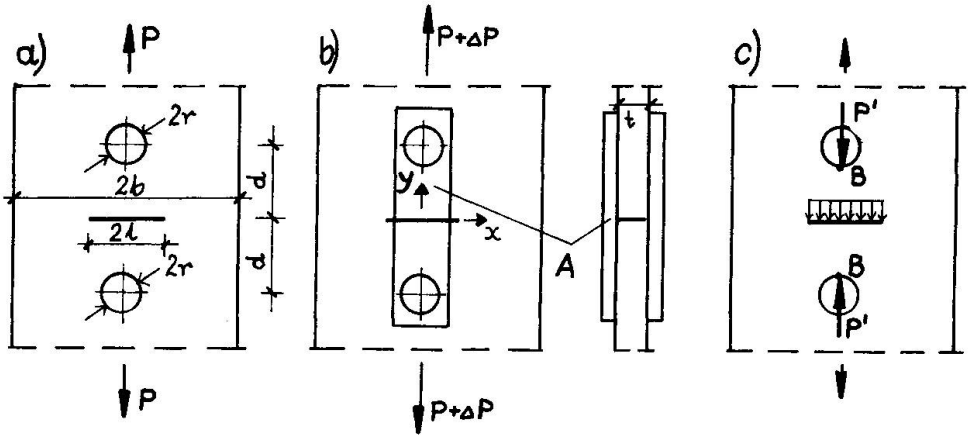

Fig.4 Strengthening method I

Newman's method [3] applied to the holes shown in Fig. 4a, gives:

$$K_I = \sigma\sqrt{\pi l}\cdot F\left(\frac{d}{r},\frac{l}{r+l}\right),$$

and the diagram of function F is presented in Fig.5. For d/r = 2 and r/l = 1, F≈ 0.6. Such a result allows to load the cracked component with the relative stress $S_r \approx 0.97$.

The holes drilled in a proposed way let to apply additional reinforcing straps (Fig.4b) connected with bolts or pins to the cracked component. The bolts or pins carry the force P' - part of load ΔP which increased the force P during strengthening. The force P' can be determined from the displacements compatibility condition in points B (Fig. 4c), as: P' = VEA / d, where:

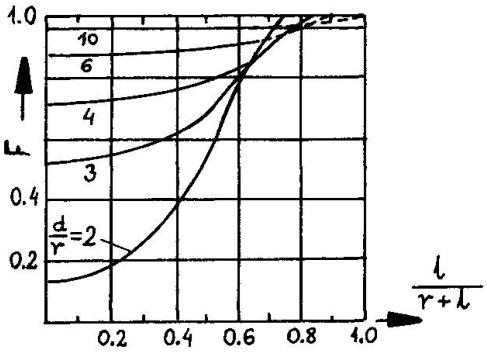

Fig. 5 Diagram of function F

$$V = \{1.82 \times \mathrm{Im}\overline{Z} - 1.3\,(d-r)\mathrm{Re}\overline{Z}\}_{z=i(d-r)},\quad \overline{Z} = \int Z\,dz,\quad z = x + iy,$$

$$\overline{Z} = \Delta\sigma\cdot z/\sqrt{z^2 - l^2} - P'l/\pi z\sqrt{z^2 - l^2}\ \text{- Westergaard's function.}$$

Force P' decreases the stress intensity coefficient K_I [5] by:

$$\Delta K_I = \Delta\sigma\sqrt{\pi l} - \frac{\left(6.6+l^2/c^2\right)\sqrt{2l/c}\,P'}{\sqrt{\pi c}\left(4+l^2/c^2\right)^{\frac{3}{2}}}$$

3.2 Method II

In the second method the component is stiffened by two-dimensional finite strap. It is supposed that the elastic strap fully cover the crack and is elastically connected with a component along its contours (Fig.6).

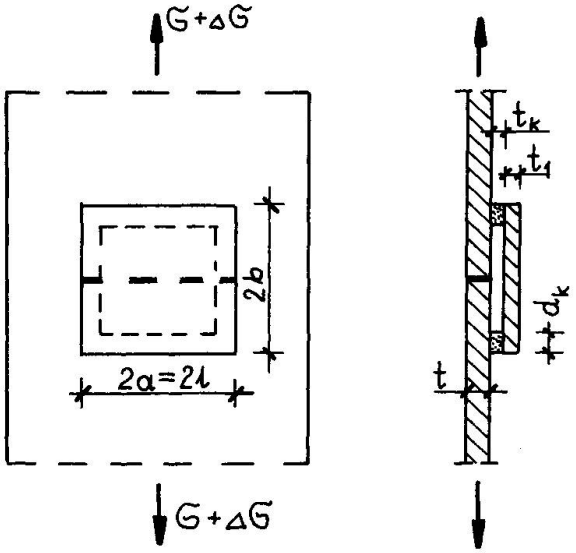

Fig.6 Strengthening method II

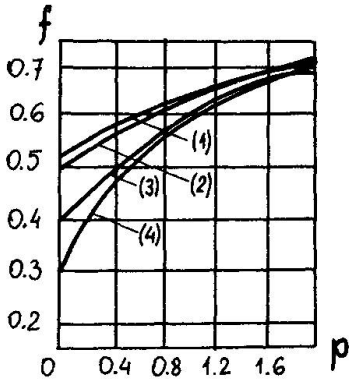

Fig.7 Diagram of function f [7]

For this method, the K_I can be calculated from the formula:

$$K_I = \sqrt{\pi l}\left(\sigma + \Delta\sigma \cdot f\right),$$

where the function f depend on the shape of straps and on the flexibility of the glue:

$$p = 2\pi G_l t_l t_k / G_k d_k l\,.$$

Diagrams of function f for some kind of straps are shown in Fig. 7 [7]:

(1) - circular shape of radius l,
(2) - ellipse with the semi-axes: l and 0.5l
(3) - square, of side 2l,
(4) - rectangular 2a * 2b (b=0.38l).

4. CONCLUSION

Steel structure with cracked structural members can be strengthened for its longer life in relatively easy ways. Obviously, the load capacity of such a strengthened structure is lower than before cracks have occurred, however, the value of capacity can be determined using clear engineering procedure.

REFERENCES

1. BARSOM J.M., ROLFE S.T., Fracture and Fatigue Control in Structures, Prentice-Hall, Inc. 1987.

2. HELLAN K., Introduction to Fracture Mechanics, McGraw-Hill Book Company, Inc., 1984.

3. NEWMAN J.C., Jr., An Improved Method of Collocation for the Stress Analysis of Cracked Plates with Various Shaped Boundaries, NASA TN D-6376, August 1971.

4. PARIS P.C., ERDOGAN F., J. Basic Eng., 85, 528÷534, 1963.

5. PARTON V.Z., MOROZOV E.M., Mechanics of elastoplastic fracture (in Russian), Nauka, Moskva 1985.

6. PD 6493: 1991. Guidance on methods for assessing the acceptability of flaws in fusion welded structures, BSI, August 1991.

7. SAVRUK M.P., KRAVEC V.C., The influence of strengthening straps on stress distribution in cracked disks (in Russian), Prikladnaja Mechanika, 29, N^{0}3, 1993, 48÷55.

8. TADA H., PARIS P., P., IRWIN G., The Stress Analysis of Cracks Handbook. Del Research Corporation, St. Louis, MO, 1985.

Toughness Evaluation and Assessment of Old Bridge Steel

Estimation et évaluation de la ténacité de l'ancien fer puddlé

Bestimmung und Bewertung der Zähigkeit alter Brückenstähle

Hans-Jakob SCHINDLER
Dr. sc. techn.
EMPA
Dübendorf, Switzerland

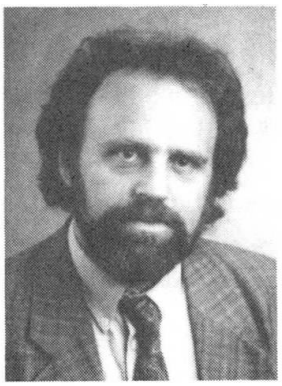

Hans-Jakob Schindler, born 1953, received his civil engineering and doctoral degrees at the Swiss Fed. Inst. of Technology (ETH), Zürich. After four years in a consulting engineering firm, he joined EMPA, as head of a research and engi-eering group. He is lecturer at ETH in fracture mechanics.

SUMMARY

Compared with the current requirements concerning toughness, the Charpy fracture ener-gy of old bridge material, especially wrought iron, is extremely low. In order to determine sufficient safety of these bridges with respect to spontaneous fracture, a simplified failure assessment based on fracture mechanics principles is recommended. A practical metho-dology to determine and to assess fracture toughness is developed and presented in this paper, which takes the special fracture behaviour of wrought iron into account.

RÉSUMÉ

Dans le cas des aciers d'anciens ponts, particulièrement en fer puddlé, la ténacité mesurée par l'essai Charpy est extrêmement basse. Pour évaluer la sécurité à la rupture spontanée, on a recours à une analyse simple basée sur des lois en mécanique de rupture. Le présent travail propose une méthode pratique d'estimation et d'évaluation de la ténacité, laquelle tient compte du comportement à la rupture du fer puddlé.

ZUSAMMENFASSUNG

Im Vergleich mit den entsprechenden Anforderungen an die heutigen Baustähle ist die Kerbschlagarbeit von Schweisseisen, dem typischen Werkstoff alter Brücken, äusserst tief. Zum Nachweis einer genügenden Sicherheit gegen Spontanbruch wird deshalb empfohlen, eine approximative bruchmechanische Analyse durchzuführen. Es wird eine praxistaugliche Methode zur Bestimmung und Bewertung der Bruchzähigkeit vorgestellt, die das spezielle Bruchverhalten dieser Werkstoffe berücksichtigt.

1. INTRODUCTION

An important part of the integrity of steel structures is the material's toughness, which has to be high enough to exclude the possibility of spontaneous brittle fracture even under the most unfavorable loading conditions. For this reason, in most of today's design standards for steel construction toughness requirements are given, in most of them in terms of Charpy fracture energy. When the safety of old steel bridges has to be assessed, these criteria often lead to difficulties: The Charpy fracture energies of these materials, especially of materials like wrought iron, which is very common for bridges that are about 100 years old, are often not high enough to meet the requirements of these standards. Furthermore, old bridges are likely to be affected by additional unfavorable factors with respect to brittle fracture, like local corrosion, unknown fatigue damage (hidden by the rivet heads and hardly detectable by nondestructive testing methods), low temperature, aging effects due to local plastic deformation, and possibly increased loading rates. So the question of the safety of the structure and whether or not the low Charpy fracture energy of these materials can be tolerated needs to be comprehensively investigated. For this purpose its is recommended to perform - complementary to the standard stress and strain analysis - a fracture mechanics analysis, which is in line with modern standards like e.g. Eurocode 3 [1].

In a fracture mechanics analysis, the applied stress intensity factor at a hypothetical crack, K_I, is compared with the fracture toughness K_{Ic} of the material (see e.g. [2]). In [3] it is shown that the fracture toughness of wrought iron is relatively high, at least higher than what is expected from the low Charpy fracture energy, indicating that the well known correlation formulas between Charpy energy and fracture toughness give overconservative predictions of the latter for this kind of material [4, 5]. Therefore it is advisable not to rely on such correlations but to perform direct fracture toughness tests. Unfortunately, such tests are in general rather time consuming and costly, and often there is not enough testing material available to determine the fracture toghness under all the relevant loading conditions the structure is subjected to in service. For these reasons testing on small specimens, especially instrumented impact tests on precracked Charpy specimens, are advantageous. However, there are two major problems arising when doing such tests: First, there is not yet a standard or generally accepted evaluation procedure available, and second, the loading rate is in general much higher than in service, so there must be a reliable way to compensate for this effect. At EMPA, simplified procedures for these purposes have been recently developed [6, 7, 8]. Nevertheless, due to the special fracture behaviour of old bridge materials like wrought iron that will be discussed in this paper, these evaluation procedures need some modifications and adjustments when applied to these materials. Another important point that is also affected by the special fracture behaviour is the required fracture toughness. Regarding the typical inhomogenity of wrought iron and the corresponding pronounced scatter of the toughness values, it is suggested to use an additional requirement which reflects not only the initiation but also the propagation resistance of cracks.

In this paper the above mentioned topics are discussed and illustrated with some examples. Simple formulas to be used in practical applications are presented. For their mathematical derivation, reference is given to further publications of the author, where also additional references can be found.

2. FRACTURE BEHAVIOUR OF WROUGHT IRON

Compared with today's structural steel there are several differences in the fracture behaviour of wrought iron. Concerning the Charpy (CVN) test results, the most striking ones are the low magnitudes of the upper shelf CVN-energies, the relatively high temperature (40°-80°C) where the upper shelf regime begins, and the large width of the brittle-to ductile transition temperature range, which results in a relatively low slope of the transition curve. In the transition regime, the force vs.

deflection diagram exhibits some noteworthy qualitative differences as well, as schematically shown in Fig. 1: Whereas ordinary steel in the brittle-to-ductile transition range (Fig. 1, (a)) exhibit a sudden steep fall at a certain (temperature-dependent) deflection due to unstable brittle cleavage crack growth, curves of wrought iron (Fig. 1, (b)) decrease more or less continuously after the maximum force, indicating a macroscopically stable crack growth behaviour (see Fig. 5 for an example). The fracture energy consumed in the crack initiation phase (i.e. area under the load-deflection-curve up to about maximum load) is very small compared with the propagation energy (after about maximum load) in the case of wrought iron, and a sharp corner at maximum load is formed, indicating a relatively sudden and well defined transition from crack-tip-blunting to crack propagation. In the upper shelf and lower shelf range, the shape of the curves is qualitatively the same for both types of materials.

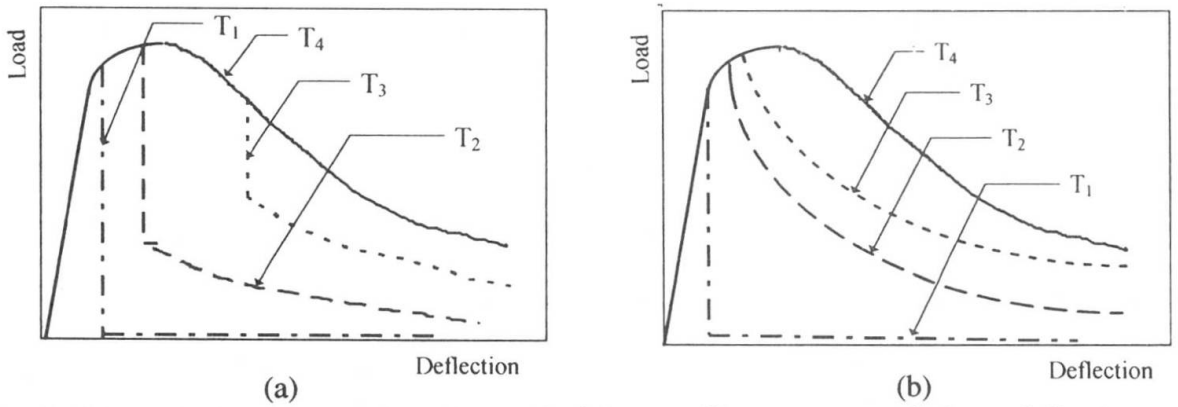

Fig. 1: Schematical representation of smoothed (i.e. oscillations removed) force-deflection curves of ferritic steel (a) and wrought iron (b) at four different temperatures $T_1<T_2<T_3<T_4$. T_1: lower shelf; T_2: lower transition range; T_3: upper transition; T_4: upper shelf

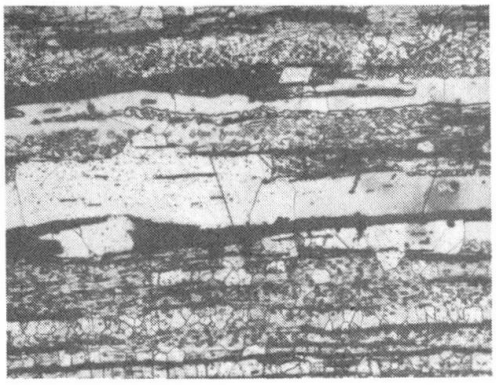

Fig. 2: Microstructure of wrought iron (L-S orientation, magn. 50x)

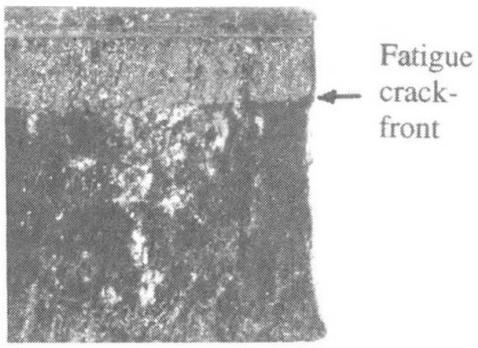

Fig. 3: Fracture surface of a precracked (L-T) Charpy specimen in the upper transition range

This fracture behaviour of wrought iron is attributed to the characteristic lamellar or fibrous microstructure of the material and its large content of nonmetallic inclusions (see Fig. 2). This leads to a fibrous, "wood-like" fracture surface in the upper shelf regime. In the transition regime, there is not a single crystalline area on the fracture surface like in the case of normal structural steel, but a number of small zones of cleavage fracture (bright spots in Fig. 3). The lower the temperature, the higher is the total area of these brittle spots, explaining the decreasing crack propagation energy with decreasing temperature as visible in Fig 1 (b). The relatively sharp corner of the load-displacement curve at maximum load is explicable by the various local cleavage events concentrated near the fatigue crack front. The macroscopic stability of the subsequent crack growth can be explained by the ability of the microstructure to arrest the local unstable cleavage cracks, which is possible by delamination and crack branching, and the corresponding reduction of local constraints as the crack

propagates. Thus, the effect of the characteristic lamellar and inhomogenious microstructure with its statistically distributed local brittle zones is twofold: On one hand it is responsible for the relatively low and scattering initiation toughness K_{Ic} (depending on whether or not a local brittle zone is present near the original crack-tip), on the other, it prevents a macroscopically unstable cleavage fracture from being triggered by the local cleavage events. So there is sort of a balance between beneficial and unbeneficial effects that should be appropriately accounted for in a failure assessment analysis.

3. EVALUATION OF FRACTURE TOUGHNESS BY INSTRUMENTED PRECRACKED CHARPY-TYPE TESTING

Instrumented impact testing on precracked Charpy specimens is very advantageous in terms of material needs and testing time consumption, especially for tests at different temperatures. Their drawback is that there is no "exact" or generally accepted procedure to determine fracture toughness from these tests. In [7] and [8] a simplified single specimen evaluation procedure is suggested. The following formula allows the approximate determination of K_{Ic} throughout the complete transition range including upper and lower shelf:

$$K_{Ic} \cong \left[\frac{0.85 \cdot F_m^2 \cdot l^2}{B^2 \cdot (W-a)^3} + \frac{4 \cdot E}{B \cdot (W-a)^{3/2}} \sqrt{U_{mp} \cdot U_t \cdot 0.2mm} \right]^{1/2} \quad (1)$$

F_m denotes the maximum force measured by the instrumented tup, U_{mp} the plastic (non-recoverable) part of the fracture energy at F_m, U_t the total fracture energy, E Young's modulus, B and W the specimen thickness and height, respectively (both =10 mm for standard Charpy geometry), and a (>0.3W required) the initial fatigue crack length (Fig. 4). In the case of wrought iron, the plastic part of the absorbed energy at maximum load is often much smaller than the elastic part, so it can hardly be determined accurately from the test diagram. For this reason, we suggest to modify eq. (1) by replacing U_{mp} by the total energy U_m at maximum load. The latter includes, as one can show, the first term of eq. (1), which represent the elastic component of the measured K_{Ic}, so this term can be omitted. Physically, this modification is justified by a virtual rounding-off of the load vs. deflection curve in the region of maximum load, as indicated by the dotted line in Fig. 5. One obtains:

$$K_{Ic} = \left(\frac{4 \cdot E}{B \cdot (W-a)^{3/2}} \cdot \sqrt{U_m \cdot U_t \cdot 0.2mm} \right)^{1/2} \quad (2)$$

The apparent advantage of this approximate evaluation formula (2) is its simplicity and unambiguity. The only parameters that have to be determined from the force-displacement diagram are the two well defined energy values U_m and U_t (see Fig. 5). Thus, (2) is well suited for automatic evaluation by means of a computer program. Note that in case of very small U_m, the kinetic energy of the specimen, which can be easily estimated, should be subtracted from U_m.

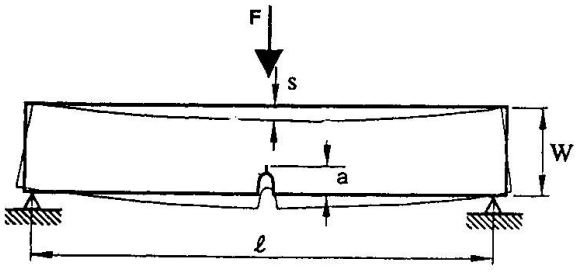

Fig. 4: Mechanical system of an impact bending test on precracked CVN- specimen

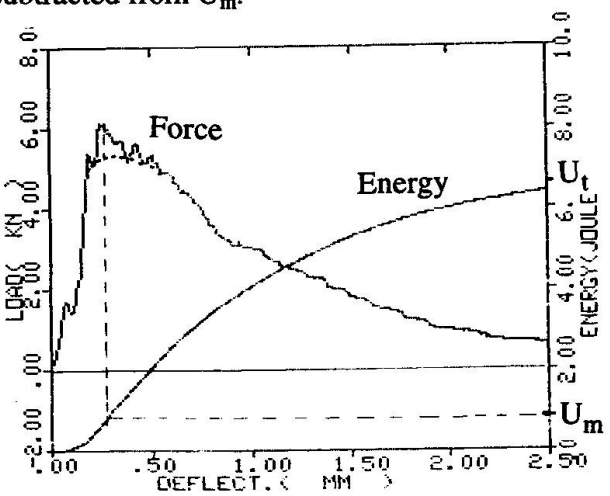

Fig. 5: Example of force (smoothed) and energy as a function of deflection, and definition of test data U_m and U_t used in eq. (2)

4. TEMPERATURE SHIFT DUE TO LOADING RATE

The crack-tip loading rate expressed in $\dot{K}_I$ is usually much higher at impact testing than in the relevant parts of the real bridge. Therefore the effect of the lower loading rate should be accounted for when transferring the toughness data from the test specimen to the real structure. Lowering the loading rate causes a shift of the K_{Ic}-vs.-temperature curve towards lower temperatures [6]. The relation between the brittle-to-ductile transition temperature, T_t, (defined as the temperature at which the fracture toughness equals a certain value K_t, usually K_t=100MPam$^{1/2}$), and the loading rate in terms of $\dot{K}_I$ is derived in [6]. Rearranging equation (2) of ref. [6] leads to the much simpler form

$$\log\frac{\dot{K}_I}{\dot{K}_{test}} = A_1 - \frac{A_2}{T_t(\dot{K}_I)} \tag{3}$$

A_1 and A_2 are material dependent constants that can be derived by performing impact tests at two different impact speeds $\dot{K}_{test}$. The latter can be roughly determined from the impact speed $\dot{s}$ by the formula

$$\dot{K}_{test} = \frac{2 \cdot E \cdot R_p \cdot b_0 \cdot \dot{s}}{K_t \cdot \ell} \tag{4}$$

The actual loading rate in service, $\dot{K}_I$, has to be estimated from the expected strain rate and a conservative assumption of a crack size. In cases where only tests at one impact velocities are performed, the temperature shift $\Delta T = T_t(\dot{K}_I) - T_t(\dot{K}_{test})$ can be estimated by the simplified relation

$$\Delta T = \left(22 - 0.016 \cdot R_p\right) \cdot \log\frac{\dot{K}_I}{\dot{K}_{test}} \ (°C) \qquad (R_p\text{: yield stress in N/mm}^2) \tag{5}$$

which follows as a first approximation of (3) and using the experimental results reported in [9]. Shifting the measured transition curve by the amount given by (5) or (3) to the left on the temperature axis delivers an approximation of the actual toughness-vs.-temperature curve, which can be used as the material data in a failure assessment procedure.

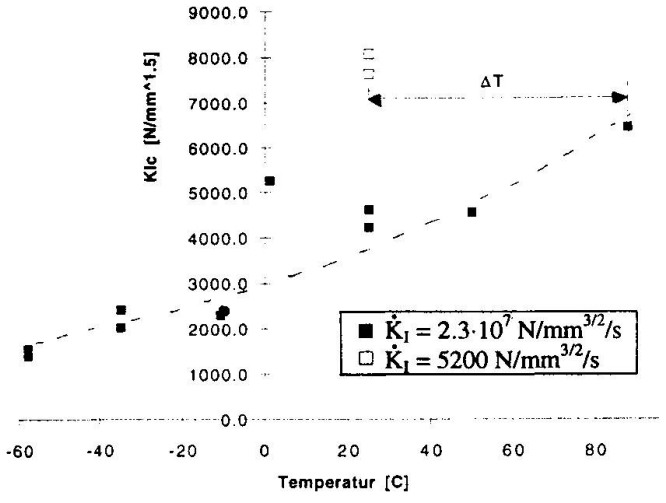

Fig. 6: Fracture toughness of wrought iron under two different impact velocities

In order to check the validity of (5) applied to wrought iron, impact bending tests on the material from a tensile rod of an old railway bridge were performed under impact speeds of 2.25 m/s and 0.5 mm/s, which correspond to crack loading rates $\dot{K}_I$ of $2.3 \cdot 10^7$ N/mm$^{3/2}$/s and 5200 N/mm$^{3/2}$/s, respectively. The yield stress was 273 N/mm^2, so eq. (5) predicts a temperature shift of ΔT=64°C. Fig 6 shows the K_{Ic} values as obtained using eq. (2). The temperature shift between the two loading rate can be estimated to be about 65°C, confirming eq. (5) Note the relatively large scatter of K_{Ic}.

5. ON THE REQUIRED TOUGHNESS

By the assumed condition that general yielding shall occur before onset of crack growth for any pre-existing crack, and using the so-called R6 failure assessment procedure [10] for the corresponding crack stability analysis, the following required toughness values K_{req} are obtained [11]:

- for plate-shaped components: $K_{req} = 1.38 \cdot R_p \cdot t^{1/2}$ (t: thickness) (6)
- for round rods under tensile loading $K_{req} = 2.08 \cdot R_p \cdot D^{1/2}$ (D: diameter) (7)

These values applied to the K_{Ic}-vs. temperature curve shifted by ΔT according to the previous chapter enables the lowest service temperature to be determined. Eq. (6) and (7) are applicable to any elastic-plastic materials, to modern structural steels as well as to wrought iron. In order to account for the relatively large scatter of K_{Ic} in the case of the latter, we recommend to use an additional criterion to make sure that there is enough crack growth resistance to stabilize crack growth in the case of unexpected initiation of local cleavage. In [12] a criterion to predict stability of tearing crack growth is derived. The key parameter therein is the crack tip opening angle (CTOA), which is related to (U_t-U_m) as shown in [4]. Using these relations and assuming the largest half-width of a hypothetical surface crack to be 4t results in the following criterion for stable tearing:

$$U_t - U_m \geq \frac{3 \cdot \pi \cdot B \cdot (W-a)^2 \cdot R_p^2}{E \cdot (1 - \sigma / R_p)} \tag{8}$$

In (8), σ denotes the maximum applied primary stress of the considered component in service.

6. CONCLUSIONS

- Wrought iron often exhibits Charpy fracture energies that are far below today's requirements. Nevertheless, thanks to its special microstructure, the fracture toughness and especially the crack growth resistance can be sufficiently high to guarantee safety with respect to brittle fracture.
- In order to assess the integrity of old bridges, it is recommended to perform a fracture mechanics analysis complementaryly to the standard stress analysis. For the testing part within such an analysis, instrumented impact tests on precracked specimens have proven to be very useful.
- The test evaluation procedure as well as the assessment methods developed for normal structural steel need some appropriate modification to account for the special fracture behaviour of wrought iron. The simple procedures presented in this paper allow for a simple as well as a reliable assessment of the materials toughness.
- The temperature shift due to loading rate is about the same as for normal steels.

References:

1. Eurocode 3, "Design of Steel Structures", CEN Prestandard, 1992
2. Rolfe, S.T., Barsoum, J.M., Fracture and Fatigue Control in Structures, Prentice-Hall Inc., 1977
3. Schindler, H.J., Morf, U., in: Report of IABSE Workshop, Lausanne, 1990, 87-94
4. Schindler, H.J., Morf, U., Int. J. Pres. Vess. and Piping, Vol 55, 1993, pp. 203-212
5. Eriksson, K., in: Report of IABSE Workshop, Lausanne, 1990, 95-101
6. Schindler, H.J., Morf, U., "Toughness Testing and Assessment of Welds", in: Proc. of Int. Conf.on Engineering Design in Welded Constructions, Madrid, 1992, pp. 205-212
7. Schindler, H.J., in: Berichtsband der 24. Vortragsveranstaltung des DVM-Arbeitskreises Bruchvorgänge, Aachen, 1992, pp.119-131 (in german)
8. Schindler, H.J., Proc. of 2nd ESIS -TC5 Workshop on instrumented Charpy Testing, Mol,Belgium, 1994 (to be published)
9. Sedlacek, G., et al., Internat. Inst. of Welding (IIW) Doc. X-1274-93
10. Central Electricity Generating Board, "Assessment of the Integrity of Structures Containing Defects", CEGB Document No. R/HR6-Rev. 3, Mai 1986
11. Schindler, H.J. "On the required toughness of structural materials", in: Proc. of the 2nd Int. Conference on Engineering Integrity Assessment, Glasgow, 1994
12. Schindler, H.J., Proc. of 9th European Conf. on Fracture, Ed. S. Sedmak, Varna, 1992

Acknowledgement:The author wishes to thank his colleagues U. Morf, M. Veidt, and R. Huwyler for helpful discussions and the experimental work behind this paper.